UNIVERSITÉ DE MONTRÉAL

MORPHOLOGY AND PROPERTIES OF POLY(ETHYLENE TEREPHTHALATE)/CLAY NANOCOMPOSITES

ABBAS GHANBARI

DÉPARTEMENT DE GÉNIE CHIMIQUE

ÉCOLE POLYTECHNIQUE DE MONTRÉAL

THÈSE PRÉSENTÉE EN VUE DE L'OBTENTION
DU DIPLÔME DE PHILOSOPHIAE DOCTOR
(GÉNIE CHIMIQUE)

NOVEMBRE 2012

UNIVERSITÉ DE MONTRÉAL

ÉCOLE POLYTECHNIQUE DE MONTRÉAL

Cette thèse intitulée:

MORPHOLOGY AND PROPERTIES OF POLY(ETHYLENE TEREPHTHALATE)/CLAY NANOCOMPOSITES

présentée par : GHANBARI Abbas

en vue de l'obtention du diplôme de : Philosophiae Doctor

a été dûment acceptée par le jury d'examen constitué de :

M. PATIENCE Gregory S, Ph.D., président

Mme. HEUZEY Marie-Claude, Ph.D., membre et directrice de recherche

M. CARREAU Pierre, Ph.D., membre et codirecteur de recherche

M. AJJI Abdellah, Ph.D., membre

M. COATES Philip David, PhD., membre

DEDICATION

“To my beloved parents, sisters, and brother”

ACKNOWLEDGEMENTS

When I sincerely acknowledge valuable people who kindly helped me my soul feels elevated with gratification and my heart feels happy with emotions. First and foremost I would like to offer my deepest and sincerest gratitude to my supervisors, Prof. Marie-Claude Heuzey, Prof. Pierre J. Carreau, and Prof. Minh-Tan Ton-That for their excellent guidance, continuous support of my research, and for the trust they placed in me to work in my own way. Their patience, warm encouragements, confidence on me, and insightful suggestions make me indebted to them more than they know. I truly appreciate constructive remarks and **S**ignificant efforts of Prof. Heuzey for improving quality of the papers, precious comments of Prof. Carreau, and productive discussions with Prof. Ton-That. I really feel lucky for having the rare opportunity to do my PhD under supervision of these famous world-class researchers.

Special thanks go to all the technical and administrative staff of the Chemical Engineering Department and technicians of Industrial Material Institute (IMI), particularly Mr. Guillaume Lessard, Mr. Eric Cloutier, and Ms. Florence Perrin-Sarazin. Many thanks to Ms. Weawkamol Leelapornpisit for providing the SEM and TEM images. A special word of thanks is owed to our brilliant and helpful research associate who has also been a magnificent friend to me, Ms. Melina Hamdine, someone you will instantly love and never forget once you meet her.

I would also like to thank my friend Marie Matet for her warm and quick response to my request for translating part of this thesis to French.

I warmly thank all my friends and my colleagues for their supports and their willing to help me with my research. I have spent memorable times with them during the past 4 years and I never forget their kind regards to me.

My heartfelt thanks to my beloved parents, sisters, and brother for their understanding, support, and encouragements during every step of my life. I cannot thank them enough for their unconditional love.

RÉSUMÉ

Le polyéthylène téréphtalate (PET), un thermoplastique semi-cristallin, est produit par une réaction de condensation soit du téréphtalate de diméthyle soit de l'acide téréphtalique et de l'éthylène glycol. Le PET est habituellement utilisé dans l'industrie de l'emballage des aliments et boissons. Toutefois le PET ne permet pas d'avoir des propriétés barrières à l'oxygène suffisantes pour l'emballage des breuvages telles que la bière et les boissons gazeuses non alcoolisées qui sont sensibles à l'oxygène ou à la perte de dioxyde de carbone. L'incorporation de silicates en feuillets imperméables à une matrice de PET et la fabrication de nanocomposites à base de PET est une méthode prometteuse en vue de l'amélioration des propriétés barrières du PET. L'objectif de la présente étude est d'améliorer les propriétés barrières du PET avec des silicates en nanocouches. Les nanocomposites à base de PET et d'argile ont été préparés par un mélange à l'état fondu. Par rapport au mélange en solution et la polymérisation *in-situ*, le mélange à l'état fondu a des avantages environnementaux et économiques car l'utilisation de solvants organiques n'est pas nécessaire. De plus, cette technique entraîne des forces de cisaillement élevées ce qui améliore le niveau d'exfoliation des particules d'argile dans la matrice. Afin de créer un long chemin tortueux et une diffusion ralentie des molécules de gaz à travers le nanocomposite, les particules d'argile doivent être bien dispersées et distribuées dans la matrice. Par conséquent, une attention particulière est apportée à l'amélioration du niveau d'exfoliation des silicates stratifiés dans la matrice de PET. À cet égard deux types différents d'argiles organomodifiées, le Cloisite® 30B (C30B) et le Nanomer® I.28E (N28E), ont été mélangées avec le PET.

Des films de nanocomposite à base de PET ont été préparés par extrusion. Un PET ionomère a été utilisé afin d'augmenter la compatibilisation et l'espacement entre les couches des particules d'argile. Il a été observé que mélanger un PET et un PET ionomère entraîne la formation d'un mélange immiscible. Des interactions favorables entre les particules d'argile et le PET ionomère localise les particules d'argile dans les domaines composés du PET ionomère et restreint la distribution des particules. Néanmoins, les études morphologiques et rhéologiques montrent que le PET ionomère agit comme un agent exfoliant et accroit l'espacement des nanofeuillets de

l’argile N28E. L'incorporation de 2 % en masse de C30B dans la matrice de PET entraîne l'amélioration de 25 % des propriétés barrières à l'oxygène.

Les effets des conditions de mise en œuvre, de la composition de l'argile, et de la concentration des argiles sur les propriétés morphologiques et rhéologiques des nanocomposites de PET et argile ont été examinés dans la seconde partie de cette étude. Différents organo-argiles comme le N28E, C30B, Cloisite 25A (C25A), et Cloisite 15A (C15A) aussi bien qu'un argile non-modifié synthétique Somasif ME100 (SM100) ont été mélangés avec le PET en utilisant une extrudeuse double vis. Les résultats morphologiques et rhéologiques montrent que l'augmentation du temps de résidence et un nombre plus grand d'éléments de cisaillement améliorent la dispersion des argiles et les propriétés viscoélastiques. Alors que le PET seul présente une viscosité non-dépendante de la fréquence, la viscosité complexe des nanocomposites montre un comportement rhéofluidifiant qui devient plus prononcé quand la quantité d'argile augmente. Le module de conservation est presque indépendant de la fréquence aux basses fréquences pour les chargements élevés d'argile, due à la formation d'un réseau interconnecté des particules d'argile. Des propriétés rhéologiques plus élevées ont été observées pour les nanocomposites les plus intercalés/exfoliés. La dégradation de la matrice de PET, due à la présence des organo-argiles, a été quantifiée en utilisant l'équation de Maron-Pierce. Parmi les organo-argiles étudiés dans ce travail, la dégradation la plus importante a eu lieu pour la matrice contenant du C30B.

Pour contrôler la dégradation thermique du PET et pour améliorer les propriétés des nanocomposites à base de PET, dans la dernière partie de cette recherche, un agent d'allongement de chaînes multifonctionnel à base de résine d'époxy, le Joncryl ADR-4368F (Joncryl), a été ajouté aux nanocomposites via un lot primaire. L'effet de l'agent d'allongement de chaînes sur les propriétés morphologiques, rhéologiques, mécaniques, thermiques, optiques, et sur les propriétés barrières aux gaz a été examiné sur le nanocomposite contenant 4 % en masse de C30B et de N28E. Grâce aux réactions entre les groupes fonctionnels de l'agent d'allongement de chaînes et les groupes terminaux du PET, les propriétés viscoélastiques des échantillons contenant du Joncryl ont été augmentées. Des contraintes de cisaillement plus élevées, dues à la présence de l'agent, entraînent une exfoliation plus élevée et par conséquent des propriétés mécaniques et barrières plus élevées. Une réduction de 46 % de la perméabilité à l'oxygène a été obtenue pour les films nanocomposites contenant du C30B et du Joncryl en comparaison aux films de PET pur.

La réduction pour les nanocomposites contenant du N28E et du Joncryl était de 40 %. Les nanocomposites contenant du N28E et du Joncryl contenant du C30B et du Joncryl l'augmentation était légèrement moindre.

ABSTRACT

Polyethylene terephthalate (PET), a semi-crystalline thermoplastic, is produced by condensation reaction of either dimethyl terephthalate or terephthalic acid with ethylene glycol. PET is commonly used in food and beverage packaging industry. However, PET does not offer sufficient oxygen barrier properties in packaging of beverages such as beer and carbonated soft drinks that are sensitive to oxygen and loss of carbon dioxide. Incorporation of impermeable layered silicates into a PET matrix and manufacturing of PET nanocomposites is a promising method to enhance barrier properties of PET. The aim of the present study is to improve barrier properties of PET with silicate nanolayers. PET clay nanocomposites were prepared via a melt blending approach. In comparison to solution blending and *in-situ* polymerization, melt blending has environmental and cost advantageous because there is no need for organic solvents. Besides, this technique provides high shear forces that improve the exfoliation level of clay particles in the matrix. To create a long tortuous pathway and slow down the diffusion of gas molecules through the nanocomposite, clay particles must be well dispersed and distributed in the matrix. Hence, a particular attention is paid to the improvement of exfoliation level of silicate layers in the PET matrix. In this regard two different types of organomodified clay, Cloisite® 30B (C30B) and Nanomer® I.28E (N28E), were melt blended with PET. PET-based nanocomposite films were prepared using cast film extrusion. A PET-ionomer was employed to compatibilize and increase the interlayer spacing of the clay particles. It was observed that mixing of PET and PET-ionomer results in an immiscible blend. Favorable interactions between the clay particles and the PET-ionomer localize the clay particles into the PET-ionomer domains and restrict the distribution of the particles. Nevertheless, morphological and rheological studies show that PET-ionomer acts as an exfoliation agent and increases the gallery spacing of N28E nanolayers. Incorporating 2 wt% C30B into PET matrix led to 25% enhancement in oxygen barrier properties.

The effects of processing conditions, clay chemistry, and concentration on the morphological and rheological properties of PET clay nanocomposites were investigated in the second part of this study. Various organoclays such as N28E, C30B, Cloisite® 25A (C25A), and Cloisite® 15A (C15A) as well as unmodified synthetic clay Somasif® ME100 (SM100) were melt blended with PET using a twin-screw extruder. Morphological and rheological results show that a longer

residence time and more shearing elements improve the dispersion of clay tactoids and enhance the viscoelastic properties. While the neat PET exhibits a frequency independent viscosity, the complex viscosity of the nanocomposites shows a shear-thinning behavior, which becomes stronger with clay loading. The storage modulus was nearly independent of frequency at low frequencies and high clay loadings, due to the formation of an interconnected network of clay particles. Larger rheological properties were observed for the most intercalated/exfoliated nanocomposites. The PET matrix degradation, due to the presence of the organoclays, was estimated using the Maron-Pierce equation. The highest degradation occurred for the matrix containing C30B among the organoclays studied in this work.

To control the thermal degradation of PET and improve the overall properties of PET nanocomposites, in the last phase of this research a multifunctional epoxy-based chain extender, Joncryl® ADR-4368F (Joncryl), was added to the nanocomposites via a master-batch approach. The effect of the chain extender on the morphological, rheological, mechanical, thermal, optical, and gas barrier characteristics of the nanocomposites containing 4 wt% C30B and N28E was examined. The viscoelastic properties of the samples containing Joncryl increased due to the reaction between functional groups of the chain extender and PET end groups. Higher shear stress induced by the presence of the chain extender resulted in higher exfoliation level and consequently better mechanical and barrier properties. A 46% reduction in oxygen permeability was obtained for the PET nanocomposites containing C30B and Joncryl, in comparison to the neat PET films. The corresponding reduction for the nanocomposites containing N28E and Joncryl was 40%. Nanocomposites containing N28E and Joncryl exhibited a 66% improvement in tensile modulus, whereas the corresponding improvement for the nanocomposites containing C30B and Joncryl was slightly less.

Abbas Ghanbari

École Polytechnique de Montréal

October 2012

TABLE OF CONTENTS

LIST OF TABLES

LIST OF FIGURES

CHAPTER 1
INTRODUCTION

Polymer/layered silicates, in comparison with unfilled polymers or common microcomposites, have shown remarkable improvements in several properties [1-3]. Incorporation of nanolayers with high aspect ratio at very low volume fractions improves tensile modulus, strength, gas barrier properties, heat resistance, and decreases flammability. One can expect reduction of the thickness of the commercial packaging containers by incorporation of nanoplatelets and improvement of barrier properties.

Polyethylene terephthalate (PET) is a linear thermoplastic polyester which has become an important commercial polymer owing to its rapid market growth. The wide field of applications of PET is due to its desirable qualities such as high tensile strength, dimensional stability, chemical resistance, resistance to abrasion, optical clarity, processability, recyclability, and reasonable thermal stability. PET is commonly used in synthetic fibers, food and non-food containers, soft drink and mineral water bottles, and engineering plastics in automobiles. Depending on the required mechanical properties, specific molecular weight is desired for each application. For instance, intrinsic viscosity of PET used for audio or video tapes is about 0.55 dL/g, while PET used for textile fibers, soft drink bottles, and industrial tire cords has intrinsic viscosities of 0.65, 0.78, and 0.85 dL/g, respectively [4]. Global demand of PET for packaging applications in 1985 was about 0.5 million metric tons, while in 1990 1.5 million metric tons of PET was consumed. Seven (7) million metric tons of PET were consumed in 2000, and this increased to more than 10 million metric tons in 2005 in the packaging industry [5].

Glass containers, usually used for beverage packaging, are fairly heavier than an equivalent PET bottle. Besides, PET bottles do not shatter or break. The world market for PET resin in packaging could be doubled if PET would gain 50% of the market share in beer bottles packaging. Delicate flavor of beer, especially light beer, is very sensitive to exposure to oxygen as presence of oxygen sours beer [1]. For example, considering that allowable oxygen concentration limit in beer is 1 ppm, it has been reported that beer quality preservation in typical 1.5 L PET bottles is around one month [6]. Loss of carbon dioxide of carbonated soft drinks leaves a flat drink. Unfortunately PET does not provide sufficient barriers to the transmission of oxygen and carbon dioxide. One promising method to enhance barrier properties of PET is the incorporation of silicate nanolayers.

Presence of obstructing platelets can slow down the transmission of gases through nanocomposites by creating a long tortuous pathway. Exfoliation of silicate layers into the matrix is the key to obtain this benefit.

To achieve that goal, in the first phase of this study a PET-ionomer was employed as an exfoliating agent to increase the gallery spacing of the clay platelets. Considering the importance of processing conditions and clay chemistry in the final morphology of nanocomposites, a systematic study was performed to examine the effect of screw geometry, clay concentration and chemistry on the rheological and morphological properties of PET-based nanocomposites. The first and second parts of this study made it very clear that the PET matrix undergoes severe degradation in the presence of the organoclays. Hence, in the last phase of this work a multifunctional chain extender was used to compensate molecular weight reduction of the matrix and improve the exfoliation level of silicate layers.

This dissertation is based on three articles that have been accepted by or submitted to scientific journals, and consists of the following chapters:

- Chapter 2 provides a literature review considering the related issues.
- Chapter 3 presents the objectives.
- In Chapter 4 the organization of the articles is introduced.
- Chapters 5, 6, and 7 comprise the three papers describing the main results obtained in this study.
- Chapter 8 gives a general discussion about the results presented in previous chapters.
- Finally, Chapter 9 summarizes the most important conclusions of this study followed by recommendations for future works.

CHAPTER 2
LITERATURE REVIEW

2.1 Structure of layered silicates

Generally, at least one dimension of dispersed particles in nanocomposites must be in the nanometer range (<100 nm). Typical nanomaterials which are currently under investigation are classified by their geometries. Silica nanoparticles and carbon black are examples of nanoparticles, while carbon nanotubes and nanofibers are classified as fibrous materials. Silicate layers with plate-like structure belongs to layered nanomaterials [7].

Silicate nanolayers which are widely used in polymer clay nanocomposites (PCN) are 2:1 phyllosilicates and contain octahedral and tetrahedral crystalline sheets. The octahedral sheet consists of hydroxyl groups, oxygen, aluminum, iron, and magnesium atoms. On the other hand, the tetrahedral sheet comprised a central silicon atom and four oxygen atoms or hydroxyl groups [8]. The structure of 2:1 phyllosilicates is shown in Figure 2-1.

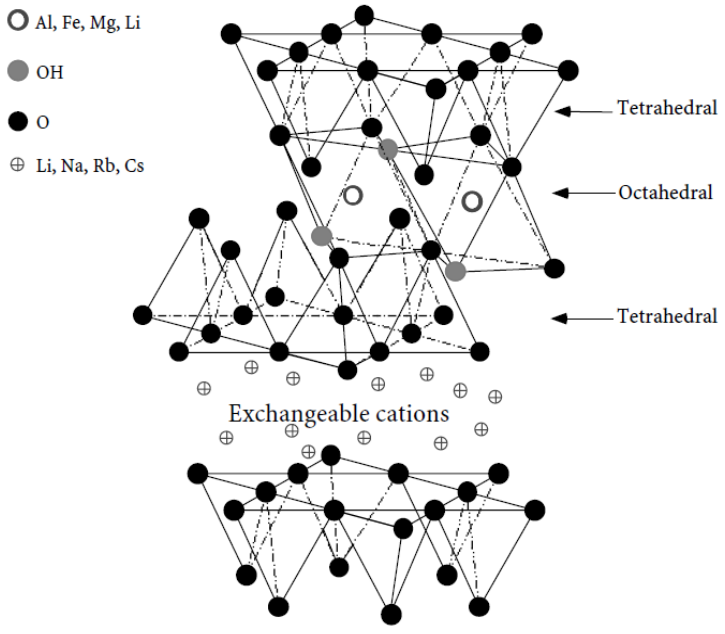

Figure 2-1: Structure of 2:1 phyllosilicates [1].

The lateral dimensions of these layers changes in a wide range, from 30 nm to some microns, while the thickness of the layer is around 1 nm. Interlayer or gallery spacing is a gap between the stacked layers. The ability of clay minerals to hold cations is named the cation exchange capacity

(CEC), which is generally expressed as meq/100 g clay. Substitution of cations in the tetrahedral sheet (e.g. Si^{4+} is replaced by Al^{3+}) or in the octahedral sheet (e.g. replacement of Al^{3+} with Mg^{2+} or Fe^{2+}) leads to the generation of a net negative surface charge. This replacement of ions with relatively similar sizes is called isomorphous substitution. The negative charge can be counterbalanced by alkali and alkaline earth cations such as Na^{+} or Ca^{2+} situated in the gallery [1].

Montmorillonite is highly polar and its surface is hydrophilic. Therefore, delamination of montmorillonite in many engineering polymeric matrices is problematic. In order to make a miscible blend from montmorillonite and polymers it is essential to render the hydrophilic silicate surface more organophilic. Via this conversion, intercalation of most polymeric matrices between silicate nanolayers becomes possible. Cationic surfactants such as alkylammonium and alkylphosphonium can penetrate into the interlayer space of silicate nanolayers via ion exchange reactions. The produced organosilicate has a lower surface energy, higher interlayer spacing, and more ability for polymer wetting in comparison with unmodified montmorillonite (Na-MMT). In some cases these organic modifiers or surfactants possess functional groups interacting with the polymer matrix [1, 2]. Figure 2-2 displays a schematic representation of a cation exchange reaction between pristine montmorillonite and a cationic surfactant.

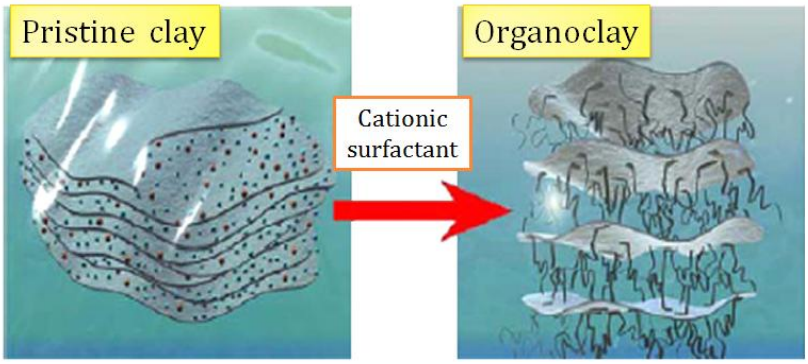

Figure 2-2: Schematic representation of a cation exchange reaction [3].

2.2 Morphologies of polymer layered silicates

Generally, depending on the interfacial interaction strength between the polymer matrix and the nanolayers, three main types of polymer layered silicates morphologies may be observed. In

immiscible or phase-separated systems, polymer chains are not able to penetrate between the silicate layers gallery spacing. Therefore, the *d*-spacing of the nanolayers remains unchanged and the properties of the resulting composites cannot be better than conventional microcomposites. Intercalated nanocomposites are obtained when polymer chains are inserted in the interlayer gap between the silicate nanolayers. In the intercalated morphology the stacking order of the nanolayers is retained, however due to the penetration of several polymer chains the interlayer *d*-spacing expands. Delaminated or exfoliated nanocomposites refer to the morphology in which silicate nanolayers are dispersed individually in the polymer host matrix. In this case, the distance between separated layers is typically 10 nm or higher, which depends on clay loading. Remarkable improvements are expected to be obtained via exfoliation of silicate nanolayers within polymer matrices [3]. Figure 2-3 illustrates a schematic representation of the three morphologies of polymer layered silicates. Generally, the final morphology of polymer layered silicates is determined by the interplay of entropy and enthalpy changes. The entropy change includes an entropy loss due to the confinement of polymer chains within the interlayer spacing of nanolayers, and an entropy gain because of gallery enhancement and increased conformational freedom of organic modifier chains. If the entropic penalty of polymer confinement is equal to or larger than the entropy gain, enthalpy will determine if intercalation is thermodynamically feasible. The enthalpy of mixing depends on the interactions of the polymer chains with the silicate nanolayer surface and the organic modifier chains [1, 9].

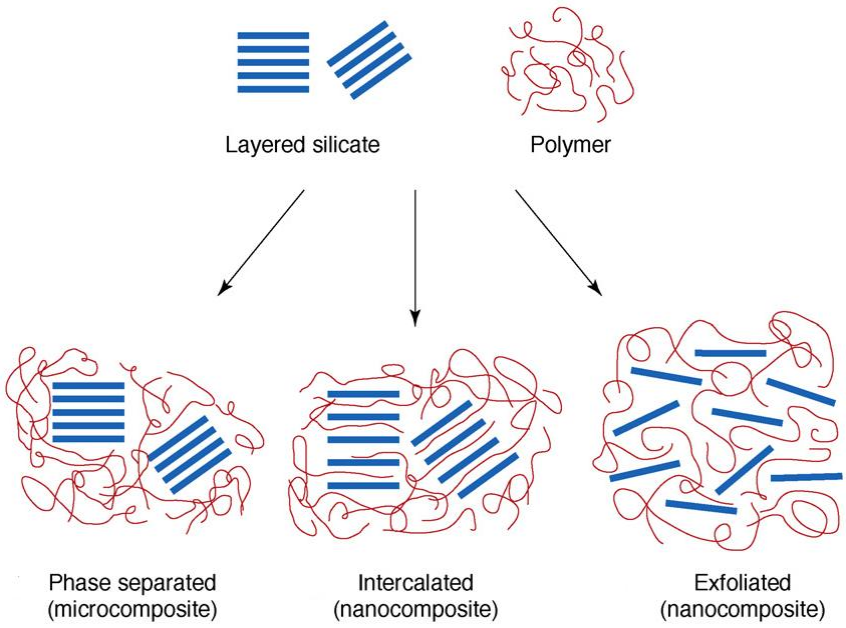

Figure 2-3: Scheme of different types of composite structures arising from the mixing of layered silicates and polymers [10].

2.3 Nanocomposite preparation methods

Solution blending, *in-situ* polymerization, and melt blending are three processing techniques for preparing polymer layered silicate nanocomposites. In solution blending a polymeric solution is prepared and layered silicates are swollen in a solvent (e.g. water, toluene, or chloroform). By mixing the polymeric and silicate nanolayers solutions, macromolecules can intercalate and displace the solvent within the silicate layers gap. By removing the solvents, polymer/layered silicate nanocomposites are achieved [1]. A schematic representation of this method is shown in Figure 2-4. Pramanik *et al*. [11] prepared ethylene vinyl acetate (EVA) nanocomposites containing 2, 4, 6, and 8 wt% dodecyl ammonium ion intercalated montmorillonite by solution blending. EVA was dissolved in toluene and the organoclay was dispersed in *N*,*N*-dimethyl acetamide. The absence of any diffraction peak in XRD for nanocomposites containing up to 6 wt% clay was attributed to the homogenously exfoliation and randomly dispersion of silicate layers within the polymer matrix. In our opinion, the absence of XRD peak, which can be due to clay dilution, is not sufficient to conclude to an exfoliated structure. It is worth noting that EVA nanocomposites containing 8 wt% organoclay exhibit the basal reflection peak at the same

position as that of the pristine organoclay. The authors reported 36% improvement in tensile strength for the nanocomposites containing 2 wt% organoclay.

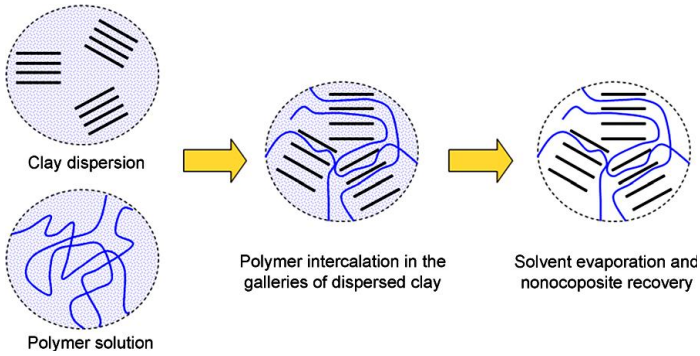

Figure 2-4: Schematic representation of nanocomposites obtained by solution blending [3].

Another technique to prepare polymer layered silicate nanocomposites is *in-situ* polymerization. This method have attracted much academic and industrial interests after Toyota research group synthesized polyamide-6 clay nanocomposites, with remarkable mechanical and thermal properties improvement, via *in-situ* polymerization. In this technique a liquid monomer or a monomer solution is used to swell the silicate nanolayers. Upon starting polymerization, macromolecule formation can occur between the silicate layers [1]. Lee and coworkers [12] prepared PET nanocomposites containing trimethyl octadecyl ammonium ion intercalated montmorillonite by ring-opening polymerization of ethylene terephthalate cyclic oligomers (ETCs). Figure 2-5 depicts the schematic of the process leading to the synthesis of a PET nanocomposite. Intercalation of the cyclic oligomer, with low molecular weight and viscosity, enhanced gallery spacing of the organoclay. Subsequent polymerization resulted in the co-existence of exfoliated and intercalated clay particles rather than perfect exfoliation. Besides, this method led to the formation of a PET with a very low intrinsic viscosity (IV= 0.55 dL/g).

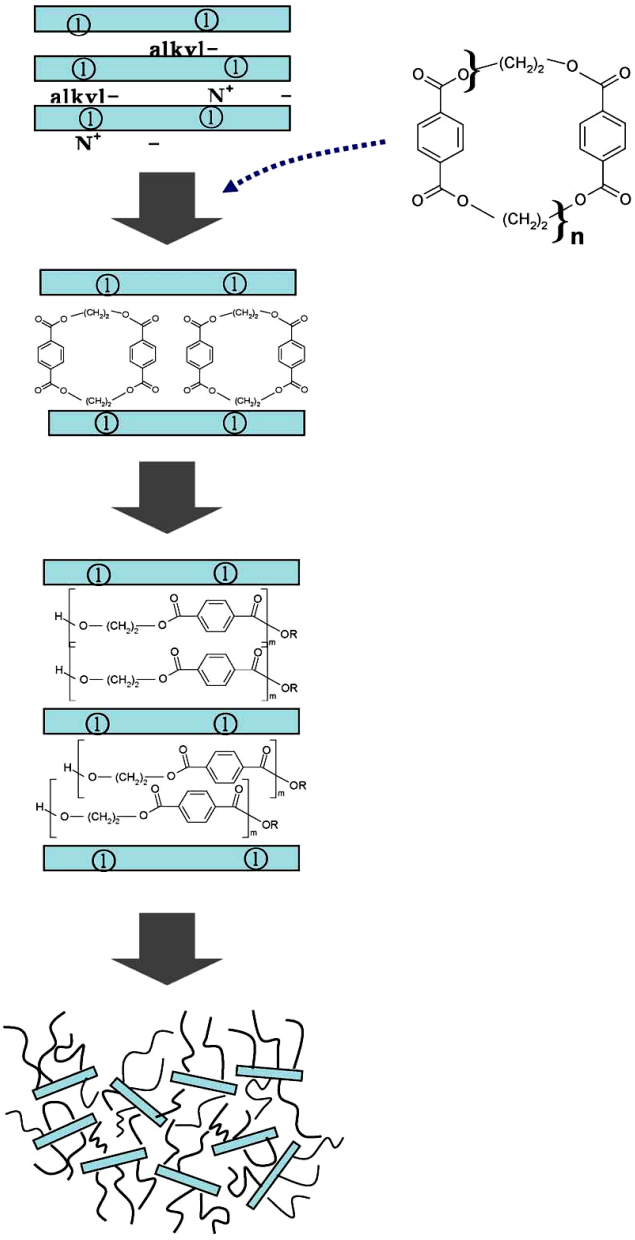

Figure 2-5: Ring-opening polymerization of cyclic oligomers in the interlayer spacing of the organoclay [12].

Melt intercalation involves direct mixing of layered silicates with a molten polymer. It is desirable that molten polymer chains diffuse into the interlayer spacing of the nanolayers and lead to delamination of the nanolayers.

The melt intercalation method has several advantages over the other mentioned methods. First of all, this is an environmental friendly method because there is no need for organic solvents. Second, common industrial processing techniques such as extrusion and injection molding can be

used by this approach. It is a cost effective method and it can be employed for the preparation of nanocomposites of a wide range of polymers, from nonpolar to strongly polar ones. Besides, the high shear forces encountered in polymer processing equipments facilitates the dispersion of the nanoparticles in the molten polymer matrix. Therefore, this method is greener and commercially more viable in comparison with the other approaches.

2.4 Polymer clay nanocomposites

2.4.1 Challenges of matrix degradation

In spite of several advantages of the melt mixing approach, this method may lead to the thermal degradation of commercial organoclays. For example, melt processing and polymerization of PET is performed at high temperatures (250-300 °C), while commercial organoclays degrade below 200 °C [13]. It seems that the thermal stability of organosilicates have a critical role in the resulting nanocomposite morphology, because upon decomposition of the silicate nanolayers organic modifier the interface between the polymer matrix and the silicate nanolayers may change. Moreover the decomposition of the organic modifiers, which leads to the collapse of the silicate nanolayers, results in an interlayer spacing decrease and the intercalation of polymer chains within the gallery spacing becomes more difficult. Color formation, enhanced degradation of the polymer matrix, plasticization effects, and physical properties deterioration may result from the thermal degradation of organoclays during melt intercalation. Therefore, if melt intercalation is chosen for producing polymer clay nanocomposites, the thermal stability of the organic modifiers which are used for the modification of the silicate nanolayers surface should be improved to avoid an anticipated collapse and agglomeration of the organoclays. Beside thermal stability of organosilicates, compatibility of organosilicates with the polymer matrix is another parameter that controls the final morphology and the level of dispersion and delamination of the silicate nanolayers in the produced nanocomposites [14, 15].

Fornes *et al*. [16] prepared Nylon-6 nanocomposites containing various quaternary alkylammonium organoclays using a twin-screw extruder. Molecular weight reduction and color formation was reported for all nanocomposites due to reactions between the matrix chains and the

organoclays. More matrix degradation was reported for the nanocomposites with higher platelet delamination, which was attributed to more exposure of the organoclays to the matrix.

Shah and Paul [17] prepared low density polyethylene nanocomposites containing 5 wt% trimethyl hydrogenated-tallow ammonium montmorillonite, $M_3(HT)_1$, and dimethyl bis(hydrogenated-tallow) ammonium montmorillonite, $M_2(HT)_2$, using a twin-screw extruder. Melt compounding was performed at 150, 165, 180, 200, and 240 °C to study the effect of processing temperature on the degradation of the quaternary ammonium surfactants of the organoclays. Change in the position of XRD peaks was assigned to the platelets collapse induced by mass reduction of the surfactants within the clay galleries. Figure 2-6 shows XRD patterns of polyethylene nanocomposites containing $M_3(HT)_1$ and $M_2(HT)_2$ organoclays. The authors did not present TEM images for direct visualization of the state of the organoclays dispersion and XRD patterns do not show evidence of intercalation.

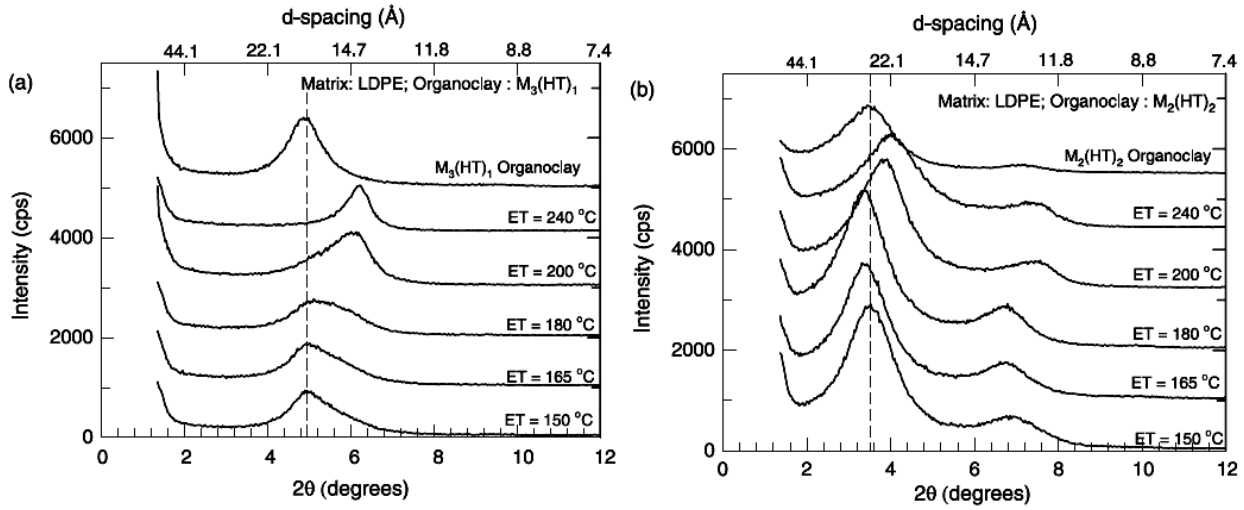

Figure 2-6: XRD patterns of low density polyethylene nanocomposites processed at several extrusion temperatures and containing $M_3(HT)_1$ (a) and $M_2(HT)_2$ (b) organoclays [17].

Polycarbonate nanocomposites were prepared by melt intercalation and the effect of organoclay structure on color formation was examined. Darker colored nanocomposites were obtained for samples containing the organoclay with double bonds in the hydrocarbon tail, in comparison to those with saturated organic modifiers. Presence of both hydroxy-ethyl groups and tallow tails led to the most color change [18].

Color formation and significant reduction of intrinsic viscosity and molecular weight of PET due to melt blending with organoclays has been reported by several researchers [19-30]. Scaffaro and coworkers [20] prepared PET nanocomposite using a twin-screw extruder. Intrinsic viscosity of virgin PET and extruded PET was reported to be 0.83 and 0.82 dL/g, respectively, while PET nanocomposites containing 10 wt% C30B show an intrinsic viscosity of 0.63 dL/g. This remarkable reduction of intrinsic viscosity was attributed to depolymerization of PET induced by the degradation of C30B organic modifier. Hwang *et al*. [27] prepared PET nanocomposites containing Cloisite® 10A (C10A) by *in-situ* polymerization at 285 °C. By incorporating 5 wt% C10A, the intrinsic viscosity of the neat PET reduced from 0.76 to 0.7 dL/g. In another work, PET nanocomposites containing synthetic mica were prepared using a twin-screw extruder at 270 °C. Molecular weight of extruded PET was reported to decrease from 90 100 to 78 500 g/mol due to incorporation of 5 wt% of the organoclay using gel permeation chromatography [22].

Chung and coworkers [31] proposed a novel method for the preparation of PET nanocomposites in the absence of organic modifiers to avoid the thermal decomposition of alkyl ammonium modifiers in silicate layers. For de-intercalation (i.e. removal) of the organic modifiers from the silicate layers a strong acid was used. Lee *et al*. [32] reported that ionic bonds between strong acids and organic modifiers are stronger than bonds between organic modifiers and negatively charged silicate layers. Figure 2-7 presents gallery spacing reduction of dodecylammonium montmorillonite (C_{12}-MMT) treated with various acids as a function of acid concentration.

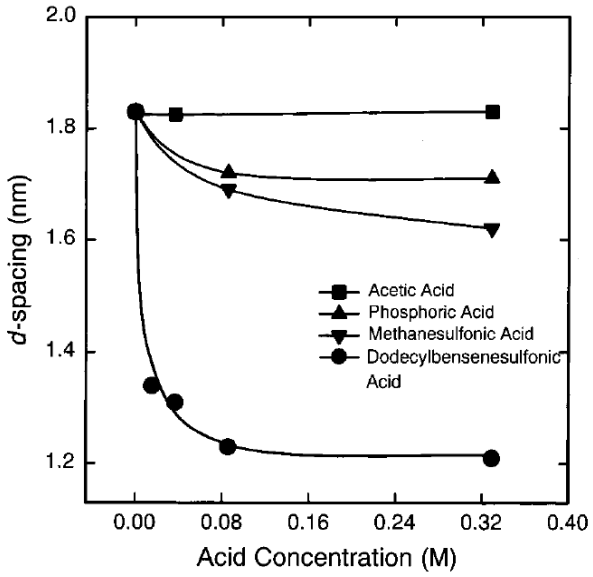

Figure 2-7: Interlayer spacing of C_{12}-MMT treated with different acids [32].

Chung *et al*. [31] employed trifluoroacetic acid (TFA) to remove the ionically attached organic modifiers (polyoxypropylene methyldiethylammonium cations) of the organically modified layered silicates (OLS). OLS were added to chloroform and TFA was poured in this solution. Then neat PET was dissolved in OLS/chloroform/TFA solution. PET/OLS/chloroform/TFA solution was added to cold methanol to obtain PET nanocomposites excluding organic modifier (S-$P_{et}LSN_{eom}$), as shown in Figure 2-8. PET nanocomposites including organic modifier (S-$P_{et}LSN_{iom}$) were prepared by removing solvents from PET/OLS/chloroform/TFA. By melt mixing of neat PET with S-$P_{et}LSN_{eom}$ and S-$P_{et}LSN_{iom}$ in a twin screw extruder (neat PET/S-$P_{et}LSN$ = 1/0.333 weight ratio), M-$P_{et}LSN_{eom}$ and M-$P_{et}LSN_{iom}$ were obtained. Direct melt mixing of OLS with PET (PET/OLS = 1/0.067) denoted by (D-$P_{et}LSN$) was performed for comparing results with this novel approach.

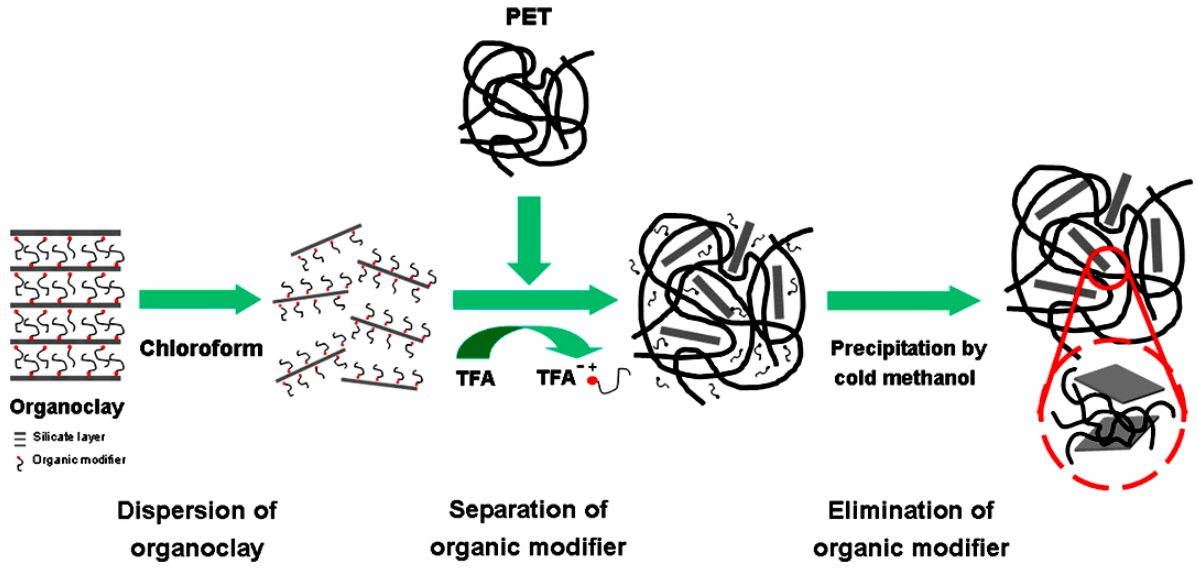

Figure 2-8: Schematic representation of the preparation of exfoliated PET nanocomposites excluding organic modifier (S-Pet-LSNeom) [31].

For characterization of the prepared nanocomposites, both WAXD and TEM techniques were employed. WAXD patterns are shown in Figure 2-9.

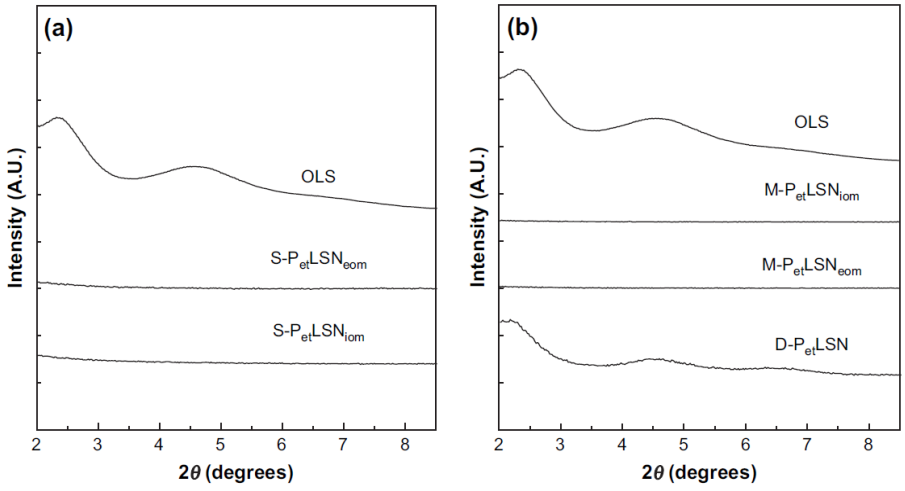

Figure 2-9: WAXD patterns of S-Pet-LSN (a), and M-Pet-LSN (b) [31].

For the OLS two peaks appeared in the WAXD patterns corresponding to 4.4 nm and 2.8 nm of gallery spacing. However, no peak was detected for both S-Pet-LSN and M-Pet-LSN, while two peaks corresponding to the OLS remained unchanged for D-PetLSN, which were attributed to the lack of intercalation of the PET chains into the interlayer spacing of the OLS. Figure 2-10 shows the TEM images of the prepared nanocomposites.

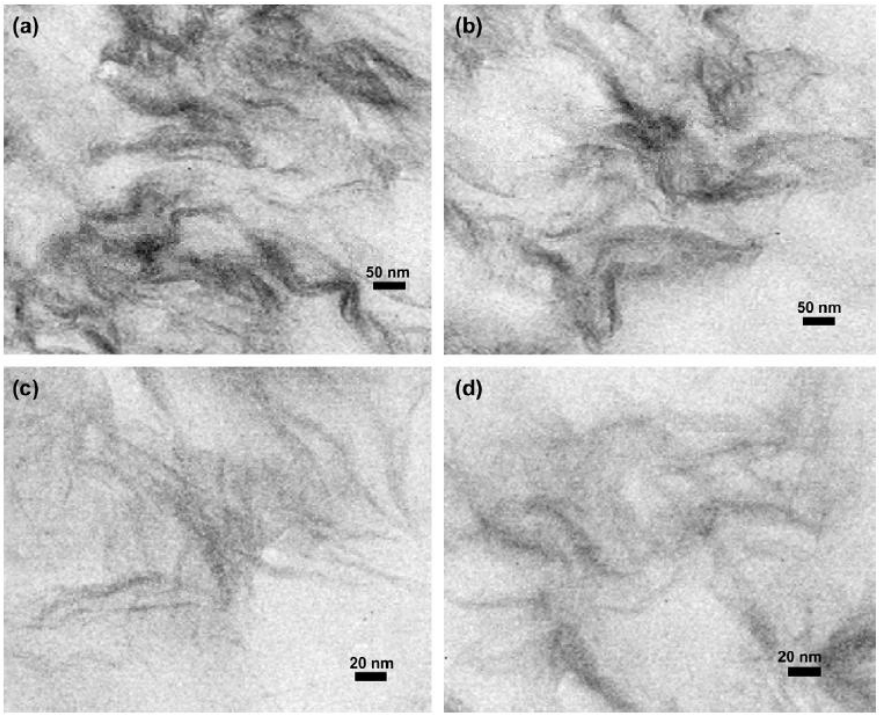

Figure 2-10: Images of S-Pet-LSNeom (a), S-Pet-LSNiom (b), M-Pet-LSNeom (c), and M-Pet-LSNiom (d) [31].

The optical transparency of neat PET film was compared with nanocomposites films, as shown in Figure 2-11 and it was found that M-P$_{et}$-LSN$_{eom}$ and neat PET showed similar transparency, while lower transparency and darker color with slight yellowing was observed for M-P$_{et}$-LSN$_{iom}$ and D-P$_{et}$LSN [31].

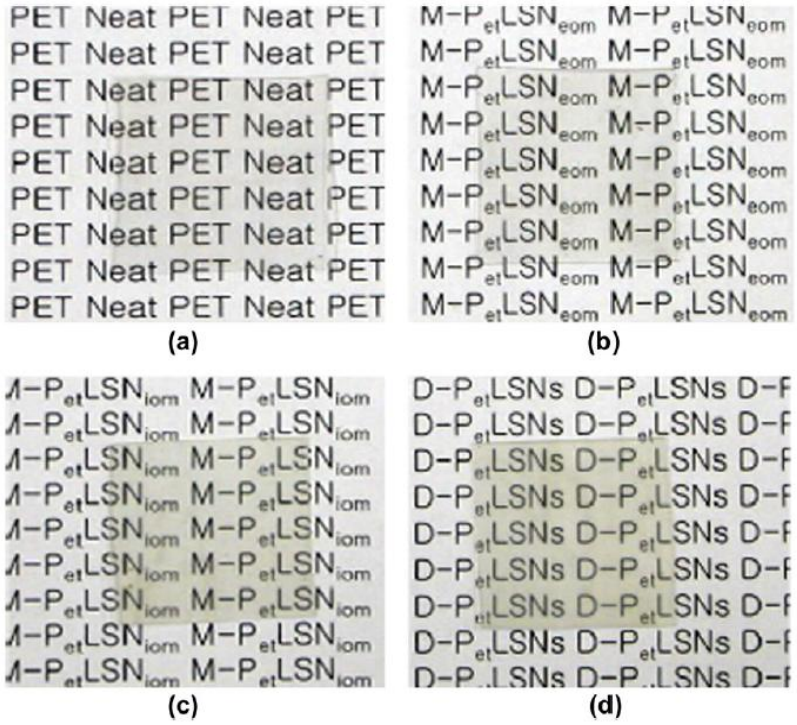

Figure 2-11: Optical aspects of neat PET (a), M-Pet-LSNeom (b), M-Pet-LSNiom (c), and D-PetLSN (d) [31].

Although better optical transparency, thermal stability and enhanced mechanical properties were obtained, this procedure is obviously tedious and not convenient because of the use of solvents.

Another approach to reduce matrix degradation is the purification of the organoclays by removing unbounded halogen impurities. Davis *et al*. [33] treated Na-MMT and synthetic mica (Na-SM) with dimethyl dioctadecyl ammonium bromide (DMDODA-Br). After the ion exchange reaction, both types of organoclays contained ionically bounded DMDODA, unbounded DMDODA-Br, and NaBr by-product. Both NaBr and DMDODA-Br decreased the thermal stability of the produced organosilicates. Therefore, it is desirable to remove these two sources of residual bromide. Ngo and coworkers [34] reported that the onset temperature of degradation of imidazolium cations reduces drastically in the presence of a halide (by about 100 °C). Cui *et al*. [35] have shown that washing organoclays to remove the excess unbounded organic modifier salt improves the thermal stability of the organoclays. Davis and coworker [33] found that thermal stability of organosilicates depends on the employed solvent for removing bromide impurities. Hot water, ethanol, and tetrahydrofuran (THF) were used for washing the organoclays. While hot water washing had no effect on the thermal stability of the organoclays, a 40 °C enhancement in

temperature at 5% mass fraction loss, $T_{5\%}$, was obtained for organoclays that experienced both ethanol and THF extraction. Stoeffler *et al*. [36] purified Cloisite® 20A (C20A) by successive washing with a water/ethanol (1:1) mixture at 70 °C to eliminate the residual chloride anions present in the organoclay. They however only reported a negligible 4 °C improvement in $T_{5\%}$ for the purified C20A.

Modification of silicate layers with highly thermally stable cationic surfactants is another approach to reduce matrix degradation. Quaternary ammonium organic modifiers are cheaper than thermally stable organic modifiers such as imidazoliums [33]. Besides, organoclays based on quaternary ammonium surfactants are already commercialized, which make purification of the alkyl ammonium-modified organoclays more reasonable. However, purification procedures are time consuming and require solvents. Besides, this approach increases the final cost of the commercialized alkyl ammonium-modified organoclays.

Kim *et al*. [13] modified Na-MMT with a thermally stable organic modifier based on dimethyl imidazolium bromide (DMIBr). PET nanocomposites containing 3 wt% of this organoclay were prepared by a melt intercalation approach at 280 °C. PET nanocomposites containing Cloisite® 15A (C15A) and C30B were also prepared for comparison. Thermogravimetric analysis (TGA) measurements were carried out for the organoclays. The onset of decomposition temperature of the imidazolium-based organoclay, C15A, and C30B was reported to be 255, 196, and 174 °C, respectively. TEM images of PET nanocomposites containing the imidazolium-based organoclay are presented in Figure 2-12 at different magnifications. Although imidazolium-based organoclay exhibits better thermal stability over C30B and C15A, the TEM images show an intercalated morphology containing tactoids of several silicate layers rather than an exfoliated structure.

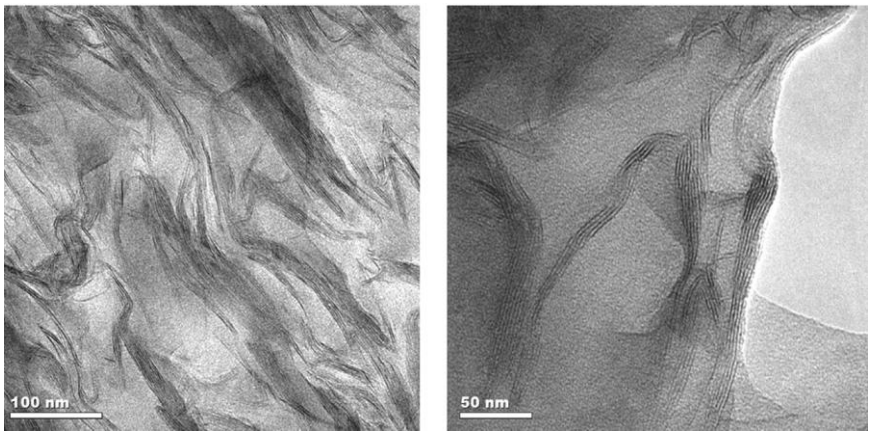

Figure 2-12: TEM images of PET nanocomposites containing imidazolium-based organoclay at various magnifications [13].

Ghasemi *et al*. [37] prepared PET nanocomposites containing C30B, and thermally stable organoclays modified with imidazolium, pyridinium, and phosphonium surfactants using a twin-screw extruder. TGA analysis confirmed that $T_{5\%}$ of the thermally stable organoclays was significantly higher than that of C30B. However, based on XRD results the highest gallery opening (i.e. PET intercalation) was obtained for C30B. Image analysis based on TEM images also confirmed a higher degree of intercalation for the nanocomposites containing C30B.

Stoeffler *et al*. [38] prepared PET nanocomposites containing alkyl phosphonium, alkyl pyridinium, and dialkyl imidazolium-modified montmorillonite using an internal mixer at 280 °C. Based on TEM images, intercalated morphologies with tactoids made of around 4-10 layers were reported for the nanocomposites. The presence of micro-aggregates, observed by optical microscopy, was also reported for all the nanocomposites. PET nanocomposites containing alkyl phosphonium and dialkyl imidazolium-modified montmorillonite exhibited a yellowish/brownish color, and those containing pyridinium-modified montmorillonite presented a dark brown color in comparison to the neat PET matrix.

Na-MMT was modified with thermally stable hexadecyl quinolinium bromide (Q16) and PET nanocomposites were prepared with an inorganic clay loading of 3 wt% using an internal mixer at 280 °C [39]. Figure 2-13 shows XRD patterns of the pristine and modified montmorillonite, as well as PET nanocomposites containing the organoclay. According to the XRD results, modification of Na-MMT with the quinolinium surfactant increases the *d*-spacing from 1.21 nm to 1.73 nm, and after melt blending with PET the gallery spacing reaches 3.15 nm.

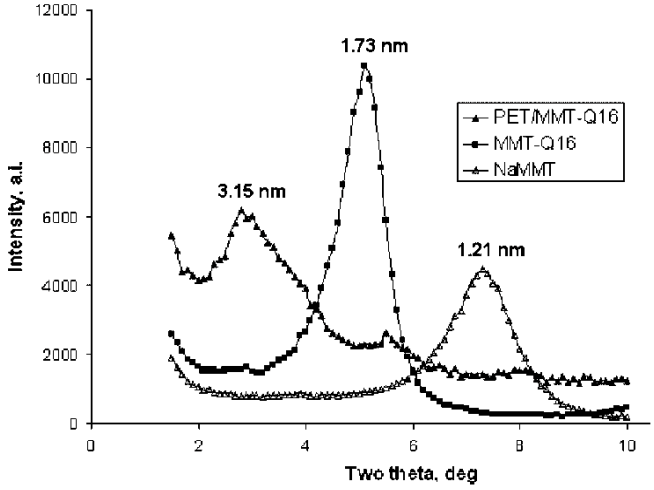

Figure 2-13: XRD patterns of Na-MMT, quinolinium modified montmorillonite (MMT-Q16), and PET nanocomposite containing MMT-Q16 [39].

Low and high magnifications TEM images of the obtained nanocomposites are presented in Figure 2-14. Based on the XRD and TEM results, a mixed morphology including immiscible, intercalated, and exfoliated silicate layer structures was reported [39].

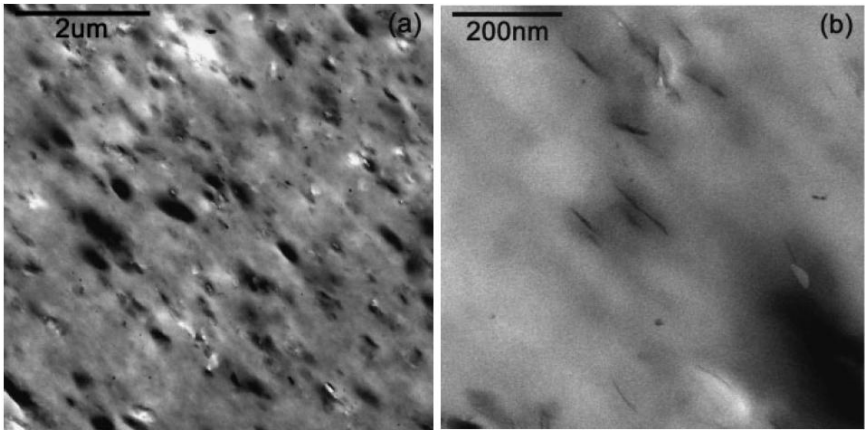

Figure 2-14: Low (a) and high magnification (b) TEM images of PET nanocomposites containing MMT-Q16 [39].

In another study PET nanocomposites containing imidazolium-modified montmorillonite were synthesized by *in-situ* polymerization. XRD and TEM results revealed the coexistence of large aggregates and intercalated silicate layers for the synthesized nanocomposites [19].

2.4.2 Nanocomposites morphology and properties

Food and beverage producers require distributing their products all over the world. This increases the time interval between production and consumption of the products. The shelf life of many

foods and beverages is strongly dependent on their packaging resistance to oxygen, carbon dioxide, and water vapor. Hence, various efforts have been devoted on the improvement of barrier properties of packaging materials. A thin layer of materials with high intrinsic barrier such as aluminum and silicon oxide has been coated on polymer substrates to reduce gas permeability. The level of adherence between the plastic substrate and the coating limits the durability of the coated article. The barrier performance significantly reduces if the interior coating delaminates or the exterior coating scratches off [40, 41].

The permeability of semi-crystalline polymers depends on the degree of crystallinity. Annealing (heat setting) of semi crystalline polymers results in crystal perfection by the reduction of defects and the enhancement of the degree of crystallinity [42]. Crystalline domains are impermeable and a higher degree of crystallinity reduces the volume of polymer available for gas penetration. Besides, impermeable crystals create tortuous path and force gas or liquid molecules to follow longer diffusion pathways within the amorphous phase [43, 44]. Therefore, crystalline domains affect both the solubility and diffusivity of gases in the matrix [45]. The influence of annealing on the degree of crystallinity and oxygen permeability of PET was studied by Perkins [46]. A 33% improvement in barrier properties was reported when crystallinity of the matrix increased from around 25% to 55% [46]. Another study showed that after 20 min annealing at 150 °C, the degree of crystallinity and oxygen barrier properties of PET increased by 7 times and 40%, respectively. However, it was reported that after annealing the sample became completely opaque and white [47]. Another drawback of annealing is brittleness of the product.

Blending with high barrier polymers is another approach to increase barrier properties of polymers like PET or polyolefines [48-50]. Yeo *et al*. [50] prepared a blend of polypropylene (PP)/ethylene-vinyl alcohol copolymer (EVOH) (85/15) using a single-screw extruder. Oxygen permeability of bi-axially stretched PP/EVOH films increased by about 10 times compared to the neat PP. A 19% improvement in oxygen barrier properties of bi-axially stretched PET films blended with 5 wt% poly(*m*-xylene adipamide) MXD6 was also reported [49]. The main problem of this approach is the immiscibility of the components in the blends, which deteriorates properties of the final product such as visual appearance. Besides, bi-axial stretching is essential to deform the droplets of the high barrier dispersed phase into parallel and extended layers to create a tortuous pathway and restrain the diffusion of gas molecules.

Another approach to increase barrier properties is employing high barrier polymers for multilayer containers. The high barrier polymers alone are not used as single material containers because of low physical properties and cost issues [51]. Packaging containers with multilayer structures (3-9 layers) comprised a main constituent polymer (e.g. PET) and high barrier polymer (e.g. EVOH). In contrast to the previous method, the multilayer approach does not cause miscibility and visual appearance problems. However, layer adherence can be a limitation and therefore an adhesive polymer is required to tie or bond the barrier layers to the main constituent polymer. Higher production and material costs is another disadvantageous of this approach. Besides, it is more economical and simpler to recycle a single component plastic than a multilayer container [41, 52, 53].

Introducing impermeable lamellar fillers with high aspect ratio in the polymer matrix is another method to enhance barrier properties [54-59]. A tortuous path is created in the polymer matrix due to the presence of the impermeable silicate layers. The impermeable obstacles force the gas permeant to travel a longer path to penetrate through the film, and consequently the permeability decreases. Permeability is the product of diffusion and solubility. The kinetic aspect of the transport is described by the diffusion coefficient, *D*, and the thermodynamic aspect of the transport is reflected by the solubility coefficient, *S*, which implies the affinity between the polymer matrix and gas molecules. The following equation shows the relationship between the permeability coefficient, *P*, with the solubility and diffusion coefficients:

$$P = DS \tag{1}$$

By ignoring the effect of the filler on the local characteristics of the host polymer matrix, the gas solubility in the nanocomposite is given by the following equation:

$$S_{PCN} = (1-\varphi)S_P \tag{2}$$

where φ is the clay volume fraction, S_{PCN}, and S_P are solubility coefficients of the polymer clay nanocomposite and the neat polymer, respectively. Presence of the silicate layers not only decreases the available area for diffusion of the solutes but, due to the tortuosity, it also reduces the diffusion rate of the nanocomposites according to the following equation:

$$D_{PCN} = \frac{D_P}{\tau} \tag{3}$$

where τ is the tortuosity, D_{PCN}, and D_P are diffusion coefficients of the polymer clay nanocomposite and the neat polymer, respectively. Relative permeability is obtained by combining Eqs. (1) - (3):

$$\frac{P_{PCN}}{P_P} = \frac{1-\varphi}{\tau} \tag{4}$$

where P_{PCN} and P_P are permeability coefficients of the polymer clay nanocomposite and the pure polymer, respectively [60]. Tortuosity must be known in order to predict the permeability of the nanocomposites. There are several models describing tortuosity of the filled systems [61-66]. For example, following model was proposed by Bharadwaj [62] for tortuosity:

$$\tau = 1 + \frac{\alpha\varphi}{2}\cos^2\theta \tag{5}$$

where α is silicate layers aspect ratio and θ is the angle between the direction of penetrate flow and the normal of the layers.

Ghasemi *et al*. [47] prepared PET nanocomposite films containing 3 wt% C30B by cast extrusion. A partially exfoliated/intercalated morphology was reported for the nanocomposite films. In comparison to the neat PET films, oxygen barrier properties and Young modulus of the nanocomposite films exhibited 23% and 20% improvement, respectively. The presence of the silicate nanolayers increased brittleness of the samples and resulted in more hazy films. In another study, they investigated the effect of processing conditions on theproperties of PET nanocomposite films containing C30B [67]. Compared with the neat PET, a 27% reduction in oxygen permeability and a 30% improvement of the tensile modulus was reported for the nanocomposites containing 3 wt% C30B, processed by employing a severe screw profile in terms of mixing and high screw rotational speed [67].

In another study, PET nanocomposites containing C15A were prepared using a twin-screw extruder. A 16% reduction in oxygen permeability was reported for the nanocomposites containing 3 wt% C15A [68].

Various blends of PET and polyamide-6 containing Nanomer® I30TC (N30TC) were prepared by injection molding. Figure 2-15 presents TEM images of a blend containing 20 wt% polyamide-6 and 5 wt% N30TC. The silicate layers are located in the dispersed phase due to a higher affinity between polyamide-6 and the organoclay. Around 14% improvement in the Young modulus was reported for the nanocomposite [69].

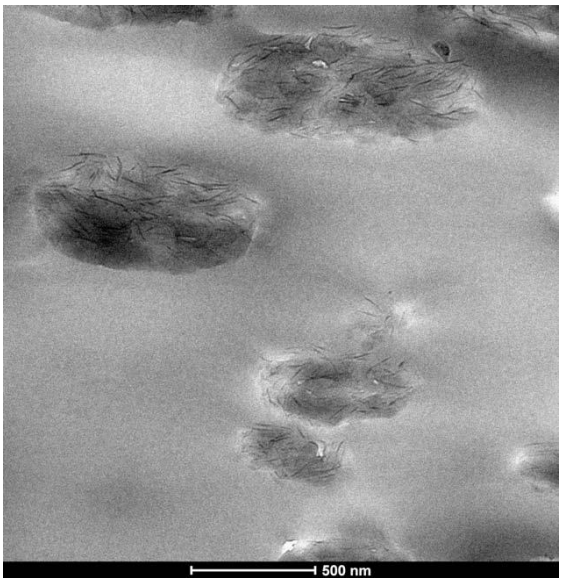

Figure 2-15: TEM images of PET nanocomposites containing 20 wt% polyamide 6 and 5 wt% N30TC [69].

Hwang and coworkers [27] prepared PET nanocomposites containing Na-MMT and C10A by *in-situ* polymerization. Figure 2-16 shows TEM images of the samples containing 2 wt% of the pristine clay and the organoclay.

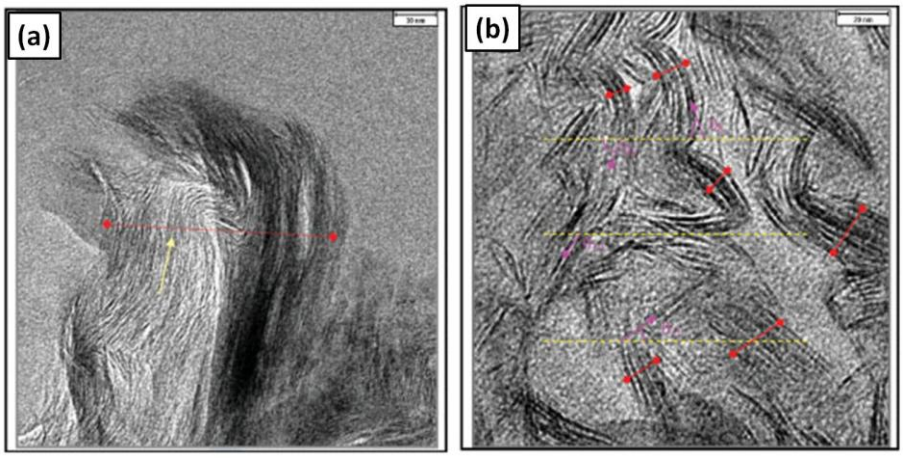

Figure 2-16: TEM images of PET nanocomposites containing 2 wt% Na-MMT (a) and C10A (b) prepared by *in-situ* polymerization [27].

A mostly intercalated morphology was obtained for the nanocomposites containing C10A; however, the pristine clay was not efficiently intercalated with the PET chains. Large aggregates containing an average of 66 platelets per particle were reported for the samples containing Na-MMT. The better morphology obtained for PET nanocomposites containing C10A, in comparison to samples containing Na-MMT, was attributed to the surfactant of the organoclay, which promotes the compatibility between the inorganic clay and the organic PET. Mechanical properties of the nanocomposites are shown in Figure 2-17. Because of extreme brittleness of the samples containing Na-MMT, mechanical properties of the corresponding samples were measured only up to 2 wt% loading. The Young modulus increased with clay concentration for both Na-MMT and C10A-containing samples. Around 35% enhancement in the Young modulus was obtained for the nanocomposites containing 5 wt% C10A. The reduction of elongation at break was attributed to the increased stiffness and formation of microvoids around clay particles during tensile testing.

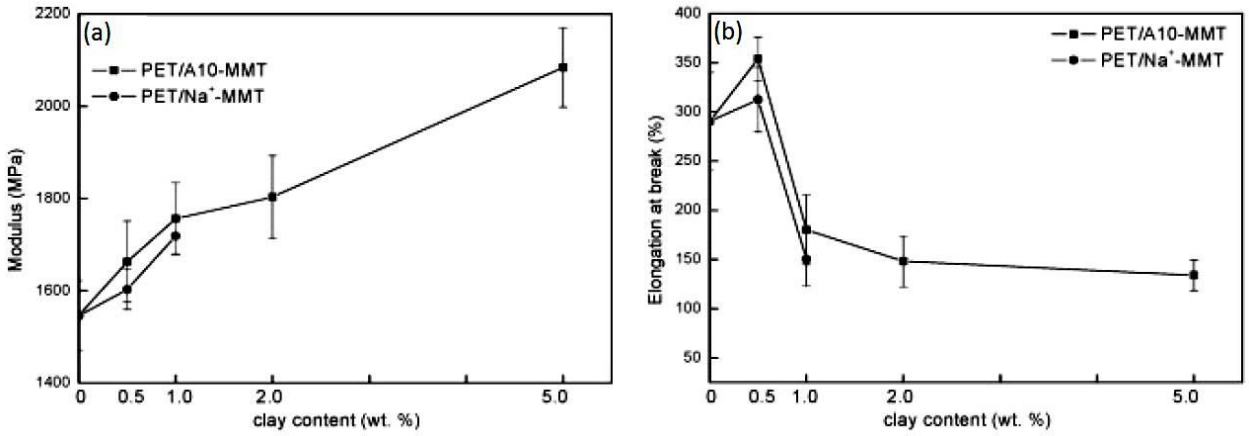

Figure 2-17: Young modulus (a) and elongation at break (b) of samples containing pristine clay and organoclay [27].

A polarizing optical microscope was employed to investigate the crystallization of the neat PET and the clay-containing samples. The samples were held at 200 and 220 °C for 5 min and the spherulite morphologies are presented in Figure 2-18. A well defined spherulite texture is observed for the neat PET, but by increasing the crystallization temperature the Maltese cross disappears. Clay-containing samples exhibit smaller spherulites with more nuclei density as compared to the neat PET [27]. Similar results (i.e. smaller spherulites size and more nuclei) were obtained by other researchers for PET nanocomposites in comparison to neat PET [70, 71].

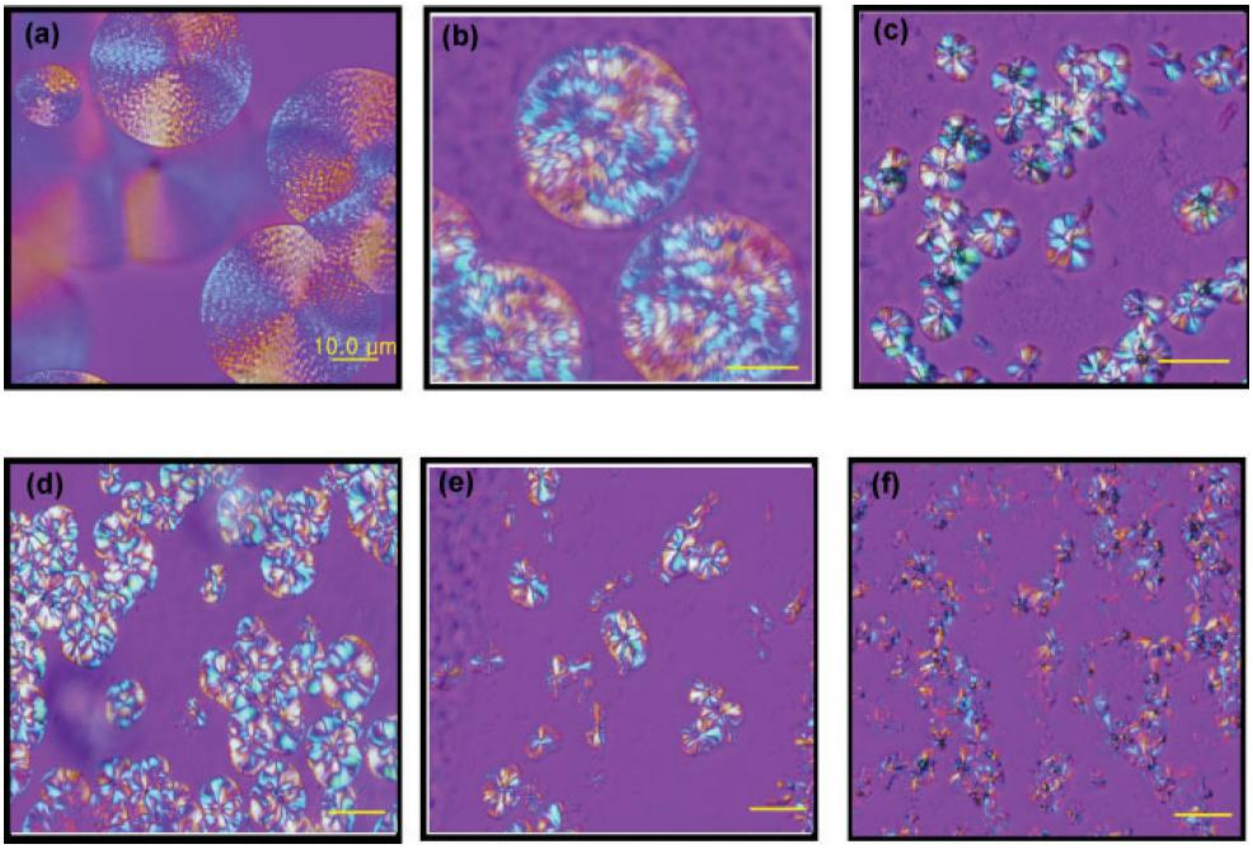

Figure 2-18: Micrographs showing spherulites of the neat PET at 200 °C (a) and 220 °C (b), PET/0.5 wt% Na-MMT (c), PET/2 wt% Na-MMT (d), PET/2 wt% C10A (e), and PET/5 wt% C10A (f) all at 220 °C [27].

PET nanocomposites containing various concentrations of Cloisite® 20A (C20A) were prepared using a twin-screw extruder. The reduction of the cold-crystallization temperature of PET in nanocomposites was attributed to the nucleating effect of C20A. XRD results indicated expansion of the gallery spacing of the organoclay due to intercalation by the PET chains. An inhomogeneous dispersion of the clay particles in the nanocomposites was reported, based on TEM images, and it was attributed to less favorable interactions between C20A and the polymer matrix. TEM images of the prepared nanocomposites with inorganic clay loading equal to 1.3 and 2 wt% are shown in Figure 2-19 [72].

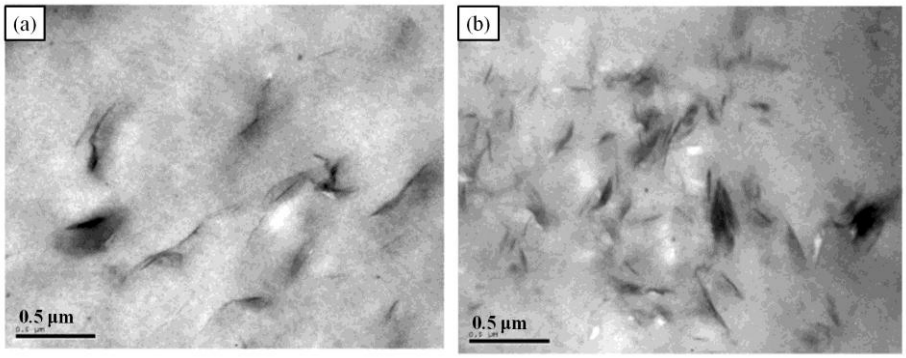

Figure 2-19: TEM images of PET nanocomposites containing C20A with inorganic clay loading equal to 1.3 (a) and 2 wt% (b) [72].

Biaxial stretching was reported to improve exfoliation of silicate layers within a PET matrix [73, 74]. Rajeev *et al*. [74] employed a twin-screw extruder to produce PET nanocomposites containing Somasif® MAE, which is an alkylammonium-modified synthetic clay. Platelets in tactoids slip past each other due to biaxial stretching. As a result, tactoid length and the frequency of single layer and double layer particles are increased. Figure 2-20 exhibit the effect of equi-biaxial stretching with a stretch ratio equal to 3 in both directions on the morphology of nanocomposites containing 2 wt% Somasif® MAE. A 22% reduction in oxygen permeability was reported for the nanocomposites, in comparison to the neat PET [74]. The Young modulus of the samples with various clay loadings and stretch ratios is shown in Figure 2-21. A 10, 20, and 30% improvements in Young modulus were reported for the unstretched samples containing 1, 2, and 5 wt% Somasif® MAE, respectively. By stretching the samples better mechanical properties were obtained, which was attributed to the reduced agglomeration and more tactoid alignment [73].

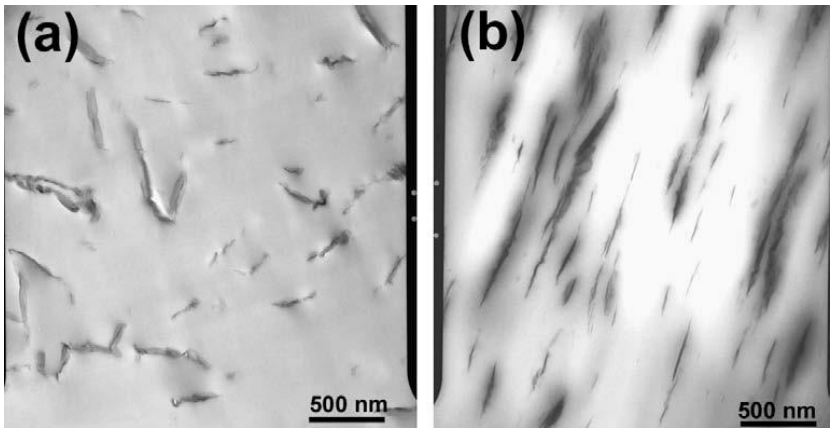

Figure 2-20: TEM images of PET nanocomposites before (a) and after stretching [74].

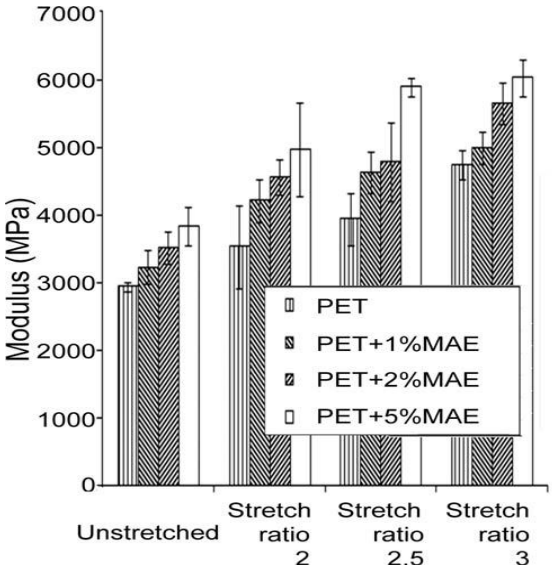

Figure 2-21: Effect of biaxial stretch ratio and clay concentration on the tensile modulus of PET and PET-based nanocomposites [73].

Efforts have also been devoted to improve the compatibility between organoclays and polyesters. Compatibilizers have been considered to improve the morphology of PET nanocomposites. Pentaerythrytol and maleic anhydride were employed to improve the compatibility between silicate nanolayers and PET chains; however, an exfoliated morphology was not achieved [75]. Chisholm and coworkers [76] investigated the effect of sodium sulfonate functionalization of poly(butylene terephthalate) (PBT) on the properties of PBT nanocomposites containing 5 wt% Na-MMT, and an alkylammonium modified montmorillonite. TEM images of PBT and PBT-ionomer samples containing the organoclay and Na-MMT are shown in Figure 2-22. PBT and

PBT-ionomer composites containing Na-MMT exhibit almost the same morphology, while the presence of sulfonated groups in PBT-ionomer/organoclay nanocomposites leads to a significant change in the morphology as compared to the reference PBT/organoclay nanocomposite. Higher exfoliation level obtained for PBT-ionomer/organoclay nanocomposites was attributed to favorable interactions between the positively charged edges of montmorillonite and the negatively charged ionomer. Other researchers also took advantage of strong affinity of negatively charged sulfonic groups of ionomers with the edges of clay nanoparticles to prepare nanocomposites with improved morphology [23, 77-81].

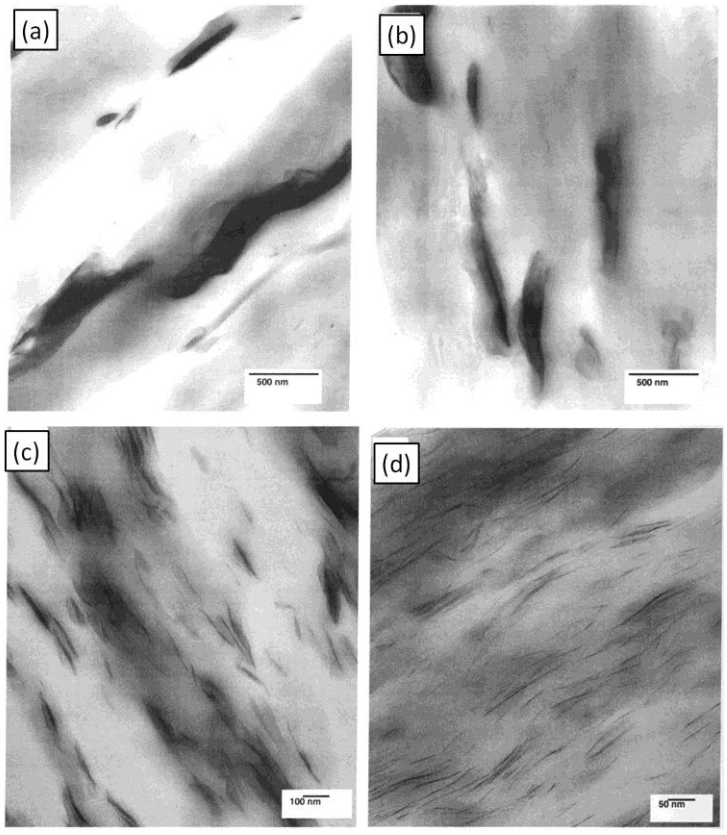

Figure 2-22: TEM images of PBT/Na-MMT (a), PBT-ionomer/Na-MMT (b), PBT/organoclay (c), and PBT-ionomer/organoclay (d) [76].

2.4.3 Rheology of nanocomposites

XRD, SEM, and TEM are widely used for morphological characterization of nanocomposites. Rheology has been used extensively in complement to these techniques in several studies as it is

very sensitive to the morphology of nanocomposites [1, 82-89]. The summary of the most significant results of these studies is the transition from liquid-like to solid-like viscoelastic behavior for nanocomposites, even at low volume fractions of silicate layers, as well as a strong shear-thinning behavior. Solid-like behavior has been attributed to the formation of a percolated network of clay particles which happens at relatively low clay loadings due to the anisotropy of the particles which prevents their free rotation and dissipation of stress.

Aubry *et al*. [86] studied rheological properties of polyamide-12 containing C30B prepared by an internal mixer. The storage modulus as function of frequency and clay volume fraction is shown in Figure 2-23. A low-frequency plateau is observed for the nanocomposites containing more than 1.5% C30B and the storage modulus increases monotonically with clay concentration.

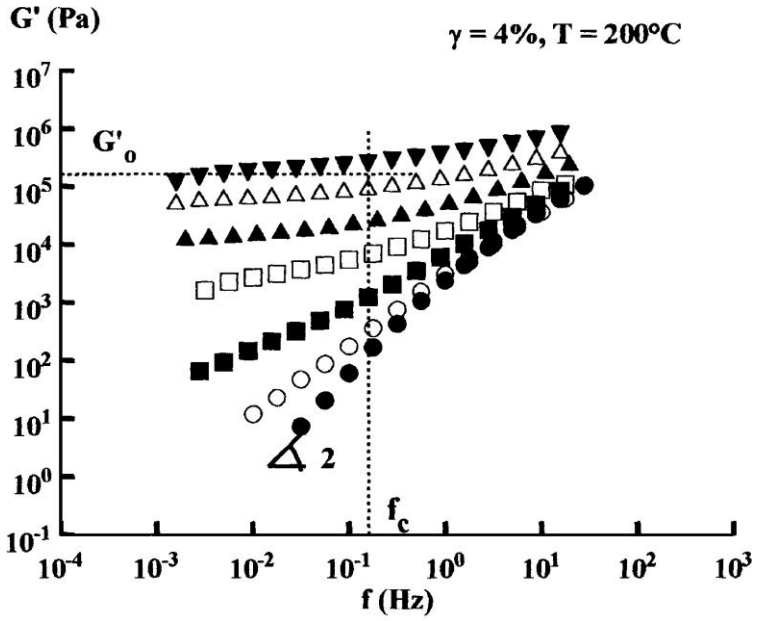

Figure 2-23: Storage modulus vs. frequency for neat polyamide-12 (●), and nanocomposites containing 0.5% (○), 1% (■), 1.5% (□), 2.5% (▲), 5% (Δ), and 10% (▼) C30B [86].

Vermant *et al*. [85] prepared polypropylene (PP) nanocomposites containing Cloisite® 20A (C20A) using a twin-screw extruder at 205 °C. Maleic anhydride grafted PP (PPMA) was employed as a compatibilizer. The prepared master-batch was diluted using a lab scale re-circulating co-rotating extruder to fabricate nanocomposites containing various concentrations of C20A while the C20A/PPMA ratio was kept at 0.67. Figure 2-24 shows the effect of the organoclay volume fraction on the storage modulus of the matrix. In comparison to the neat

samples, larger storage modulus was obtained for the nanocomposites, which increases with clay loading. At high volume fractions clay particles may touch each other, which leads to the formation of a space filling network and appearance of a low frequency plateau.

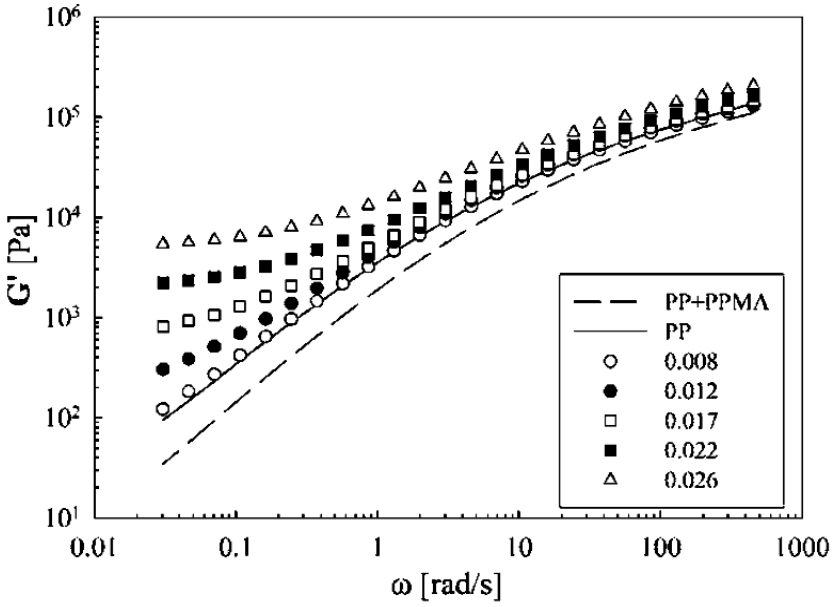

Figure 2-24: The storage modulus as a function of frequency and C20A volume fraction, as indicated in the legend, measured at 220 °C [85].

It has been reported that the empirical Cox-Merz rule is inapplicable in case of nanocomposites [90, 91]. Poly(butylenes succinate-*co*-adipate) (PBSA) nanocomposites containing 6 wt% C30B, C15A, and Cloisite® 93A (C93A) were prepared using an internal mixer [84]. Figure 2-25 exhibit the viscosity of PBSA and the nanocomposites as a function of frequency or shear rate. While the Cox-Merz rule holds for the neat PBSA, the complex viscosity of the nanocomposites is always above their corresponding steady shear viscosity. This was attributed to the alignment of the silicate layers in the flow direction due to steady shear.

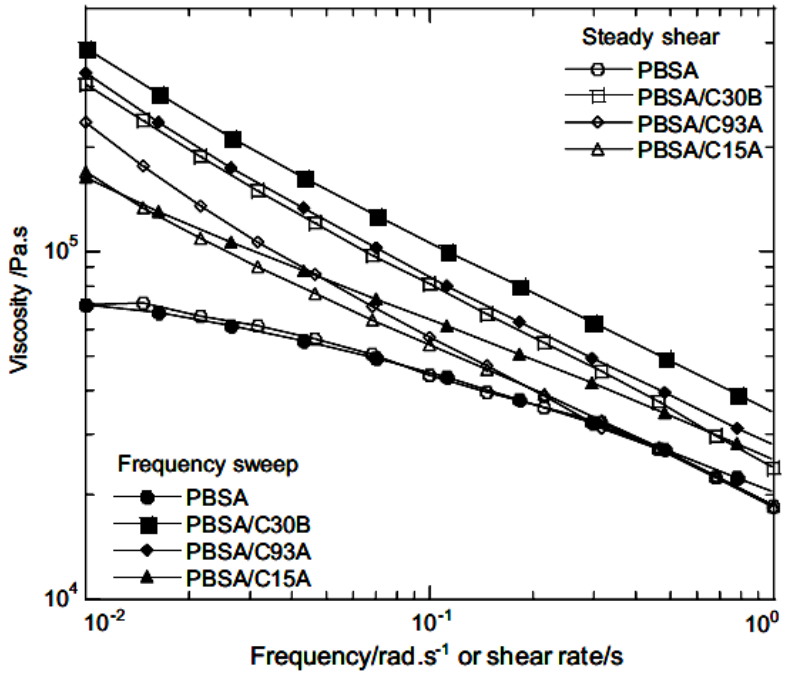

Figure 2-25: Cox-Merz representation of the neat PBSA and the nanocomposites: open symbols, steady shear data; filled symbols, dynamic data [84].

It was demonstrated that the formation of a percolated network increases the viscoelastic properties of nanocomposites significantly. Therefore, a remarkable decrease in the viscoelastic properties is expected if the percolated network is destroyed. Several studies have shown that steady pre-shearing can disrupt internal percolated networks of nanoparticles [92-94]. Wu *et al*. [92] prepared poly(butylene terephthalate) (PBT) nanocomposites containing C10A using an internal mixer. Figure 2-26 shows the effect of steady pre-shearing on the rheological behavior of PBT nanocomposites containing 4 wt% C10A. A significant reduction in the elastic modulus of the pre-sheared sample is observed. Besides, the low-frequency dependence of the elastic modulus is enhanced in the pre-sheared nanocomposites. These were attributed to the preferential orientation of the silicate layers in the shear direction and disruption of the percolation network.

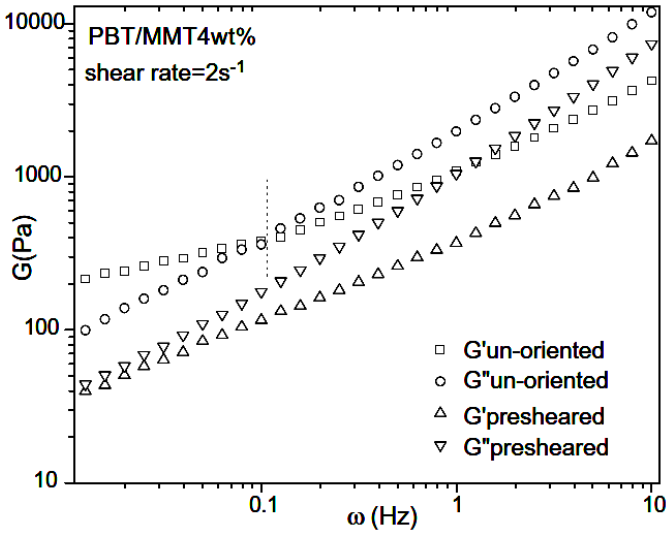

Figure 2-26: Effect of steady pre-shearing on the viscoelastic properties of PBT nanocomposites containing 4 wt% C10A [92].

Li *et al*. [93] studied rheological behavior of PP nanocomposites containing an alkylammonium-modified montmorillonite prepared by an internal mixer. PP nanocomposites containing 6 wt% the organoclay was first sheared at shear rate equal to 0.1 s^{-1} for 5 min. Then, the flow was stopped and after different rest times the sample was sheared in the reverse direction for 5 min at 0.1 s^{-1} and 200 °C. The transient stress response of the sample is shown in Figure 2-27. The magnitude of the stress overshoot depends on the rest time significantly, which was attributed to structural evolution in the sample during the quiescent period.

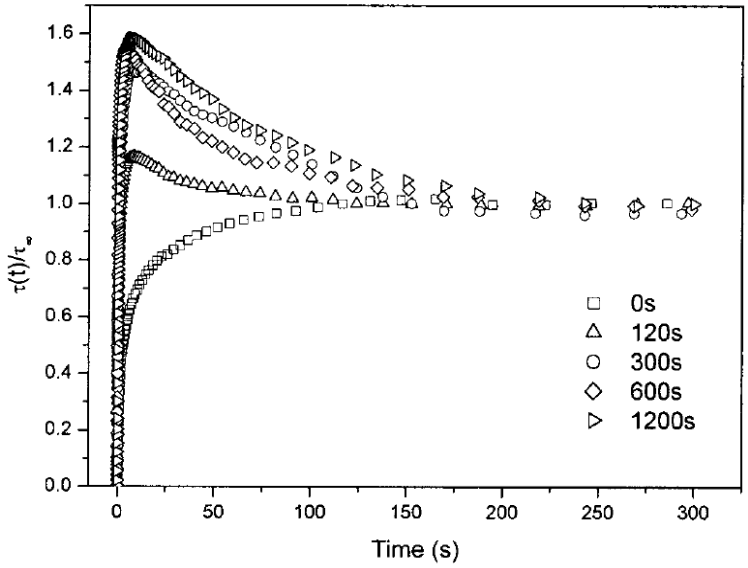

Figure 2-27: The stress response to the startup of steady shear in reverse flow measurements for PP nanocomposites containing 6 wt% the organoclay at 200 °C [93].

2.5 Summary

Many efforts have been made to improve barrier properties of polymers against oxygen, carbon dioxide, and water vapor. One promising approach, which has attracted considerable attention in recent years, is incorporating impermeable silicate layers with high aspect ratio in the polymer matrix. It has been observed that properties of the nanocomposites are influenced by the exfoliation level of the silicate layers, which depends on the compatibility between the host polymer matrix and nanoclay, as well as the employed processing techniques and conditions.

Many studies have been aimed at delaminating silicate layers within a PET matrix. A mostly intercalated morphology was reported for PET nanocomposites prepared by *in-situ* polymerization. Lack of exfoliation may be due to the absence of high shear forces as well as the long time procedure of the technique at high temperatures (e.g. 280 °C), which led to the degradation of the organic modifiers and the polymer matrix. While employing twin-screw extrusion in the melt blending approach provides high shear forces, the degradation of the matrix and organoclays remained unsolved. Purification of the commercial organoclays by removing unbounded halogen impurities led to negligible improvement in thermal stability of the organoclays, and no significant improvement in morphology was obtained. Employing solvents

makes this method even less interesting. PET nanocomposites containing silicate layers modified with thermally stable cationic surfactants exhibit an intercalated morphology containing tactoids of several silicate layers, rather than an exfoliated structure. In addition, several studies reported severe matrix degradation by incorporating organoclays. In summary the preparation of PET nanocomposites with exfoliated morphology and good barrier properties remain challenging, and novel approaches need to be undertaken to improve these materials.

CHAPTER 3
OBJECTIVES

Taking into account the significant demands in the packaging industry for single layer containers with high barrier and mechanical properties, and considering the various drawbacks of previous approaches to improve barrier properties of PET to fabricate food and beverage containers, the main objective of this study is:

"To improve barrier properties of PET by incorporating silicate layers via melt compounding"

To meet this objective, PET nanocomposite films containing different organoclays are prepared by cast extrusion. A PET-ionomer is employed to improve exfoliation of the organoclays, and its effect on morphology and properties of the nanocomposites is examined.

Subsequently, PET nanocomposites containing various organoclays and pristine synthetic clay are prepared and the effects of clay loading and organic modifier on the morphology and rheology of PET nanocomposites are investigated. By changing screw configuration the effect of processing conditions on the morphology and rheology of the nanocomposites are studied as well.

Finally, to control the thermal degradation of the matrix induced by the presence of the organoclays, a multi-functional epoxy-based chain extender is employed to rebuild the molecular weight and viscoelastic properties. The effects of the chain extender on the morphology and various properties (e.g. optical, thermal, barrier, mechanical, and rheological properties) of the nanocomposites are examined.

CHAPTER 4
ORGANIZATION OF THE ARTICLES

The following three chapters comprise the articles containing the main results of this study.

Chapter 5 presents the first article entitled "*Morphology and properties of polymer organoclay nanocomposites based on PET and sulfopolyester blends*". In this work, PET nanocomposite films containing C30B and N28E were prepared by extrusion casting. A PET-ionomer was employed to increase basal spacing of the organoclays and enhance exfoliation level of the nanocomposites. Scanning electron microscopy (SEM) and transmission electron microscopy (TEM) revealed that PET and PET-ionomer are immiscible and silicate layers are preferentially localized in the more polar PET-ionomer phase. Although homogeneous distribution of silicate layers in the nanocomposites is restricted due to their migration into the PET-ionomer domains, x-ray diffraction (XRD), TEM, and rheological results show that the presence of the PET-ionomer improved the exfoliation level of N28E. A 25% improvement in oxygen barrier properties was obtained for the nanocomposites containing 2 wt% C30B. This paper has been accepted by *Polymer International*.

Chapter 6 presents the second article entitled "*Morphological and rheological properties of PET/clay nanocomposites*". This work investigates the role of clay chemistry and concentration on the morphological and viscoelastic properties of the nanocomposites. A twin-screw extruder was used and the effect of screw configuration was examined on the rheology and morphology of the nanocomposites. The neat PET displays a Newtonian-like behavior while the complex viscosity of PET nanocomposites exhibits shear-thinning, which becomes stronger with clay loading. A pseudo-solid like behavior due to the formation of a network-like structure was observed for the nanocomposites at high clay concentrations and low frequencies. The highest degree of intercalation was obtained for C30B and the corresponding nanocomposites exhibit the largest values of the complex viscosity and storage modulus. It is worth noting that the solubility parameter of PET is closer to that of C30B than the other organoclays. The matrix degradation due to the presence of the organoclays was estimated using the Maron-Pierce equation and high frequency data. The apparent molecular weight of the PET matrix was found to decrease from 65

kg/mol for the neat PET to 29.8 kg/mol for the PET nanocomposites containing 8 wt % C30B. This work has been submitted in June 2012 to *Rheologica Acta*.

Finally, Chapter 7 presents the third article entitled "*Influence of chain extension on the morphology and properties of PET nanocomposites*". According to the rheological results of the second article, the PET matrix undergoes a remarkable degradation in the presence of the organoclays. Hence, in the third phase of this project a multifunctional chain extender, Joncryl® ADR-4368F (Joncryl), was added to the nanocomposites via a master-batch approach. XRD and TEM were used for morphological characterization and it was found that the presence of the chain extender improves the level of exfoliation. The complex viscosity and storage modulus of the nanocomposites increased significantly by incorporation of the chain extender, which is attributed to the reactions between functional groups of Joncryl and PET end groups. PET nanocomposites containing Joncryl exhibit higher barrier and mechanical properties. A 46% and 40% improvement in barrier properties were obtained for the nanocomposite films containing Joncryl and 4 wt% C30B and N28E, respectively. PET nanocomposite films containing N28E and Joncryl exhibit 66% improvement in the Young modulus, slightly more than the corresponding C30B nanocomposites. Compared to the neat PET, larger crystallinity and lower cold-crystallization temperature were obtained for the nanocomposites due to the nucleation effect of the silicate layers. This article has been submitted in August 2012 to *Polymer*.

CHAPTER 5

MORPHOLOGY AND PROPERTIES OF POLYMER ORGANOCLAY NANOCOMPOSITES BASED ON PET AND SULFOPOLYESTER BLENDS

A. Ghanbari[a], M.C. Heuzey[a], P.J. Carreau[a], M.T. Ton-That[b]

[a] *Center for Applied Research on Polymers and Composites (CREPEC), Chemical Engineering Department, Ecole Polytechnique de Montreal, PO Box 6079, Stn Centre-Ville, Montreal, QC, Canada H3C 3A7*

[b] *Automotive Portfolio, National Research Council Canada, 75 Mortagne Blvd, Boucherville, QC, Canada J4B 6Y4*

This work was accepted by *Polymer International* and was presented at Polymer Processing Society (PPS), Niagara Falls, Canada (2012)

5.1 Abstract

Poly(ethylene terephthalate) (PET) nanocomposite films containing two different organoclays, Cloisite 30B® (C30B) and Nanomer I.28E® (N28E), were prepared by melt blending. In order to increase the gallery spacing of the clay particles, a sulfopolyester (PET-ionomer or PETi) was added to the nanocomposites via a master-batch approach. The morphological, thermal and gas barrier characteristics of nanocomposite films were studied using several characterization techniques such as scanning electron microscopy (SEM), transmission electron microscopy (TEM), x-ray diffraction (XRD), differential scanning calorimeter (DSC), dynamic mechanical analysis (DMA), rheometry and oxygen permeability. The PET and PETi were found to form immiscible polymer blends and the nanoparticles were preferably located in the PETi dispersed phase. A better dispersion of clay was obtained for nanocomposites containing N28E with PETi. On the contrary, for nanocomposites containing C30B and PETi the number of tactoids increased and the clay distribution and dispersion became worse than for C30B alone. Overall, the best properties were obtained for the PET/C30B nanocomposite without PETi. Higher crystallinity was found for all nanocomposite films in comparison to that of the neat PET.

Keywords*:* Poly(ethylene terephthalate); nanocomposite; organoclay; rheology, ionomer.

5.2 Introduction

Nowadays PET is one of the most widely used engineering polymers due to its good processability, high transparency, mechanical and gas barrier properties, as well as chemical resistance and low cost. This semi-crystalline thermoplastic has found wide applications in the form of fibers and non-fibers (such as food and beverage packaging, automotive, electrical devices and construction). For some applications it is desirable to increase specific characteristics

such as barrier properties for beverage and food packaging. Incorporation of silicate nanolayers into a PET matrix has been demonstrated to enhance various physical properties.[1,2]

Large efforts have been devoted to achieve well dispersed and delaminated silicate nanolayers in a PET matrix. In most studies, the coexistence of a PET microcomposite along with an intercalated structure has been observed.[3-7] The processing temperature of PET is around 260 ºC while commercial organoclays start degrading around 200 ºC. The decomposition of the organic modifier leads to a collapse of the silicate nanolayers and to a decrease of the interlayer spacing, thus impedes the intercalation of polymer chains within the gallery spacing. Moreover, the lack of a delaminated or exfoliated morphology in PET nanocomposites is often due to the lack of compatibility of the organic modifiers used in commercial organoclays with the PET macromolecules. For these reasons, several studies have been performed to modify silicate nanolayers with various cationic surfactants[6,8-10], mostly aimed at improving the thermal stability of commercial organoclays. Efforts have also been devoted to improve the compatibility between the organoclay and polyesters. Chisholm and coworkers[11] have synthesized sulfonated poly(butylene terephthalate) copolymers (PBT-ionomers) by the melt polymerization of dimethyl terephthalate, dimethyl-5-sodiosulfoisophthalate, and 1,4-butanediol. They found that the incorporation of 5% mol. of -SO_3Na groups into PBT had no significant effect on the morphology of composites containing pristine clay (i.e. Na-MMT). However, the presence of sulfonated groups in PBT-ionomer/organoclay nanocomposites led to a dramatic change in the morphology, in comparison to the reference PBT/organoclay nanocomposites. It was suggested that the better intercalated and delaminated morphology obtained in the presence of sulfonated groups was attributed to the binding of these negatively charged groups to the edges of the clay

platelets that bear positive charges. This attachment could facilitate the diffusion of mobile polymer chain segments into the gallery spacing of the organoclay. Improvements on the processing and formulation sides have also been considered. Ghasemi et al.[12] prepared nanocomposites containing 3 wt% C30B using a PET experimental grade of high viscosity (Selar PTX 295, Dupont) blended with a commercial grade PET (9921, Eastman Chemical Company) at a ratio of 1:4. They studied the effect of feeding rate and screw speed using two screw geometries with different mixing elements. For the best case (higher screw speed), 27% reduction in oxygen permeability was achieved. In another study, Xu and coworkers[13] prepared nanocomposites containing 2 wt% N28E and 6 wt% PETi using the same experimental grade high viscosity PET (Selar PTX 295, Dupont). The best improvement of the barrier properties achieved via their procedure was 19%.

In this work a commercial sulfopolyester (PET-ionomer, or PETi) is used to improve the compatibility between a PET matrix and two different organoclays. Formulation and compounding are entirely based on a melt processing approach. In the current work a thorough investigation of the state of miscibility between PET and PETi is carried out. Furthermore we show that the dispersion and delamination of the clay are dependent on the organo-modifier chemistry. The interactions between the clays and the ionomer are studied through rheological measurements in order to explain the resulting morphologies.

5.3 Experimental

5.3.1 Materials

A commercial grade PET (PET 9921), with intrinsic viscosity of 0.8 dL/g, was obtained from Eastman Chemical Company. The PET ionomer, PETi AQ55S, with an ionic content of 9 mol%, and inherent viscosity of ~ 0.3 dL/g, was also kindly supplied by Eastman Chemical Company. The chemical formula of the PETi is shown in Figure 5-1. The organically modified montmorillonites, Cloisite 30B® (C30B) and Nanomer I.28E® (N28E), were obtained from Southern Clay Products Inc. and Nanocor Inc., respectively. C30B is modified with methyl, tallow, bis-2-hydroxyethyl, quaternary ammonium (MT2EtOH), while N28E is modified with octadecyl ammonium (ODA) according to R&D of Nanocor Inc. It has also been proposed that the Nanomer and Cloisite montorillonites do not have the same origin, since they contain different amounts of Fe^{3+}.[14]

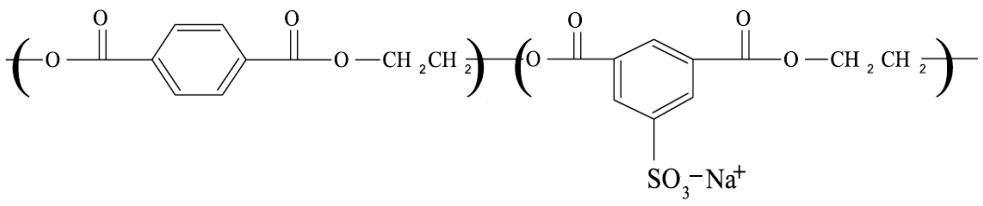

Figure 5-1: Repeat unit of the PET-ionomer. The ionic comonomer is randomly incorporated within the structure.15

5.3.2 Samples preparation

The PET, PETi, and the organoclays were vacuum dried at 80 ºC for 24 h before processing. For all blends the organoclay nominal content was 2 wt% of the total mass, while the amount of the PETi was 6 wt% in the nanocomposites containing the compatibilizer. The nanocomposites

containing PETi were prepared by a master-batch approach: 25 wt% PETi, 8.3 wt% clay, and 66.7 wt% PET were melt blended using a small co-rotating twin-screw Leistritz extruder (screw diameter = 18 mm and L/D = 40). Then the prepared master-batch was diluted with the neat PET using a larger Leistritz extruder (screw diameter = 34 mm and L/D = 42). Figure 5-2 shows the larger extruder screw geometry. The first and third mixing zones contained 10 and 15 kneading elements, respectively, with 7.5 mm width kneading lobes with right hand (positive) and left hand (negative) 60º staggering angles. The second mixing zone was composed of two left and right-handed gear type mixing elements. There were 8 tooths around each circumference and 5 gears in each block, while the total length of the mixing block was 30 mm. The screw speed and feed rate were kept at 200 rpm and 3 kg/h, respectively. The extrusion temperature profile from the feed to the die was set between 240 and 265 ºC. Table 5-1 shows the nanocomposite compositions and nomenclature.

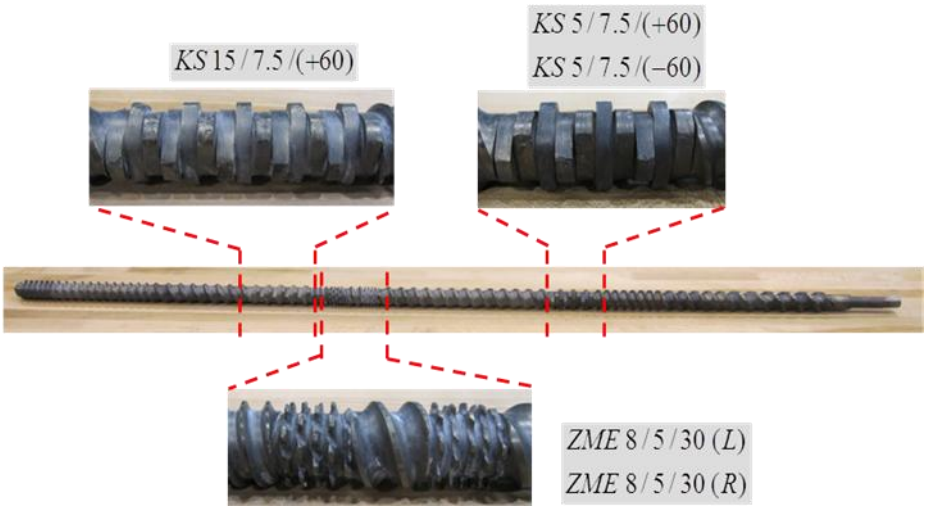

Figure 5-2: Screw geometry of the Leistritz 34 mm twin-screw extruder.

To prepare the PET-based films, a 20 cm wide slit die with a 1.42 mm die gap was used. An air knife was mounted on both sides of the die. To stretch the extrudate, chill rolls (20 ºC) were employed and the distance between the die and the chill rolls was approximately 10 cm. The width of the films was 16 cm and the average neck-in due to stretching was 20%. The draw ratio was around 44 and the corresponding thickness of the films was 40 µm.

Table 5-1: Nomenclature and compositions of the nanocomposite films.

Nomenclature	**PET wt%**	**PETi wt%**	**C30B wt%**	**N28E wt%**
Neat PET	100	0	0	0
PET/PETi	94	6	0	0
PET/C30B	98	0	2	0
PET/PETi/C30B	92	6	2	0
PET/N28E	98	0	0	2
PET/PETi/ N28E	92	6	0	2

Finally, to investigate the miscibility between PET and PETi, several PET/PETi blends containing 0, 10, 20, 30, 50, 70 and 100 wt% PETi were prepared using a 30 mL Plasti-Corder internal mixer (Brabender). Melt compounding was performed at 260 ºC and 100 rpm for 10 min under dry nitrogen. Also, PET/PETi blends containing 6 and 20 wt% PETi and 2 wt% C30B were

prepared using the same instrument and conditions (except at 250 ºC) to detect preferential localization of clay particles.

5.3.2 Characterization of the polymer blends and nanocomposites

DMA was carried out on a TA Instruments DMA 2980 from 40 to 120 ºC at a heating rate of 5 ºC/min and frequency of 1 Hz. Rectangular-shaped samples were prepared via compression molding in a hot press at 265 ºC for 9 min under a nitrogen atmosphere, followed by quenching using a cold press for 5 min. The curves of tan δ as a function of temperature were analyzed to obtain the glass transition temperature, T_g, of the PET/PETi blends.

XRD patterns were obtained using a Bruker D8 Discover with Cu K_α radiation operating at an incident X-ray wavelength λ = 0.15406 nm and a scan rate of 0.6 º/min. The spectra were recorded over the 2θ range of 0.8 -10 º.

The level of clay distribution and dispersion were determined using SEM and TEM at the micro- and nano-level, respectively. SEM observations were carried out using a cold Field Emission Gun SEM (FEG-SEM), Hitachi S4700, with an operation voltage of 2 kV. All the specimens were prepared by employing an Ultracut FC microtome (LEICA) with a diamond knife followed by coating with Pt vapor. TEM images were obtained using a JEOL JEM 2100F microscope operating at 200 kV. The samples were ultramicrotomed into ultrathin slices of about 50-80 nm thickness at Cryo temperature (i.e. -100° C) using the aforementioned microtome system. To determine if PET and PETi were miscible, PET/PETi samples of different compositions were

etched in deionized hot water to selectively extract the PETi domains prior to SEM characterization.

The thermal behavior of the nanocomposites was analyzed using a DSC TA Instruments Q1000. All the measurements were performed under a helium atmosphere. The samples were heated from room temperature to 300 ºC and held at that temperature for 3 min, then cooled to 30 ºC and heated again to 300 ºC at a constant rate of 10 ºC/min.

Molten state rheological measurements were performed using a strain-controlled rotational rheometer Advanced Rheometric Expansion System (ARES, TA Instruments) and a stress-controlled Bohlin Gemini, both with a parallel plate flow geometry (25 mm diameter, 1 mm gap). Dynamic linear frequency sweeps were carried out for the neat PET and PET-based nanocomposites at 265 ºC under a nitrogen atmosphere. The time for the measurements was restricted to 5 min to avoid a severe change of the molecular weight of the samples.

Finally, to determine oxygen transmission rates (OTRs), an OX-Tran model 2/21 apparatus (Mocon Inc.) with an oxygen permeability MD module was employed. All measurements were performed at 23 ºC under a pressure of 690 mmHg (0.91 atm) of 100% dry oxygen. The permeability coefficient [*P*, in L/(m.day.atm)] was obtained from the OTR values using the following formula:

$$P = \mathrm{OTR} \times L/p \tag{5-1}$$

where L is the film thickness (m) and p is the testing pressure (atm).

5.4 Results and discussion

5.4.1 Investigation of PET and PETi miscibility

The compounding of two polymers may lead to miscible, partially miscible and immiscible blends.[16] In the scientific literature[16-18], a single glass transition temperature T_g for a polymer blend is generally recognized as a sign of miscibility (where the size of the domains is below 15 nm), while a blend is qualified as immiscible if it exhibits two or more T_gs at a given composition. To use the T_g approach, the content of each component in the blend should be more than 10 wt%, and their T_gs should differ by at least 10 ºC. The melting point depression of a semi-crystalline polymer in the presence of an amorphous polymer is also used to examine the miscibility of a blend. Based on this method, a blend is considered miscible if the melting point T_m decreases with composition, while a constant T_m is a characteristic of immiscible polymer blends.[17,18] There are, however, several publications reporting that these two methods may lead to contradictory results regarding the miscibility state of a blend.[17,19-21] For example, for a blend exhibiting two T_gs, a melting point depression was observed[20], and a single T_g with no melting point depression has been reported as well.[21] On the basis of the above observations, it seems that a conclusion on the miscibility of two polymers based on the T_g and melting point depression may be uncertain. In this work, the miscibility between PET and PETi was investigated by the former two methods, as well as via a selective solvent dissolution technique followed by SEM.

DMA data for the neat PET, neat PETi and their blends (70-30, 50-50 and 30-70 wt%) are reported in Figure 5-3 in terms of the loss tangent (tan δ). The T_g of the neat PET and neat PETi

are 88.1 and 73 ^{o}C, respectively. A single T_g is observed for all blends, and this value is composition dependent, suggesting miscibility of the two polymers. DSC data are shown in Figure 5-4, illustrating the melting behavior of PET in the presence of the amorphous PETi. The melting point drops monotonically with increasing PETi content: however, at the largest PETi concentration (70 wt%), the melting peak disappears completely. It seems that a less stable crystalline phase, which melts at lower temperature, is formed in the presence of PETi. The observation of a single T_g for all blend compositions (Figure 5-3) along with the melting point depression shown in Figure 5-4 strongly suggest miscibility of the two polymers. However, after further investigation by solvent extraction, the blends showed phase separated domains as illustrated in the SEM micrographs of Figure 5-5 for PET/PETi blends containing various amounts of PETi. Separated droplet-like domains, of the order of several hundreds of nanometer to microns, are observed, indicating the non-miscibility of PET and PETi at this scale. In blends containing 50 wt% PETi a co-continuous structure is generated during the phase separation process, while in blends containing 20 and 30 wt% PETi phase separation leads to a droplet-matrix type of morphology. As expected, droplets are larger for blends containing 30 wt% PETi in comparison to those containing 20 wt% PETi. To explain the apparent contradiction between the DMA and SEM results, it is necessary to have a closer look at Figure 5-3. The broad peak associated to the pure PETi in the DMA data suggests that it may be a two-phase system itself, with separation of the ionic copolymer (with the sulfonated groups in Figure 5-1) from the PET homopolymer in PETi. Hence, there may be the possibility that the phase-separated portion of PETi interferes with the crystallization of the other PET in the blends, leading to the melting point depression observed in Figure 5-4.

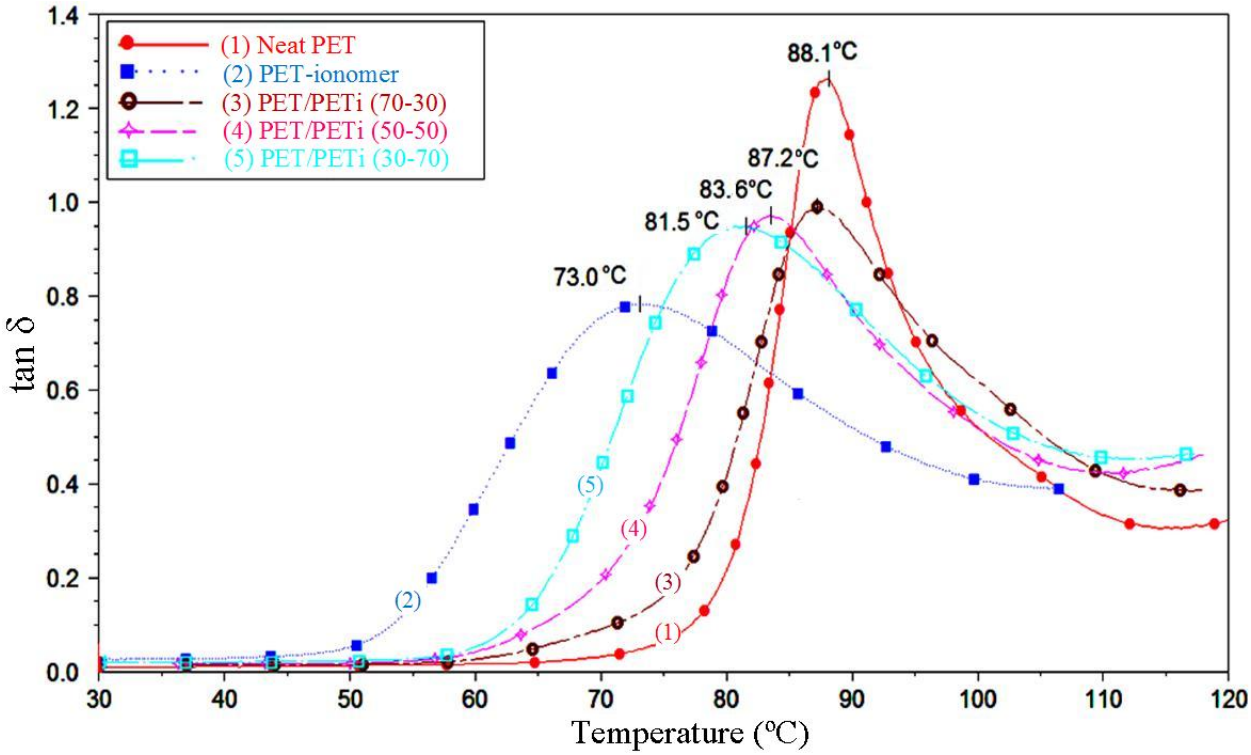

Figure 5-3: Tan δ vs. temperature for several blend compositions of PET and PETi.

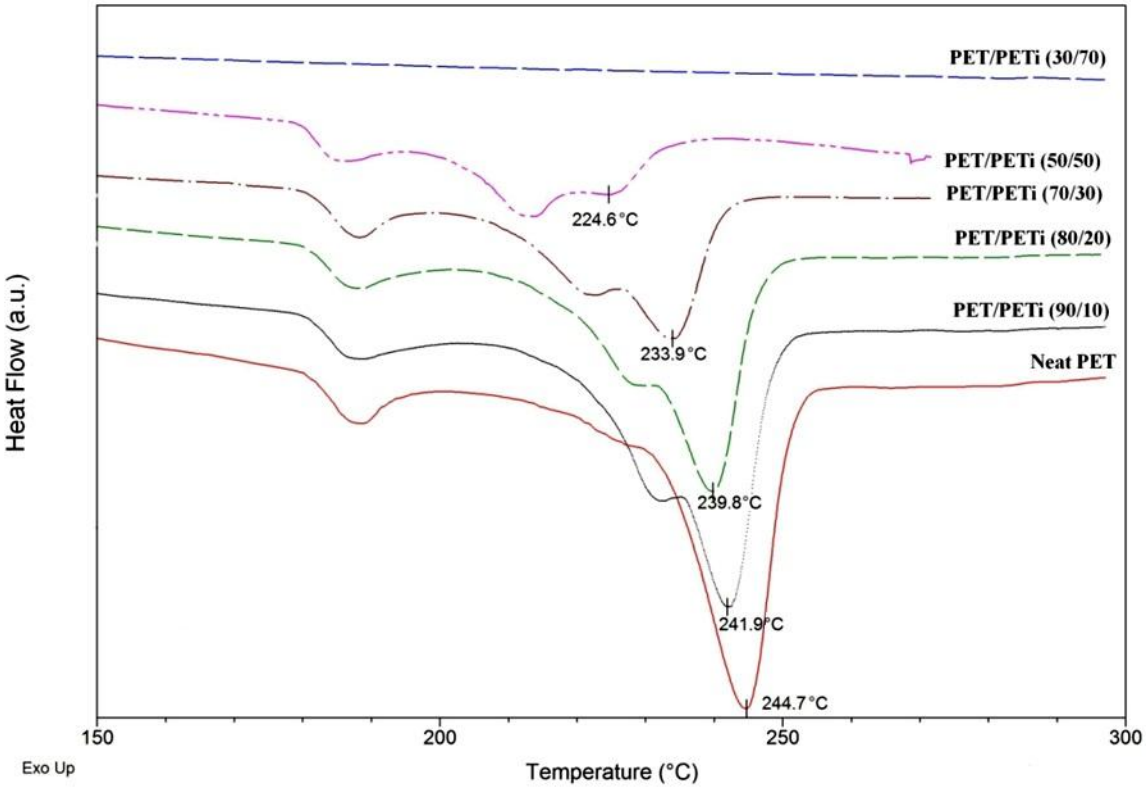

Figure 5-4: Melting behavior of PET/PETi blends containing 0 to 70 wt% PETi.

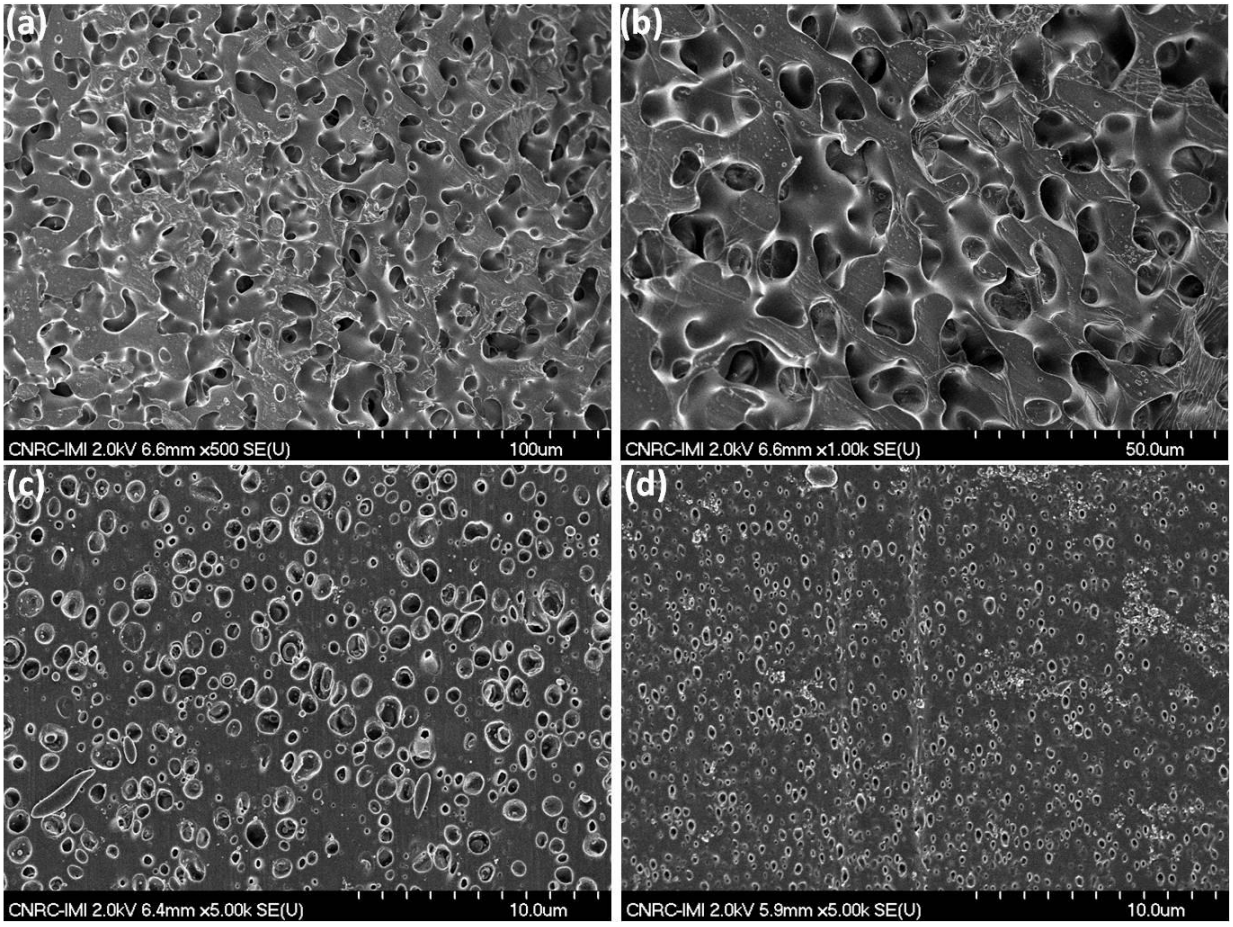

Figure 5-5: SEM micrographs of PET/PETi blends initially containing (a, b) 50 wt% PETi at different magnifications, (c) 30 wt% PETi and (d) 20 wt% PETi. All micrographs were taken after extraction of the PETi phase.

5.4.2 Morphology of PET-PETi nanocomposites

As the organoclays have positive charges on the edges while the PETi exhibits negative charges at the sulfonated groups[3,11], and as higher affinity of silicate nanolayers to polar polymers has been reported in the literature[22,23], it is anticipated that the organoclays will have greater affinity with the PETi phase. Thus the phase separation behavior of PET and PETi discussed in the previous section may cause migration and partitioning of the clay particles. Figure 5-6 shows

TEM images at different locations of nanocomposites containing 2 wt% of C30B and 20 and 6 wt% of PETi, respectively. This figure reveals that the C30B clay particles are indeed preferentially localized in the PETi domains than in the PET matrix. As expected, the greater PETi concentration of 20 wt% generates larger domains of the PETi in the nanocomposites (Figure 5-6a-d versus Figure 5-6e-f). As a consequence, the clay distribution density in the separated (PETi) domains is indeed expected to be higher in the lower PETi content system (6 wt%), since the overall clay concentration remains the same in both cases.

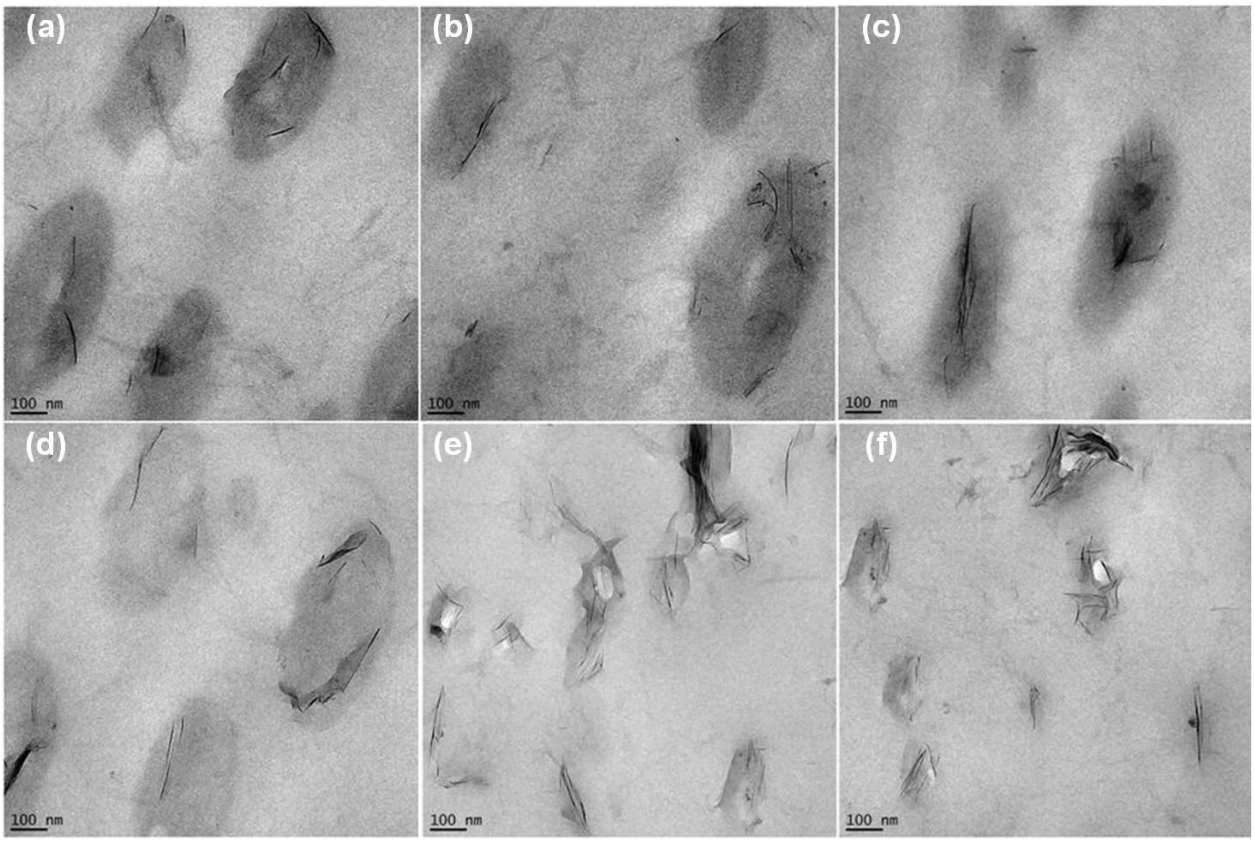

Figure 5-6: TEM images of nanocomposites containing 2 wt% C30B and 20 wt% PETi (a-d) and 6 wt% PETi (e,f).

The preferred affinity of the organoclay for the PETi phase may impede its efficient distribution within the bulk phase. A “good distribution” refers to a case where single layers and/or multilayer

clay particles show a uniform presence within the whole material, both the domains and the matrix, even if clay aggregates might be observed. On the other hand, the term "dispersion" refers to how well the clay layers are delaminated and form single layers at the nanoscale.[24] Figure 5-7 shows the SEM micrographs of various PET-based nanocomposites with and without PETi, at a nominal content of 2 wt% of organoclay C30B or N28E.

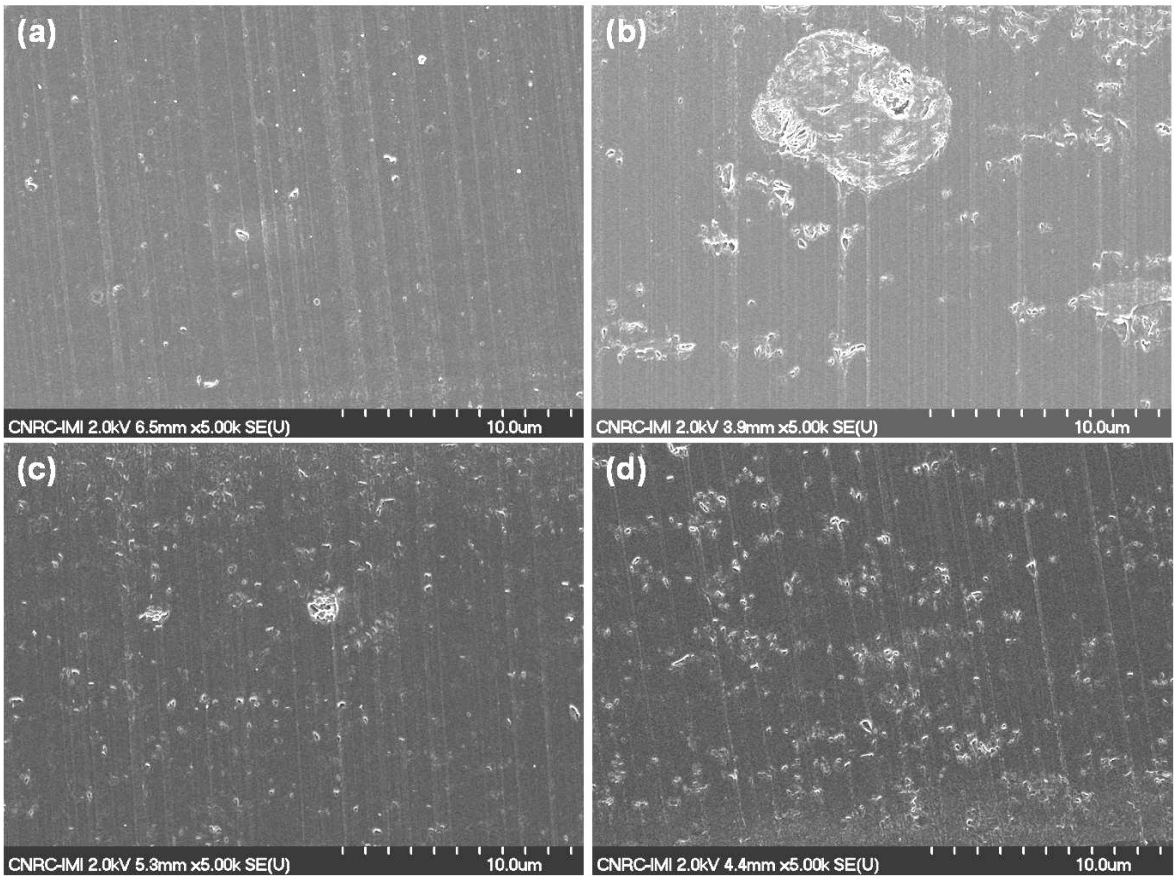

Figure 5-7: SEM micrographs of (a) PET/C30B, (b) PET/PETi/C30B, (c) PET/N28E, (d) PET/PETi/N28E.

In the nanocomposite containing C30B in the absence of ionomer (Figure 5-7a), the observed clay density is low and the particle size is smaller than for samples containing the PETi (Figure 5-7b). The low density of clay particles may be due to the limitation of SEM for sub-micron

levels while smaller aggregates suggest that clays are well dispersed in the PET matrix. By adding the PETi in nanocomposites containing C30B, more and larger clay particles are visible in the SEM image and there are several “empty” spaces neighboring large agglomerates (Figure 5-7b), indicating a bad distribution and dispersion of C30B particles in this system. The presence of large aggregates is due to concentration of particles in the PETi domains as discussed earlier. However, it is interesting to note that this phenomenon is not observed in the nanocomposites containing N28E (Figure 5-7c-d).

In order to complement the information provided by the SEM micrographs, XRD and TEM techniques were employed to have a better understanding of the nanocomposites morphology. Investigation of XRD patterns is among the important tasks to evaluate the overall morphology of nanocomposites. Morphological information on the nanocomposites can be inferred from the position, shape and intensity of the reflected X-ray beam. Figure 5-8 shows the XRD patterns of nanocomposites containing N28E and C30B, respectively. The basic interlayer spacing of N28E is 2.4 nm. The interlayer spacing of the organoclay in the PET/N28E nanocomposite increases up to 3.4 nm (Figure 5-8a). This increase is assumed to be the result of the diffusion of PET macromolecules within the silicate layers, and suggests an intercalated morphology. For the N28E nanocomposite containing PETi, no peak is observed. This can be due to the delamination of silicate nanolayers within the PET matrix and disruption of the well-ordered structure of the nanolayers. The weaker second-order peak also disappears for nanocomposites containing PETi, which is another sign that the high degree of the periodic order of N28E does not exist in these nanocomposites. By incorporation of C30B into the PET matrix, the interlayer spacing of this organoclay increases from 1.8 nm to 3.6 nm (Figure 5-8b). This is in agreement with the findings

of Ghasemi et al.[12,25] The increment is here also attributed to the intercalation of PET chains within the clay galleries. The C30B nanocomposites containing the PETi show no diffracted peak, possibly because of clay dilution due to aggregate formation as illustrated by Figure 5-7b. However, the disappearence of a diffraction peak cannot always be directly attributed to an exfoliated morphology. For these reasons, XRD analysis is not sufficient for morphological characterization of nanocomposites, and TEM imaging is required for a better understanding of the internal structure.

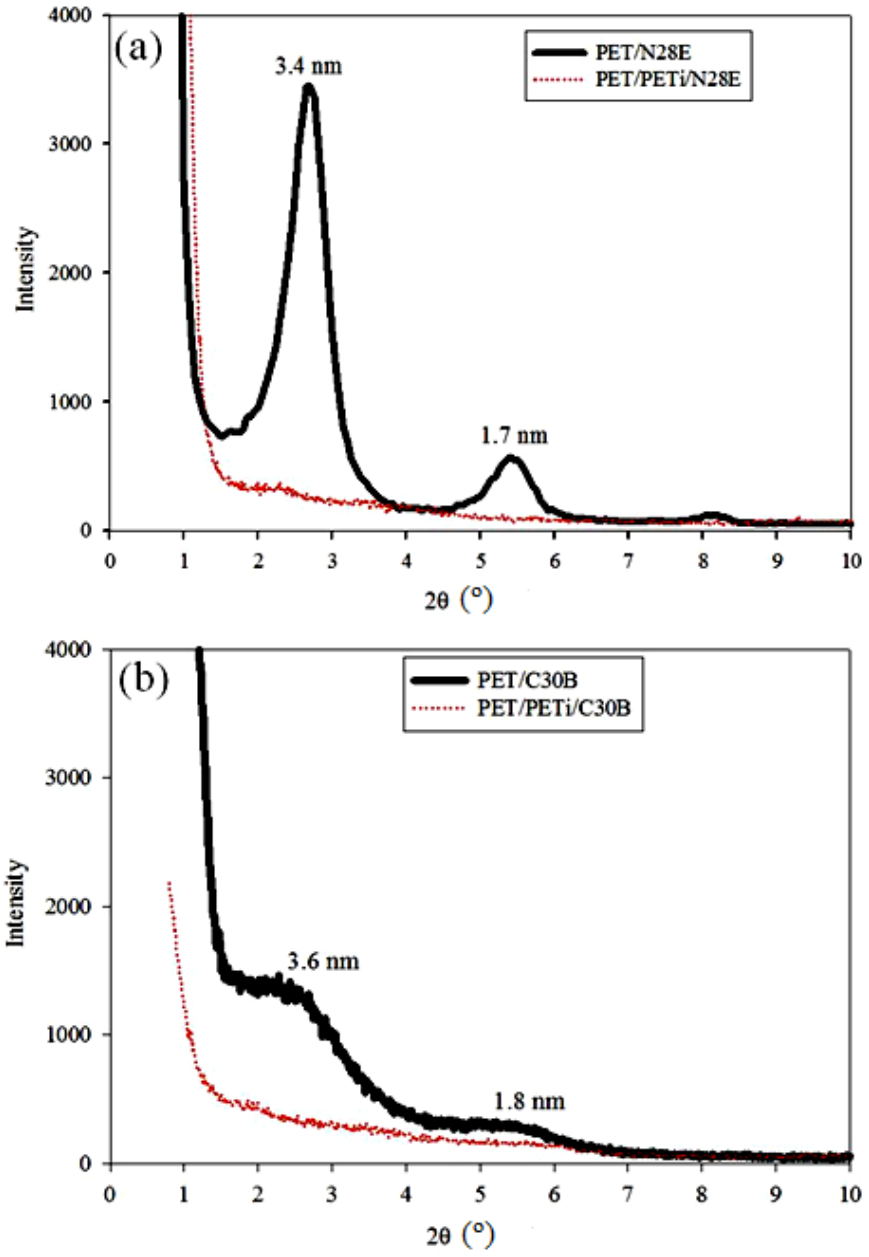

Figure 5-8: XRD patterns of PET nanocomposites containing 2 wt% N28E (a) and C30B (b). Nanocomposites without ionomer (thick solid line) and nanocomposites containing the ionomer (narrow dotted line).

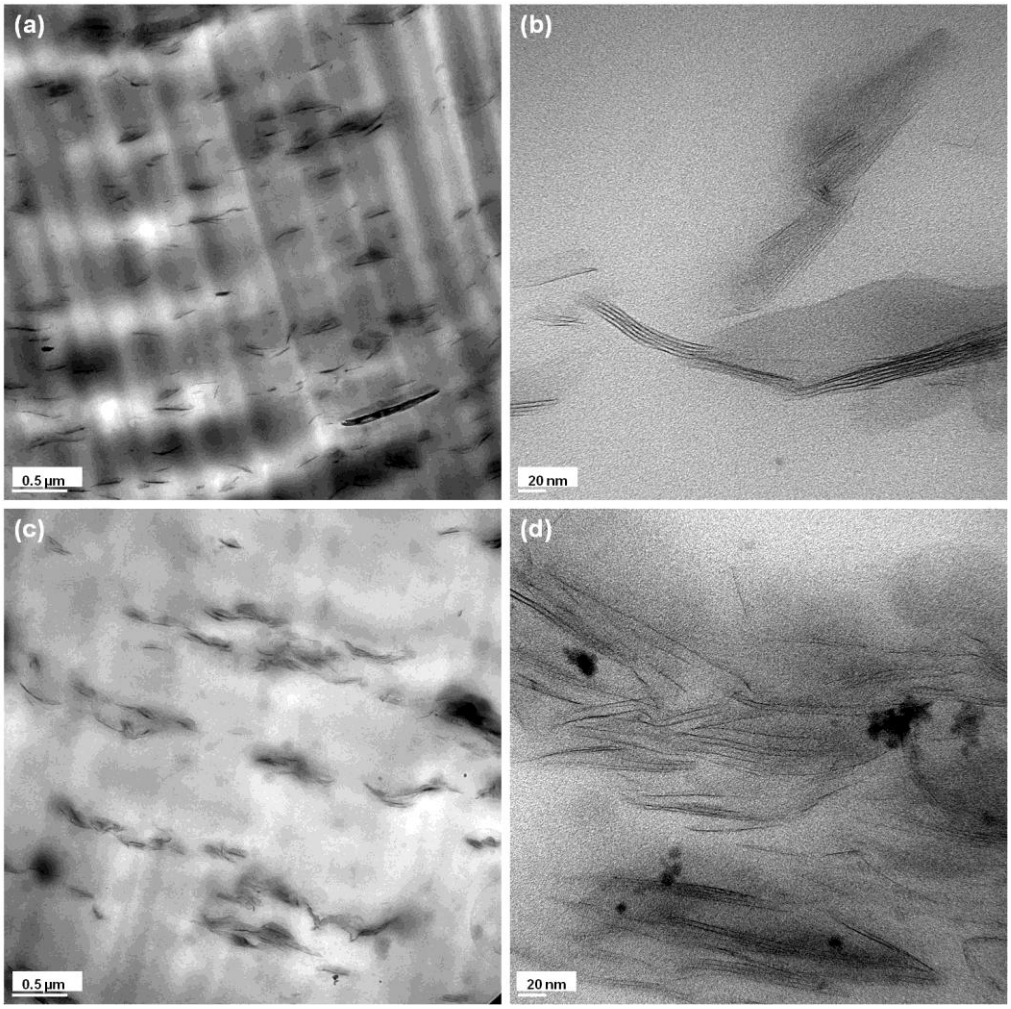

Figure 5-9: TEM images of PET/N28E (a,b) and PET/PETi /N28E (c,d) at various magnifications.

Figure 5-9 shows TEM images of PET-based nanocomposites containing 2 wt% of N28E. For these nanocomposites, a better distribution of clay particles is achieved for samples containing no PETi (Figure 5-9a) as the particles have a larger area to be distributed in. In contrast, in nanocomposites containing PETi the clay particles are trapped in the restricted PETi phase as discussed earlier and their distribution is hence constrained (Figure 5-9c). However, the presence of PETi results in a better dispersion of the clay layers due to a better affinity between PETi and

clay, as mentioned before. A larger gallery spacing and a greater clay layer disorder due to the addition of PETi can be observed by comparing the TEM images of nanocomposites with and without PETi (Figure 5-9d and Figure 5-9b, respectively). It seems that a semi-exfoliated morphology is achieved for nanocomposites containing PETi and N28E (Figure 5-9d). For these systems, a significant amount of individual clay layers can be observed in the TEM images.

TEM images of nanocomposites containing C30B are shown in Figure 5-10 for various magnifications. The TEM observations are in good agreement with the SEM ones. Figure 5-10a reveals a good distribution of the C30B clay particles within the PET matrix. At high magnifications, single layers, double layers and tactoids containing a few layers can be observed (Figure 5-10b) indicating a good level of dispersion and exfoliation. However, after adding PETi, the clay particles are not distributed as well as in the PET matrix alone (Figure 5-10c). This is related to the lack of miscibility between the PETi and PET phases and greater affinity of clay for the PETi phase as discussed above. The TEM observations also demonstrate that the morphology of the N28E systems (Figure 5-9c-d) is very different from that of the C30B systems (Figure 5-10c-d), in which the PETi domains are larger and less uniform. As clays are mainly concentrated in the PETi domains in both cases, it can explain for the appearance of large clay aggregates in the C30B-PETi systems and not in the N28E-PETi ones.

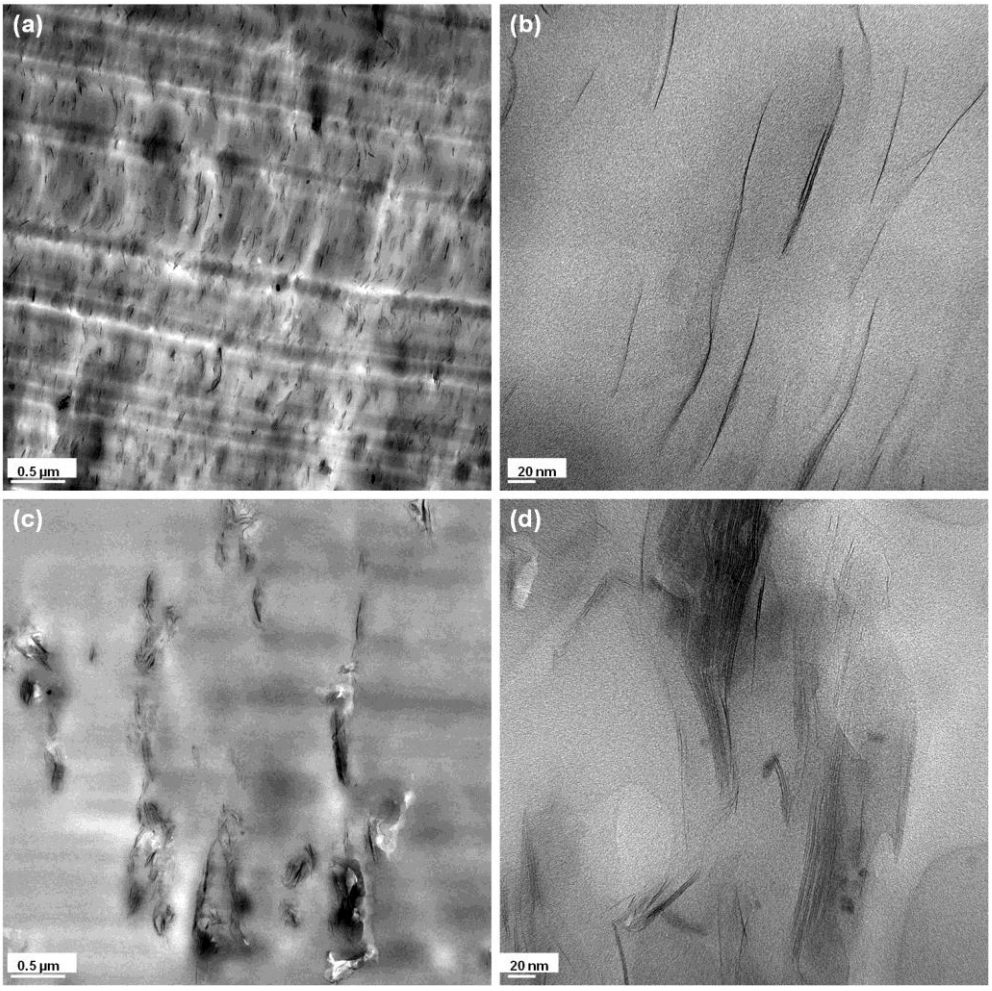

Figure 5-10: TEM images of PET/C30B (a,b) and PET/PETi /C30B (c,d) at various magnifications.

To evaluate quantitatively the effect of the compatibilizer on the PET-based nanocomposites containing the two organoclays, the number of platelets per clay particle was manually counted using the TEM images. Around 400 particles were counted to ensure statistical validity of the analysis. The corresponding data are shown in Figure 5-11. In the case of PET/C30B nanocomposites, the count for single and double layer particles is the highest among all of the nanocomposites (around 80%), indicating that this organoclay is both well dispersed and distributed in the PET matrix. In the presence of PETi, the amount of C30B clay aggregates (five

or more platelets/particle) increases due to the confinement of the clay particles within the small available area of the PETi phase. On the contrary, for the PET/N28E nanocomposites the count for single and double layer particles is the lowest one and this kind of organoclay is neither well dispersed nor distributed in the PET matrix alone (Figure 5-9a-b). However, by adding the PETi to the nanocomposites containing N28E, the counts for single and double layer particles increase. While it was seen that the addition of PETi leads to C30B aggregate formation resulting in a worse morphology, the use of a more polar polymer enhances the gallery spacing in the case of N28E and results in more single and double layer particles. The better dispersion of C30B over N28E in the PET can be due to the presence of the two ethoxy (or ethyloxy) groups in the intercalant of the former that can facilitate the interaction with the carboxylic and hydroxyl groups of PET molecules via hydrogen bonds or even chemical bonds (etherification or esterification). The better dispersion of N28E over C30B in the PETi domains should be explained by the better affinity of PETi with N28E over C30B. The primary amine used in the intercalant in N28E should provide a less crowded surface as opposed to the quaternary amine used in the intercalant in C30B, thus allowing a better interaction between the clay surface and the PETi.

To quantify further the degree of layer dispersion in the nanocomposites, the free-path spacing measurement introduced by Luo and Koo is employed.[26] According to this method, a dimensionless dispersion value $D_{0.1}$ is calculated based on the distribution of the free-path spacing distances between the clay layers according to the following equation:

$$D_{0.1} = 1.1539*10^{-2} + 7.5933*10^{-2}\left(\mu/\sigma\right) + 6.6838*10^{-4}\left(\mu/\sigma\right)^2 - 1.9169*10^{-4}\left(\mu/\sigma\right)^3 + 3.9201*10^{-6}\left(\mu/\sigma\right)^4 \quad (5\text{-}2)$$

where μ is the mean spacing between the clay layers, and σ is the standard deviation.

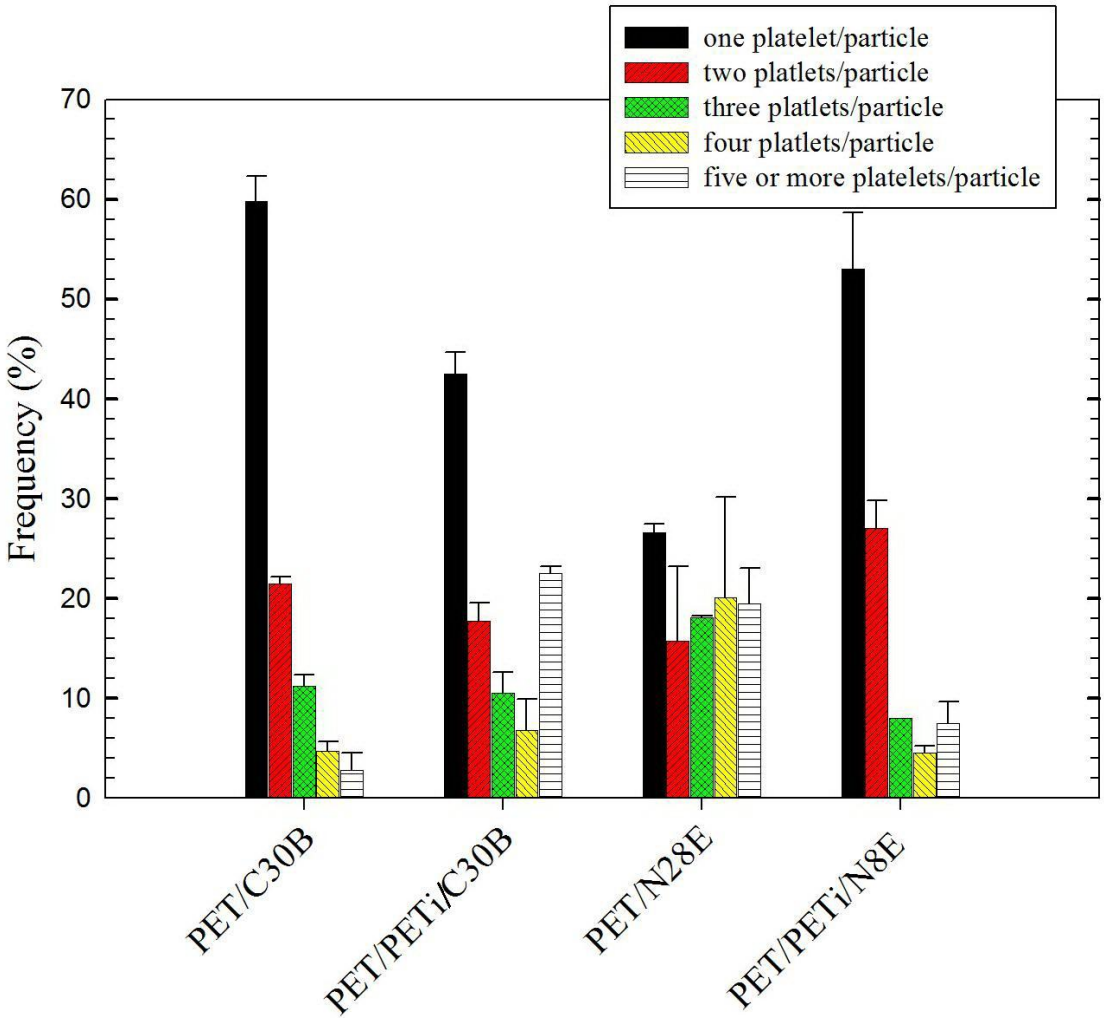

Figure 5-11: Number of platelets per particle histogram. The total number of counted particles was around 400 for each nanocomposite.

A value below 4% for the dimensionless dispersion parameter $D_{0.1}$ suggests an immiscible system or microcomposite; an intercalated nanocomposite displays a dispersion value between 4-8%,

while for an exfoliated nanocomposite this value is above 8%.[26] While the $D_{0.1}$ value increases from 4.3 to 6.3% for PET/N28E and PET/PETi/N28E, respectively, for samples containing C30B a reverse trend is observed. The $D_{0.1}$ values for PET/C30B and PET/PETi/C30B is 7.5 and 4.6 %, respectively. PET/C30B has the highest $D_{0.1}$ value with 7.5% which is close to that of a fully exfoliated system. This value is in agreement with the one obtained by Ghasemi et al.[12] for PET nanocomposites containing C30B obtained under the best processing conditions. For the N28E nanocomposites, the addition of PETi transforms a nearly microcomposite ($D_{0.1}$ = 4.3%) to an intercalated system ($D_{0.1}$ = 6.3%), in agreement with previous observations.

5.4.3 Rheological properties of PET-PETi nanocomposites

Figure 5-12 reports the complex viscosity and storage modulus of the neat PET and its nanocomposites. The various nanocomposites show a shear-thinning behavior while the neat PET displays a pseudo-Newtonian behavior on the whole frequency range. The lowest viscosity and storage modulus are observed for the nanocomposite containing C30B and PETi. However, at high frequency, where the behavior of the matrix is dominant, all the nanocomposites show a lower viscosity and lower storage modulus than the neat polymer, presumably due to the degradation induced by the presence of the organic modifiers. The addition of PETi in the nanocomposites containing N28E increases the melt viscosity and storage modulus on the whole range of frequency, in comparison to the PET/N28E samples. This is most probably due to the better dispersion of the N28E particles in the nanocomposites containing PETi. In contrast, the presence of PETi in the nanocomposites containing C30B decreases the melt viscosity and storage modulus on the whole range of frequency in comparison to the PET/C30B samples. This

may be the results of two factors: the poor dispersion of the C30B particles in the presence of the ionomer, and a plasticization effect.

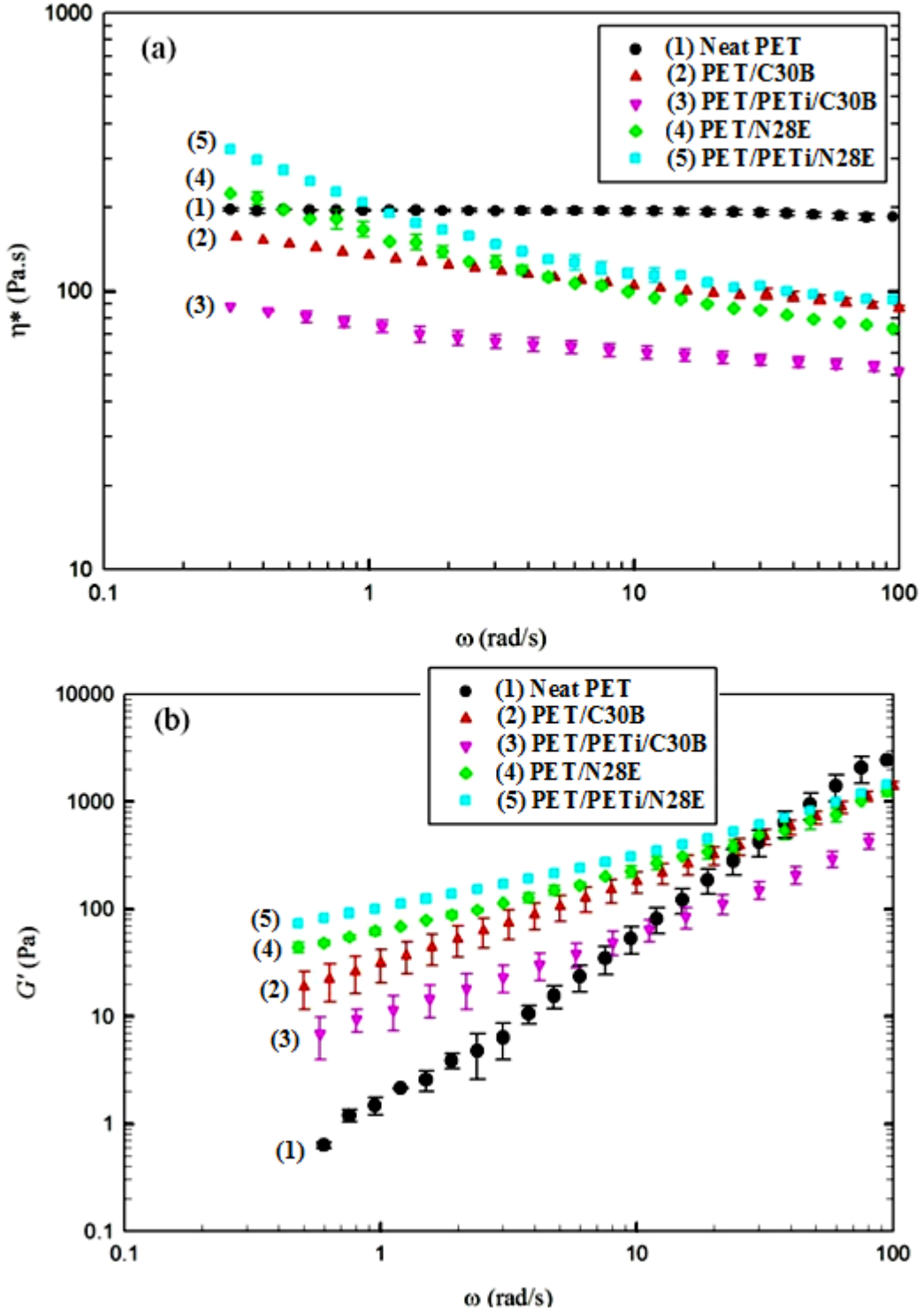

Figure 5-12: Complex viscosity (a), and storage modulus (b) as functions of frequency for the neat PET and its nanocomposites at 265 ºC.

In order to understand better the interactions between PETi and the two nanoclays, the complex viscosity and storage modulus of the neat PETi and its corresponding composites containing 6 wt% N28E and C30B were measured. This large concentration of clay was used to amplify its effect on the rheological properties of PETi, and results are presented in Figure 5-13. Both the neat PETi and the PETi/6 C30B samples display a pseudo-Newtonian behavior, while the sample containing N28E exhibits a marked shear-thinning behavior, which is one of the characteristics of nanocomposites with a favorable morphology. In the case of PETi/6 C30B, most probably C30B particles form large aggregates leading to a pseudo-Newtonian behavior as for the neat PETi. In contrast, it seems that N28E particles form an interconnected network-like structure, which is obvious at low frequency and suggests a strong interaction between the PETi and N28E. The lower complex viscosity of the PETi/6 C30B sample in comparison to the neat PETi is largely due to the degradation of the matrix induced by the organic modifier used for the C30B particles. In addition, it may suggest a low interaction between this clay and the ionomer, which was already shown in the SEM (Figure 5-7b) and TEM (Figure 5-10c-d) images.

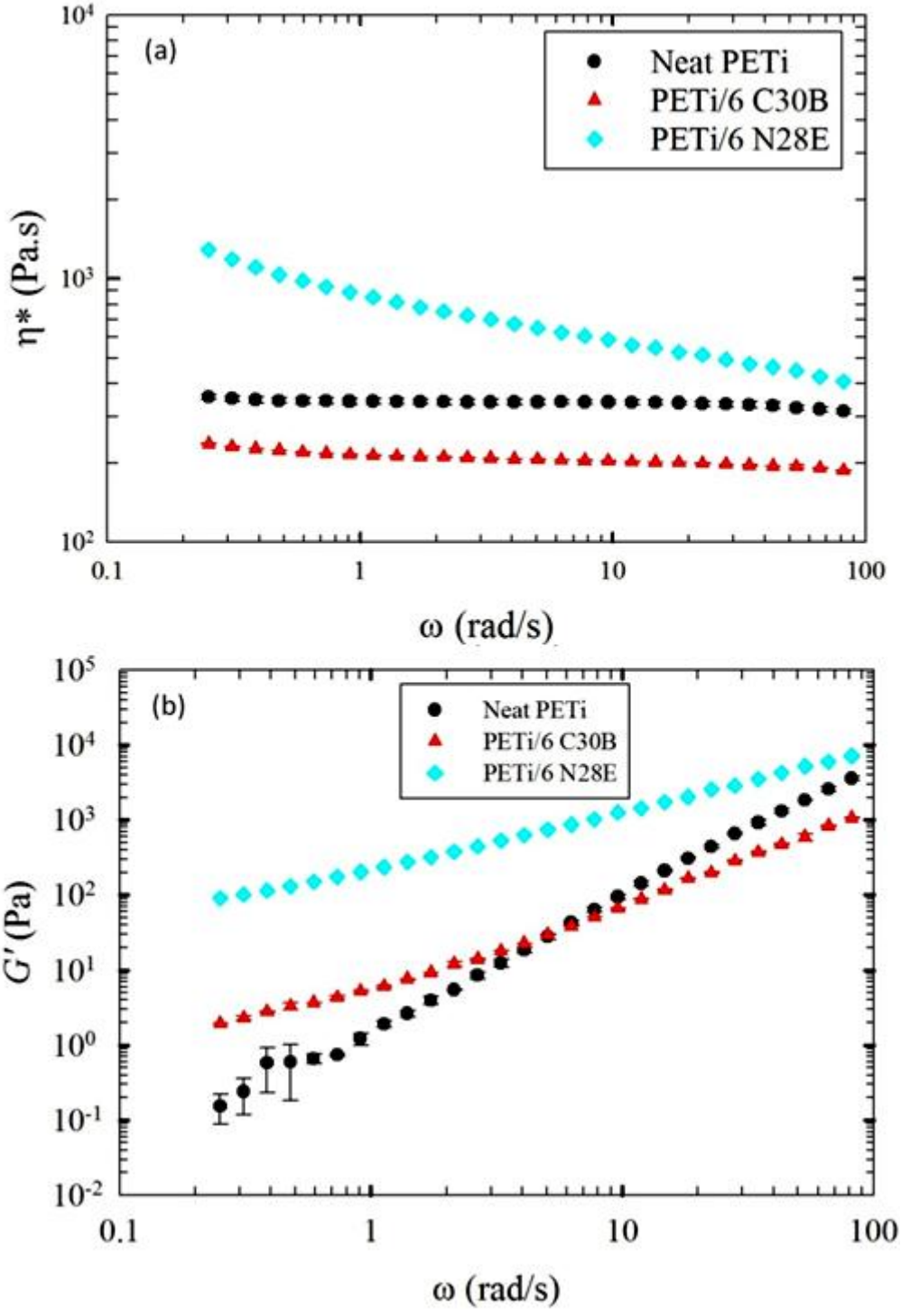

Figure 5-13: Complex viscosity (a), and storage modulus (b) as functions of frequency for the neat PETi (●), PETi/6 C30B (▲), and PETi/6 N28E (♦) at 250 ºC.

5.4.4 Thermal properties

The influence of clay platelets on the glass transition temperature T_g, the melting temperature T_m, cold crystallization temperature T_{cc}, hot crystallization temperature T_{hc}, and crystal content of PET nanocomposite films was investigated by DSC. The thermal characteristics of the various films are given in Table 5-2. The glass transition temperature of the nanocomposite films is somewhat lower than that of the neat PET, with a slightly larger reduction for nanocomposites containing PETi, which suggests thermal degradation of PET chains and/or plasticization. No significant difference is observed in the melting point of the nanocomposites in comparison with the neat PET. For all the nanocomposites, cold crystallization and hot crystallization temperatures decreases and increases, respectively, in comparison to the neat PET. This reveals that clay particles act as heterogeneous nucleating agents and promote nucleation of the semi-crystalline PET. The crystal content of the nanocomposite films is evaluated according to the following equation:

$$X_C = \frac{(\Delta H_m - \Delta H_{CC})/\alpha}{\Delta H_m^o} \qquad (5\text{-}3)$$

where α is the PET weight fraction, ΔH_m the enthalpy of melting, ΔH_{CC} the enthalpy of cold crystallization and ΔH_m^o the enthalpy of melting of 100% crystalline PET (140 J/g).[27] As shown in Table 5-2, the crystalline content of nanocomposite films is slightly larger than that of neat PET films, which is another indication of a promoted crystallization in the presence of clay.

Table 5-2: DSC results for neat PET and nanocomposites films containing C30B and N28E.

Sample	$T_g(°C)$	$T_{cc}(°C)$	$T_{hc}(°C)$	$T_m(°C)$	Crystalline fraction (%)
Neat PET	78.7 ± 0.1	135.7 ± 0.1	174.8 ± 0.1	243.1 ± 0.1	8.6 ± 0.5
PET/C30B	76.5 ± 0.2	126 ± 0.1	193.8 ± 1	244 ± 0.1	13.0 ± 0.3
PET/PETi /C30B	74.8 ± 0.1	129.2 ± 0.2	194 ± 2	244 ± 0.1	12.9 ± 0.1
PET/N28E	77.5 ± 0.1	133.3 ± 0.1	197 ± 3	244.2 ± 0.1	11.1 ± 0.5
PET/PETi /N28E	75.2 ± 0.1	125.9 ± 0.1	198 ± 0.3	244 ± 0.2	14.3 ± 0.3

5.4.5 Barrier properties

The barrier property improvement of nanocomposites is generally explained by the tortuous path model.[28,29] The presence of silicate nanolayers, which are assumed impermeable lamellar fillers with a high aspect ratio, induce a more tortuous gas path. Longer diffusion pathways are created, hence preventing the gas to pass directly through the material.[28,29] Crystallinity is another important factor, which can promote barrier properties of a material. Figure 5-14 shows the measured oxygen permeability of the neat PET and its nanocomposites. For all the nanocomposite films, the permeability is decreased in comparison to the neat PET due to both the presence of clay particles and a higher crystallinity. The best barrier properties are obtained for the nanocomposite film containing C30B, for which a reduction of oxygen permeability up to 25% is observed in comparison to the neat PET, confirming the results of Ghasemi et al.[12] By comparing Figure 5-9a and Figure 5-10a, it can be concluded that the better distribution of C30B

within the PET matrix and the larger $D_{0.1}$ value, as compared to N28E, explain the permeability results. These data clarify the strong role of the nanoclay distribution on the barrier properties. However in the case of clay particles like N28E, which cannot be well dispersed, employing a more polar polymer (the sulfopolyester) can be helpful to achieve a better dispersion level. Miscibility between the more polar polymer and polymer host matrix plays a key role as properties of nanocomposites is controlled by the level of clay distribution too. In this work, a fundamental study was performed to investigate the state of miscibility between PET and PETi and clarify the effect of PETi on the migration and partitioning of two different clay particles within a PET matrix. Unfortunately the immiscibility of PETi in PET does not permit a good distribution and dispersion of the clay particles outside of the PETi domains. Thus the advantage of the good clay dispersion in an immiscible system such as PET-PETi does not lead to improved barrier properties.

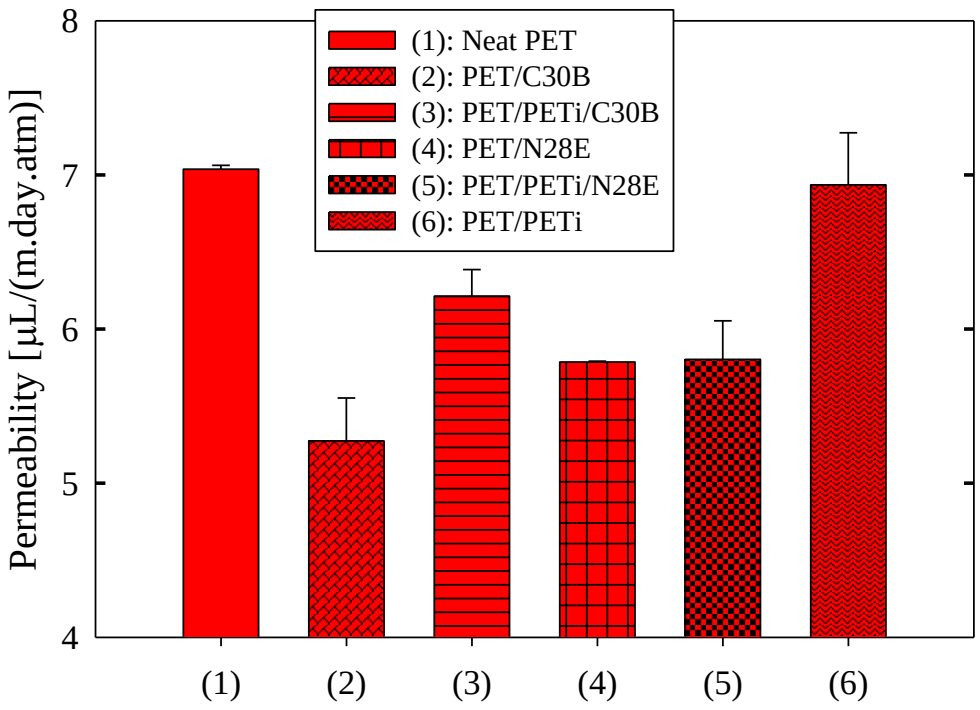

Figure 5-14: Oxygen permeability of the neat PET and its nanocomposite films.

5.5 Conclusion

In this work, morphological, rheological, thermal and gas barrier properties of PET nanocomposites containing C30B and N28E were studied. The effect of a sulfopolyester (PETi) on the morphology of nanocomposites was investigated. Based on SEM and TEM results, PETi was found to be immiscible with PET although the PET backbone of this copolymer influences the crystallization of the PET matrix and leads to a melting point depression. Nanoclay particles have greater affinity with the PETi phase due to the formation of favorable electrostatic interactions between the ionic groups of this copolymer and nanoclay particles, which localize themselves preferentially into the PETi domains. Although migration of clay particles into

droplets of the PETi phase restricts distribution of the particles, XRD, TEM and rheological results show that for nanocomposites containing N28E, PETi acts as an effective exfoliation agent and improves the dispersion of the clay particles.

Higher crystallinity was observed for all nanocomposite films in comparison to that of neat PET. Finally, it was found that the gas barrier properties of nanocomposites were improved by a good distribution of clay particles within the matrix. The best nanoclay distribution and barrier properties were obtained for C30B in the absence of PETi.

5.6 Acknowledgements

The authors thank Drs. H. Ghasemi and X-F. Xu for their valuable help in producing the nanocomposite films. They are also thankful to W. Leelapornpisit for preparing SEM and TEM images. Financial support from NSERC (Natural Science and Engineering Research Council of Canada) in the context of the NRC-NSERC-BDC Nanotechnology Initiative is gratefully acknowledged.

5.7 References

1. S.N. Bhattacharya RKG, M.R. Kamal. Polymeric Nanocomposites :Theory and Practice. Hanser Gardner Pubns; 2007.
2. Todorov LV, Viana JC, *J Appl Polym Sci* **106:**1659-69 (2007).
3. Ammala A, Bell C, Dean K, *Compos. Sci. Technol.* **68:**1328-37 (2008).
4. Calcagno CIW, Mariani CM, Teixeira SR, Mauler RS, *Polymer* **48:**966-74 (2007).
5. Chung JW, Son SB, Chun SW, Kang TJ, Kwak SY, *Polym Degrad Stabil* **93:**252-9 (2008).
6. Stoeffler K, Lafleur PG, Denault J, *Polym Degrad Stabil* **93:**1332-50 (2008).

7. Shen YC, Harkin-Jones E, Hornsby P, McNally T, Abu-Zurayk R, *Compos. Sci. Technol.* **71:**758-64.
8. Jung MH, Chang JH, *Polymer-Korea* **31:**518-25 (2007).
9. Monemian SA, Goodarzi V, Zahedi P, Angaji MT, *Adv Polym Technol* **26:**247-57 (2007).
10. Mun MK, Kim JC, Chang JH, *Polym Bull* **57:**797-804 (2006).
11. Chisholm BJ, Moore RB, Barber G, Khouri F, Hempstead A, Larsen M, et al., *Macromolecules* **35:**5508-16 (2002).
12. Ghasemi H, Carreau PJ, Kamal MR, Chapleau N, *Int Polym Process* **26:**219-28 (2011).
13. Xu XF, Ghanbari A, Leelapornpisit W, Heuzey MC, Carreau PJ, *Int Polym Process* **26:**444-5 (2011).
14. Cole KC, *Macromolecules* **41:**834-43 (2008).
15. Barber GD, Calhoun BH, Moore RB, *Polymer* **46:**6706-14 (2005).
16. Sepe MP. Thermal Analysis Of Polymers. Rapra Technology Ltd; 1997.
17. Utracki LA. Polymer Blends Handbook. 1st Edition ed.: Springer; 2002.
18. Yang F, Qiu ZB, Yang WT, *Polymer* **50:**2328-33 (2009).
19. Cheung YW, Stein RS, *Macromolecules* **27:**2512-9 (1994).
20. Prud'homme RE, *Polym Eng and Sci* **22** (1982).
21. James M. Jonza RSP, *Macromolecules* **19:**1946–51 (1986).
22. Martin Z, Jimenez I, Gomez-Fatou MA, West M, Hitchcock AP, *Macromolecules* **44:**2179-89.
23. Kontopoulou M, Liu YQ, Austin JR, Parent JS, *Polymer* **48:**4520-8 (2007).
24. Abbasi S, Carreau PJ, Derdouri A, Moan M, *Rheol Acta* **48:**943-59 (2009).
25. Ghasemi H, Carreau PJ, Kamal MR, Tabatabaei SH, *Polym Eng and Sci* **in press** (2011).
26. Luo ZP, Koo JH, *Polymer* **49:**1841-52 (2008).
27. Soon KH, Harkin-Jones E, Rajeev RS, Menary G, McNally T, Martin PJ, et al., *Polym Int* **58:**1134-41 (2009).
28. Bharadwaj RK, *Macromolecules* **34:**9189-92 (2001).
29. Russo GM, Simon GP, Incarnato L, *Macromolecules* **39:**3855-64 (2006).

CHAPTER 6
MORPHOLOGICAL AND RHEOLOGICAL PROPERTIES OF PET/CLAY NANOCOMPOSITES

A. Ghanbari[a], M.C. Heuzey[a], P.J. Carreau[a], M.T. Ton-That[b]

[a] *Center for Applied Research on Polymers and Composites (CREPEC), Chemical Engineering Department, Ecole Polytechnique de Montreal, PO Box 6079, Stn Centre-Ville, Montreal, QC, Canada H3C 3A7*

[b] *Automotive Portfolio, National Research Council Canada, 75 Mortagne Blvd, Boucherville, QC, Canada J4B 6Y4*

This work was submitted to *Rheologica Acta* and parts of it were presented at 83rd annual meeting of the Society of Rheology (SoR), Cleveland, USA (2011) and 16th International Congress on Rheology (ICR), Lisbon, Portugal (2012)

6.1 Abstract

This work investigates the effects of clay chemistry and concentration on the morphology and rheology of polyethylene terephtalate (PET)/clay nanocomposites. The complex viscosity of the PET nanocomposites exhibited a more solid-like behavior, in contrast to the matrix that had a frequency independent viscosity. In addition, at high frequencies where the behavior of the matrix should be dominant, a lower complex viscosity of the nanocomposites was observed due to PET degradation in the presence of the organoclays. The high frequency data were used to estimate the matrix degradation using the Maron-Pierce equation. The apparent molecular weight of the PET matrix was found to decrease from 65 kg/mol for the neat PET to 30 kg/mol for a PET nanocomposite containing 8 wt% Cloisite® 30B. The apparent yield stress in the nanocomposites was determined using the Herschel-Bulkley model. Yield stress increased with the level of exfoliation and clay concentration, from ~ 0 to 166 Pa when the clay concentration increased from 2 to 8 wt%.

Keywords: Polyethylene terephtalate. Nanocomposites. Organoclay. Rheology. Morphology.

6.2 Introduction

Polymer/layered silicate nanocomposites have attracted remarkable scientific and technological interests due to significant improvement of material properties, at low clay loadings, in comparison with unfilled polymers or common micro composites. These notable changes include enhancements in mechanical properties, thermal stability, barrier and flame retardant properties (Gupta et al. 2009; Ray and Okamoto 2003).

To prepare polymer/layered silicate nanocomposites, three main approaches consist of solution blending, *in-situ* polymerization, and melt blending. Melt blending is an environmental friendly

method because there is no need for organic solvents. Besides, low cost and common industrial processing techniques such as extrusion can be used for the preparation of nanocomposites from a wide range of thermoplastic polymers. In addition, the high shear force in polymer processing equipments facilitates the dispersion of the nanoparticles in the molten polymer matrix. Therefore, melt blending is industrially a more viable method in comparison to other approaches (Pavlidou and Papaspyrides 2008; Ray and Okamoto 2003).

Wide angle X-ray diffraction (WAXD), scanning electron microscopy (SEM), and transmission electron microscopy (TEM) are the most common techniques to characterize the nanocomposite morphology. WAXD is a convenient and rapid method to determine the gallery spacing of silicate layers for both pristine clays and organically modified clays and when polymer chains penetrate into the galleries. However, little information about the distribution of the silicate layers can be obtained by this method. On the other hand, although TEM provides direct visual information about the distribution of the silicate layers, it is a time-consuming and expensive technique which covers only a very small portion of the sample, with the possibility of micro-scale inhomogeneity. SEM is used to characterize the particle distribution at the micrometer scale and to assess the presence of large aggregates. In conjunction with the aforementioned techniques, rheology is employed as an indirect tool for the microstructure characterization of nanocomposites. The advantage of rheological methods is that they probe the bulk of nanocomposite materials on a significant volume of sample tested, which increases the reliability of the data. In addition measurements are performed in the melt state, which can provide valuable information about the processability of the nanocomposites. Furthermore the interactions between the nanoparticles and the matrix can also be detected and quantified. Finally, detailed

information about molecular level changes in the structure (e.g. oxidation, degradation, crosslinking, etc.) can be obtained by employing rheometry (Pogodina et al. 2008; Galindo-Rosales et al. 2011; Bhattacharya et al. 2007; Gupta et al. 2009; Vermant et al. 2007).

A large number of rheological studies have been carried out to assess the state of clay dispersion in polymer matrices, especially thermoplastics (Nazockdast et al. 2008; Wu et al. 2005; Vermant et al. 2007; Eslami et al. 2010; Wang et al. 2011; Aubry et al. 2005; Manitiu et al. 2009; Ayyer and Leonov 2004; Gahleitner et al. 2006; Lim and Park 2001; Mobuchon et al. 2007, 2009a; Mobuchon et al. 2009b). Large increases in viscoelastic properties, storage modulus and complex viscosity, as well as a slower relaxation and a transition from liquid-like to solid-like behavior are the most significant findings of these studies. The appearance of a solid-like terminal plateau in the storage modulus of nanocomposites has been commonly attributed to the formation of a space-filling percolated network of individual clay platelets and/or intercalated tactoids acting like a weak solid (Pujari et al. 2011; Utracki and Lyngaae-Jorgensen 2002; Solomon et al. 2001; Ren et al. 2000; Ray and Bousmina 2005). Therefore, by destroying this interconnected network of clay particles (for example by pre-shearing) a remarkable reduction of viscoelastic properties is expected. Orientation of clay particles in the shear direction and a transition from solid-like behavior to liquid-like behavior has been observed by many researchers (Nazockdast et al. 2008; Wu et al. 2005; Dykes et al. 2012; Solomon et al. 2001). The presence of a percolation network is also inferred by the stress response upon start-up of steady shear. The stress overshoot observed in transient rheological response of nanocomposites depends on rest time duration and applied shear rate, and is attributed to both interaction between nanoparticles and the viscoelastic properties of the polymer matrix.

PET is a semi-crystalline thermoplastic polymer widely used in soft drink bottles as well as both food and non-food containers. PET is non-toxic, shows high dimensional stability, high transparency, and good mechanical and thermal properties. Barrier properties of PET to oxygen should however be improved for some applications like packaging of oxygen-sensitive beverages such as soft drinks and beer. Incorporation of silicate nanolayers into a PET matrix has been shown to enhance the barrier properties of PET (Ghanbari et al. In press.; Ghasemi et al. 2011a; Xu et al. 2011; Frounchi and Dourbash 2009; Soon et al. 2009; Ghasemi et al. 2012).

Several studies have been performed on PET/organoclay nanocomposites. It was observed that introducing a PET-ionomer as an exfoliating agent, which has a higher polarity than PET, improved the dispersion of clay particles and increased the viscoelastic properties of the nanocomposites (Ghanbari et al. In press.; Xu et al. 2011). In another study, it was demonstrated that contrary to thermally stable phosphonium and imidazolium modified clays, ammonium-modified Cloisite® 30B (C30B) exhibited good dispersion and distribution within a PET matrix (Ghasemi et al. 2011b). The incorporation of 3 wt% of C30B into PET led to a 27% reduction in oxygen permeability (Ghasemi et al. 2011a). Sanchez-Solis *et al*. (Sanchez-Solis et al. 2004) observed that the incorporation of 3 wt% silicate nanolayers in a PET matrix resulted in a 45% enhancement of the Young's modulus.

Although several studies have been devoted to polymer/clay nanocomposites, the rheological behavior of PET/clay nanocomposites is not fully understood. For example, it has been observed that the incorporation of 2 wt% Nanomer® I.28E (N28E) and C30B in the PET matrix reduces the complex viscosity (Ghanbari et al. In press.; Xu et al. 2011). Scaffaro et al. [20] prepared PET nanocomposites containing C30B and C15A using a twin-screw extruder. They observed that the

complex viscosity of the nanocomposites containing 3, 5, and 10 wt% of the organoclays was smaller than that of the neat PET at high frequencies. More severe degradation was observed for the nanocomposites containing C30B than those containing C15A.

In the present work, various clay particles (from unmodified synthetic clay to commercially available organoclays) at different concentrations (from 0 to 8 wt%) were used to study the effect of surfactant and clay concentration on the rheological properties of PET nanocomposites. In addition, by changing the twin-screw configuration, the effect of processing was also examined. To our knowledge, there is no work addressing the effects of these parameters on both the rheology and morphology of PET nanocomposites in order to have a more in-depth comprehension. Particular emphasis is placed on studying the yield stress of the solid-like network induced by the presence of the clay particles at clay concentrations higher than the percolation threshold. High frequency data are used to estimate the thermal degradation of the PET matrix and analyze the influence of clay content on a more solid basis. Rheological properties are also correlated with morphological observations.

6.3 Experimental

6.3.1 Materials

The polyethylene terephtalate used in this study, PET 9921, is a commercial product of Eastman Chemical Company with intrinsic viscosity of 0.8 dL/g and a melting point of 243 °C. The following natural organoclays have been used: C30B, Cloisite® 15A (C15A) and Cloisite® 25A (C25A) from Southern Clay Products Inc., and N28E from Nanocor Inc. Unmodified synthetic

clay Somasif® ME100 (SM100) from CBC Co. Ltd was also utilized. The chemical composition of the organic modifiers (when applicable), the interlayer spacing of the clays, and the solubility parameter of the organic modifiers are summarized in Table 1. The content of organic modifier presents in the various organoclays was determined by thermogravimetric analysis (TGA Q500, TA Instruments). For these tests, samples of 10 mg were heated from room temperature to 800 °C with a heating rate of 10 °C/min under an air atmosphere. In Table 6-1 it is observed that the organoclays *d*-spacing is correlated with the organic modifier content.

Table 6-1: Characteristics of the clay particles.

Organoclay	Organic modifier	*d*-spacing (nm)	Organic modifier (wt%)	δ of organic modifier[a,b] ($J^{1/2}.cm^{-3/2}$)
C30B	methyl, tallow, bis-2-hydroxyethyl, quaternary ammonium	1.85	29	21.5
C25A	dimethyl, dehydrogenated tallow, 2-ethylhexyl quaternary ammonium	1.86	31	17.2
N28E	octadecyl ammonium	2.4	33	16.0
C15A	dimethyl, dehydrogenated tallow, quaternary ammonium	3.15	40	16.9
SM100	none	0.96	0	-

[a] δ is the solubility parameter calculated based on the Fedors group contribution method (Van Krevelen and Te nijenhuis 2009)

[b] experimental value of δ for PET is between 19.9 and 21.9 (Van Krevelen and Te nijenhuis 2009)

6.3.2 Melt Compounding

The PET and clay particles were vacuum dried at 90 ºC for 24 h before extrusion. A co-rotating twin-screw Leistritz extruder (screw diameter = 18 mm and L/D = 40) was used to prepare

samples containing 0 to 8 wt% of clay particles. Figure 6-1 depicts two different screw configurations (SC1 and SC2) which were used in this study. Both screw geometries have the same conveying and pressuring elements, followed by the first mixing zone with 30, 60 and 90° elliptical kneading elements 4 mm thick. The second and third mixing zones, with 30 and 60° elliptical elements, respectively, are also the same for both screw configurations. The only difference is that SC2 has a fourth mixing zone with 30 and 60° elliptical elements and a reverse element located between the third and the fourth mixing zones. It was observed that residence time at 200 rpm increases from 51 s for SC1 to 90 s for SC2. The residence times were estimated, 15 min after starting the extrusion, by adding a colored resin while feeding the neat PET. The measured torque value of the second screw was about 8% larger than the first one for nanocomposites containing 8 wt% C30B.

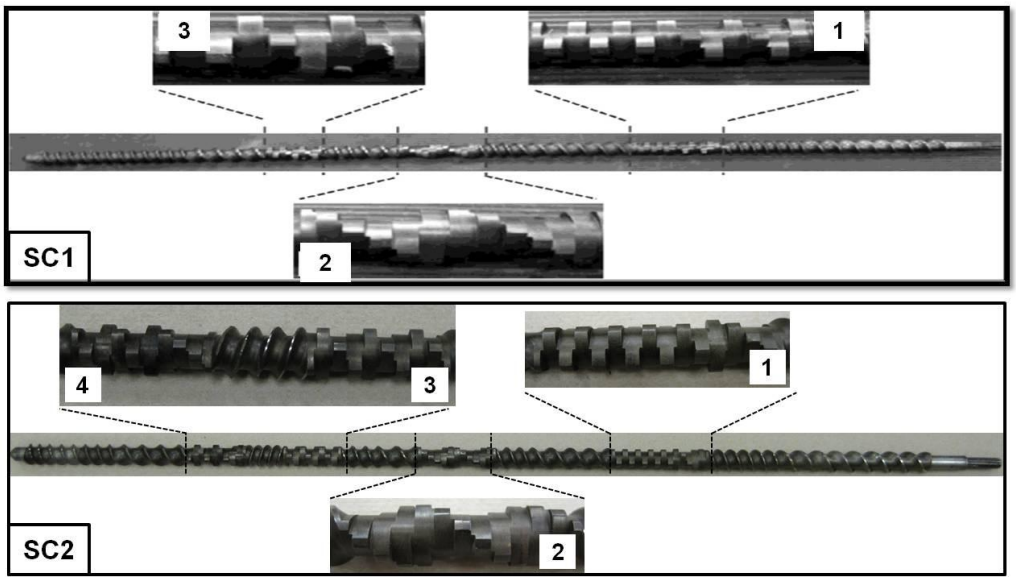

Figure 6-1: Screw configurations SC1 and SC2.

The extrusion conditions were the same for both screw configurations. Melt blending was performed at a screw speed of 200 rpm and feeding rate of 2 kg/h. The temperature profile from the feed to the die was set between 240 and 265 ºC. To cool the extrudate, a bath containing a mixture of water and ice was used. The extruded samples were granulated and vacuum dried at 90 ºC for 24 h. Compression molding was subsequently performed to obtain disk-shape samples of approximately 2 mm thickness and 25 mm diameter by employing a Carver® laboratory press (model 3912) at 265 ºC for 9 min at a pressure of 20 MPa and under a blanket of nitrogen, followed by quenching in another Carver® laboratory press (model 30-12H) for 5 min. The disk-shape samples were vacuum dried at 90 ºC for 24 h before being subjected to rheological testing.

6.3.3 Characterization

WAXD was used to obtain the basal distance of the clay layers by employing a Bruker D8 Discover with Cu K_α radiation of wavelength $\lambda = 1.5406$ Å. The generator was operated at 40 kV and 40 mA. The spectra were recorded over a 2θ range of 0.8 -10 º using a scan rate of 0.6 º/min.

SEM observations were done to evaluate the micro-scale distribution of the clay particles in the PET matrix using a Field Emission Gun SEM (FEG-SEM), Hitachi S4700, operating at 2 kV. The specimens were prepared using an Ultracut FC microtome (LEICA) with a diamond knife and then coated with platinum. TEM images were obtained using a JEOL JEM-2100F microscope operating at 200 kV to assess the quality of clay dispersion in the samples. For TEM imaging the samples were microtomed into ultrathin slices about 50-80 nm thick at a cryogenic temperature (i.e. -100° C) using the aforementioned microtome system.

Rheological measurements in oscillatory mode were performed using a Bohlin Gemini rheometer, with a parallel plate flow geometry (25 mm diameter, 1 mm gap). Time and frequency

sweeps in small-amplitude oscillatory shear were carried out on the neat PET and PET-based nanocomposite samples at 265 ºC under a nitrogen atmosphere to avoid oxidative degradation. The time sweep test of each sample was repeated twice, always with a fresh specimen, at 0.628 rad/s over 900 s. The frequency sweep tests were repeated four times for each sample, always using a fresh specimen and carried out in the linear regime. Two specimens were subjected to frequency sweep from low to high frequency, and two more from high to low. Strain sweeps were applied at a frequency of 6.28 rad/s and strain amplitudes from 0.01 to 1. After adjusting the gap, the samples were hold in quiescent state for 3 min before starting the rheological tests. This should allow orientation relaxation if there was any induced by sample loading. We also verified the effect of gap size on the viscoelastic properties of the nanocomposites at the maximum clay loading of C30B (i.e. 8 wt%). We observed that gap size had no significant effect on the results.

6.4 Results and discussion

6.4.1 Morphology of nanocomposites prepared using screw configuration #1 (SC1)

XRD patterns of PET nanocomposites with various C30B concentrations are shown in Figure 6-2. The nanocomposite samples are denoted with a nomenclature "PET/*x y*", where *x* and *y* denote concentration and type of clay particles, respectively. The gallery spacing of C30B powder (d_{001} diffraction), which is 1.85 nm, increases up to 3.4 nm ($2\theta \approx 2.5^{o}$) after being melt blended with PET. The enhancement of C30B basal spacing is due to the diffusion of the PET chains into the interlayer spacing of the layered silicate. Although the peak position of the XRD curves does not change with clay concentration, the intensity of the peaks increases

monotonically with clay concentration, which is a sign of more extensive domains of periodicity, (Delozier et al. 2003; Bhattacharya et al. 2007). Note that the second peaks observed at $2\theta \approx 5.2°$ may be attributed to the d_{002} diffraction and/or clay gallery collapse.

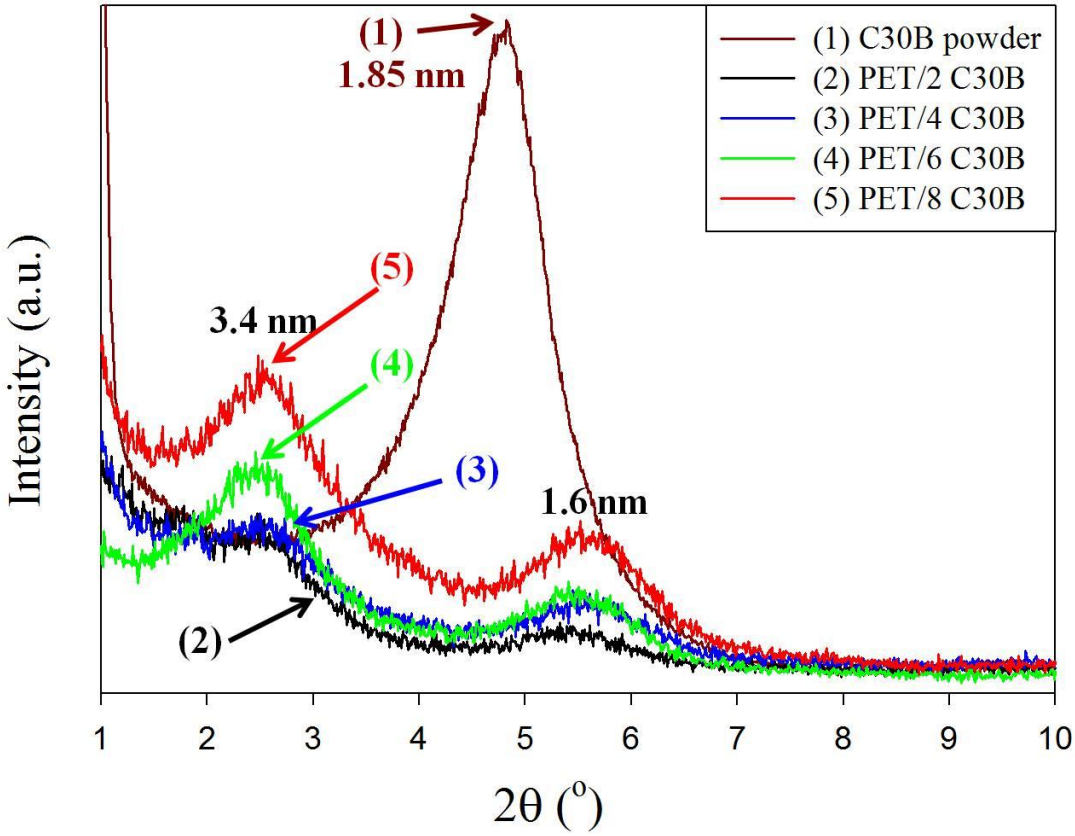

Figure 6-2: X-ray diffractograms of PET nanocomposites containing different weight fractions of C30B prepared by screw configuration #1 (SC1).

Figure 6-3 shows the SEM images of PET nanocomposites containing 2, 4, 6, and 8 wt% of C30B prepared using screw configuration #1 (SC1). This figure illustrates the state of the clay particles distribution within the PET matrix and the efficiency of SC1 in breaking down C30B aggregates. SEM results also show large aggregates for the nanocomposites at high clay loadings

(Figure 6-3b–d). Thirty-five (35) SEM micrographs were examined and it was concluded that the number of kneading elements and the residence time in SC1 for compounding are not sufficient to break down all the large aggregates.

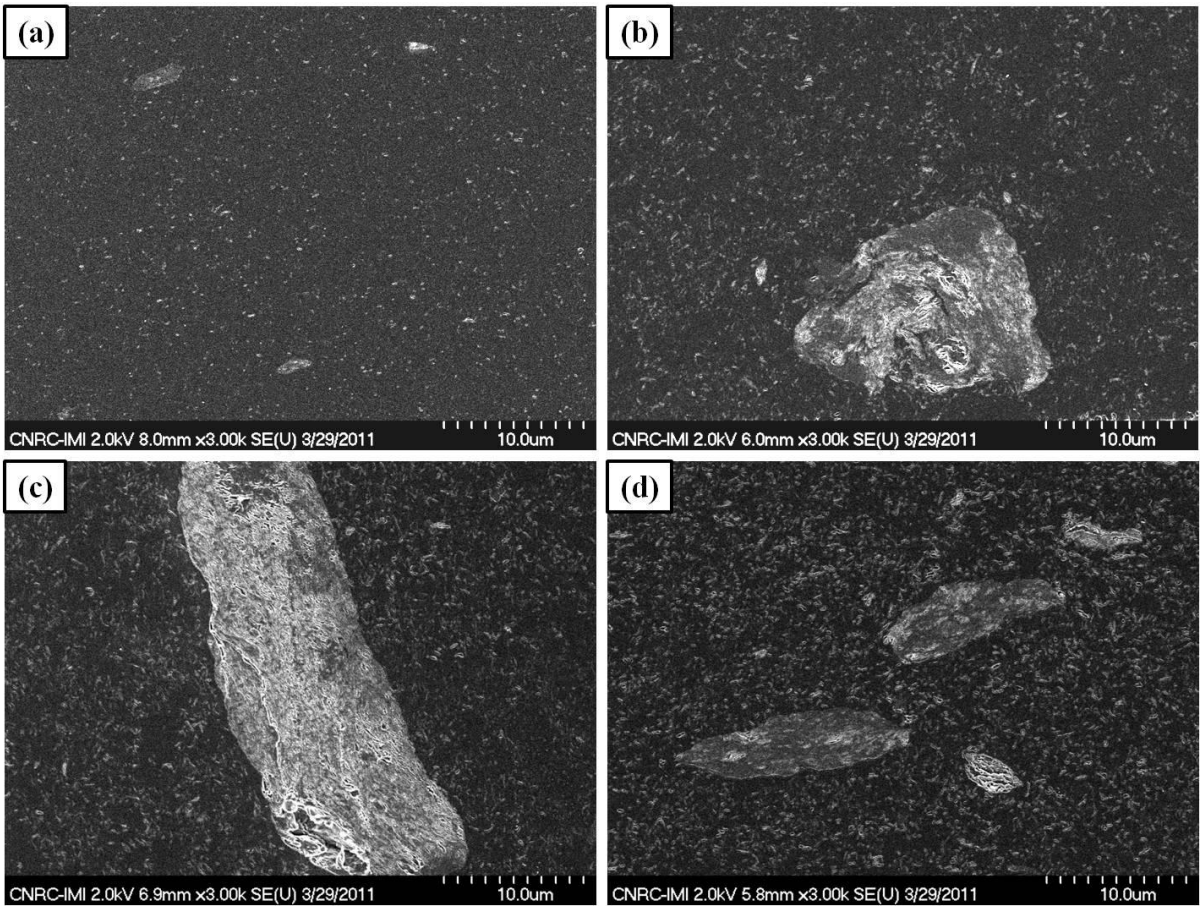

Figure 6-3: SEM micrographs of (a) PET/2 C30B, (b) PET/4 C30B, (c) PET/6 C30B and (d) PET/8 C30B nanocomposites prepared using screw configuration #1 (SC1).

6.4.2 Morphology of nanocomposites prepared using screw configuration #2 (SC2)

As the SC1 was not efficient for the compounding, additional kneading elements were employed in screw configuration #2 to increase the shear stresses. In addition, by placing reverse conveying

elements between the two last kneading blocks, a longer residence time was achieved for screw configuration #2 in comparison to screw configuration #1 (90 s vs. 51 s). Figure 6-4 presents the SEM micrographs of PET nanocomposites containing 2 and 6 wt% C30B prepared using screw configuration #2. The PET nanocomposite containing 2 wt% C30B exhibits a homogenous distribution of the clay particles all over the sample (Figure 6-4a). Using this screw configuration, even by incorporating 6 wt% C30B, no large aggregates are observed and the clay particles are well distributed within the PET matrix (Figure 6-4b). By comparing the morphologies of PET/6 C30B nanocomposites prepared using screw configurations #1 and #2 (Figure 6-3c and Figure 6-4b, respectively) it is seen that SC2 is more efficient than SC1 in breaking down the large clay aggregates, as expected. Changing screw configuration did not have a pronounced effect on XRD patterns of nanocomposites in terms of the peak position and shape of the peak (data are not shown here). Based on the poor morphology obtained using SC1, this screw configuration is not discussed further and all following results were obtained with SC2.

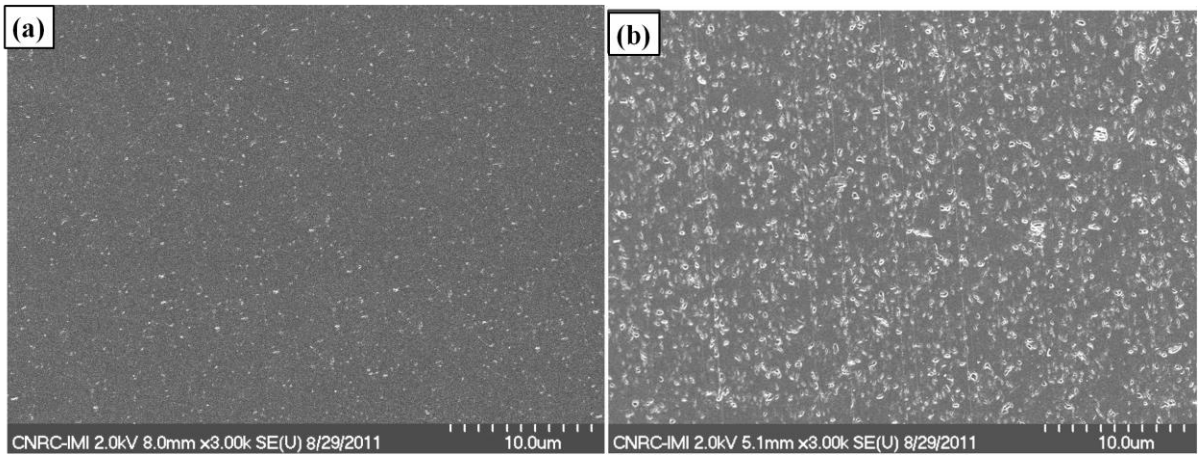

Figure 6-4: SEM micrographs of (a) PET/2 C30B and (b) PET/6 C30B (b) nanocomposites prepared using screw configuration # 2 (SC2).

6.4.3 Effect of clay concentration on the rheological properties of PET nanocomposites

Oscillatory time sweep tests were performed to examine if the neat PET and its corresponding nanocomposites had time-dependent rheological properties due to thermal degradation and/or possible chemical reactions between PET and the clay organo-modifiers. The complex viscosity and storage modulus of the neat PET and PET nanocomposites containing 2 to 8 wt% C30B are shown as functions of time in Figure 6-5a and Figure 6-5b, respectively. As stated before the time sweeps were repeated twice for each sample, always with a fresh specimen, and the results are shown in Figure 6-5 in the form of filled and unfilled symbols. These tests confirmed that for all samples a period of up to 10 min resulted in less than 10% changes in the viscoelastic properties. The complex viscosity of the PET nanocomposite containing 2 wt% C30B is observed to be lower than that of the neat PET. This is attributed to the severe degradation of the PET matrix in the presence of the organoclay. This aspect is discussed in more details below. A lower complex viscosity for PET nanocomposites containing 2 wt% of N28E and C30B in comparison to the same neat PET has been reported before (Ghanbari et al. In press.; Xu et al. 2011). For the nanocomposites containing 4, 6 and 8 wt%, the linear viscoelastic properties increase markedly with clay loading. For example the PET/8 C30B sample is more than 20 times more viscous than the neat PET.

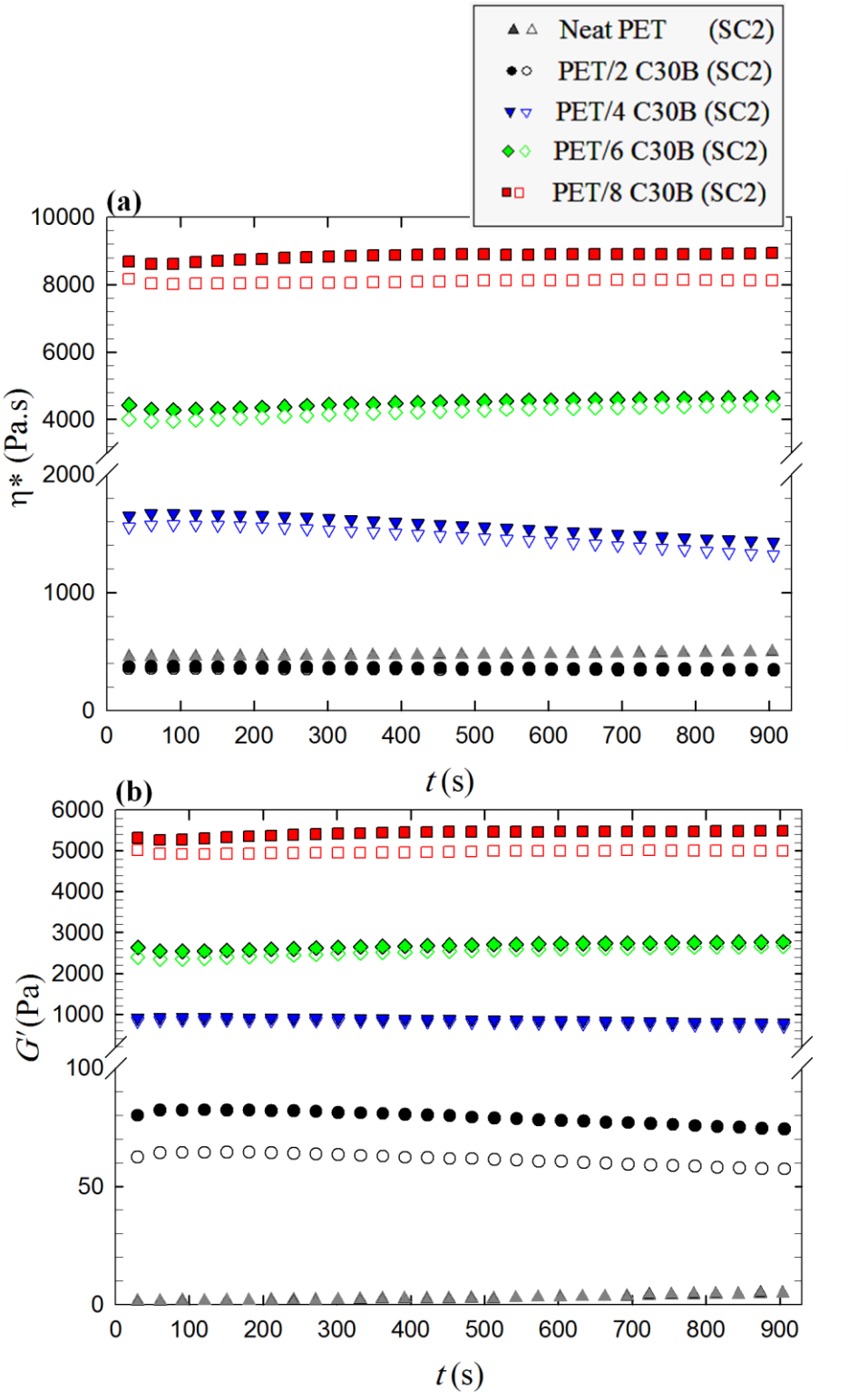

Figure 6-5: Modulus of complex viscosity (a) and storage modulus (b) as functions of time for the neat PET and PET/C30B nanocomposites.

The complex viscosity and storage modulus as functions of frequency for the neat PET and PET-based nanocomposites with various C30B loadings are presented in Figure 6-6a and Figure 6-6b, respectively. While the neat PET displays a pseudo-Newtonian behavior, the nanocomposites exhibit a marked solid-like behavior (Figure 6-6a), which becomes stronger with C30B concentration. Except for the sample containing 2 wt% C30B, the complex viscosity of PET increases with clay concentration at low frequencies. It seems that the incorporation of a small amount of C30B (2 wt%) lowers considerably the complex viscosity of the PET matrix. This behavior has been reported previously (Ghanbari et al. In press.; Wang et al. 2011). At low clay concentration, particle-particle interactions are not pronounced and the viscosity of PET nanocomposites is governed by the host polymer matrix. It has been well documented that the presence of organoclays leads to a severe chain scission of a PET matrix (Davis et al. 2002; Todorov and Viana 2007; Stoeffler et al. 2008; Litchfield et al. 2010). At high frequencies, where the behavior of the matrix is dominant, all PET nanocomposites show a lower viscosity than that of the neat polymer, which again can be attributed to the degradation induced by the presence of the organoclay.

One approach to determine the apparent viscosity of the degraded matrix in the nanocomposites is to use the Maron-Pierce empirical model:

$$\frac{\eta^*}{\eta_M^*} = (1 - \frac{\varphi}{\varphi_m})^{-2} \tag{6-1}$$

where η^* and η_M^* are the complex viscosity of the nanocomposite and the matrix, respectively, φ is the volume fraction of the clay and φ_m is the maximum packing volume fraction which is set

here as $\varphi_m = \frac{3.55}{p}$, where *p* is the clay aspect ratio (Sun et al. 2009; Wan et al. 2011). In that method TEM images are used to determine the length to thickness ratio of clay particles. For overlapped tactoids, the average thickness and overall length were used, while an end-to-end vector was considered for length of curved tactoids. The aspect ratio of the clay particles was determined by the method described by Ghasemi *et al*. (Ghasemi et al. 2012). A value of 46 was obtained for the average aspect ratio of the silicate particles in the PET matrix. Ghasemi *et al*. (Ghasemi et al. 2012) and Fornes and Paul (Fornes and Paul 2003) reported values of 47 and 57, respectively, for the aspect ratio of C30B layered silicates in nanocomposites prepared by melt blending.

The matrix apparent viscosity, $\eta^*_{M(100rad/s)}$, is evaluated at 100 rad/s where the contribution of the matrix should be dominant, using the Maron-Pierce empirical model (Equation 6-1). The calculated apparent matrix viscosity is presented in Table 6-2 for neat PET and PET-based nanocomposites.

From the apparent matrix viscosity, it is possible to estimate an apparent matrix molecular weight in order to quantify the degradation induced by the presence of the organoclay. To this end the classical relationship between the zero-shear viscosity, η_0, and the weight average molecular weight, M_w, has been used, assuming a pseudo-Newtonian behavior for the PET matrix:

$$\eta^*_{M(100rad/s)} \approx \eta_0 = kM_w^{3.4} \tag{6-2}$$

where *k* is taken as $3.02\times10^{-4}(mol^{3.4}/s.kg^{3.4})$ considering the neat PET's molecular weight and complex viscosity. The apparent matrix molecular weight is reported in Table 6-2 for the neat

PET and PET-based nanocomposites. Both the zero-shear viscosity and molecular weight of the PET matrix for PET/C30B nanocomposites are found to decrease with clay concentration, and this behavior is attributed to the severe degradation (i.e. chain scission) of the PET matrix in the presence of the organoclay. It explains the lower complex viscosity for the nanocomposites at high frequencies observed in Figure 6-6a, in comparison to the neat sample. The results for the apparent matrix viscosity and apparent matrix molecular weight of PET nanocomposites containing 6 wt% C15A, C25A, and N28E reported in Table 6-2 will be discussed later.

Table 6-2: Apparent complex (≈ zero-shear) viscosity and apparent molecular weight for the neat PET and the PET matrix in nanocomposites calculated from Equations 6-1 and 6-2, respectively.

Sample	Matrix apparent complex viscosity at 100	Matrix apparent molecular weight (kg/mol)
Neat PET	440	65.0*
PET/2 C30B	174	49.5
PET/4 C30B	98	41.8
PET/6 C30B	51.9	34.7
PET/8 C30B	30.9	29.8
PET/6 C15A	57	35.6
PET/6 N28E	64.6	37.0
PET/6 C25A	91.6	41.0

* This value is reported based on the works of Fox et al. (Fox et al. 1997) and Champagne et al. (Champagne et al. 1999) using the same grade of PET.

The effect of C30B content on the storage modulus of the PET nanocomposites can be observed in Figure 6-6b. The storage modulus increased significantly with C30B concentration at low frequencies. With increasing clay loading, the dependence of storage modulus on frequency

decreases (slope of G' vs. ω at low frequencies reported in text boxes), and at high clay concentrations (6 and 8 wt%), the storage modulus is nearly independent of frequency at low frequencies. This pseudo-solid-like behavior is attributed to the formation of a space-filling interconnected network of clay particles. This percolated three-dimensional network acts like a weak solid and causes significant enhancement of the storage modulus, as well as the emergence of a low frequency plateau (Mobuchon et al. 2007; Aubry et al. 2005; Eslami et al. 2010; Solomon et al. 2001; Vermant et al. 2007; Wu et al. 2005; Mobuchon et al. 2009a; Pujari et al. 2011). Although the incorporation of 2 wt% C30B in the PET matrix enhances the low frequency storage modulus, a sharp increment is seen when the clay concentration reaches 4 wt%, implying the formation of a percolated network.

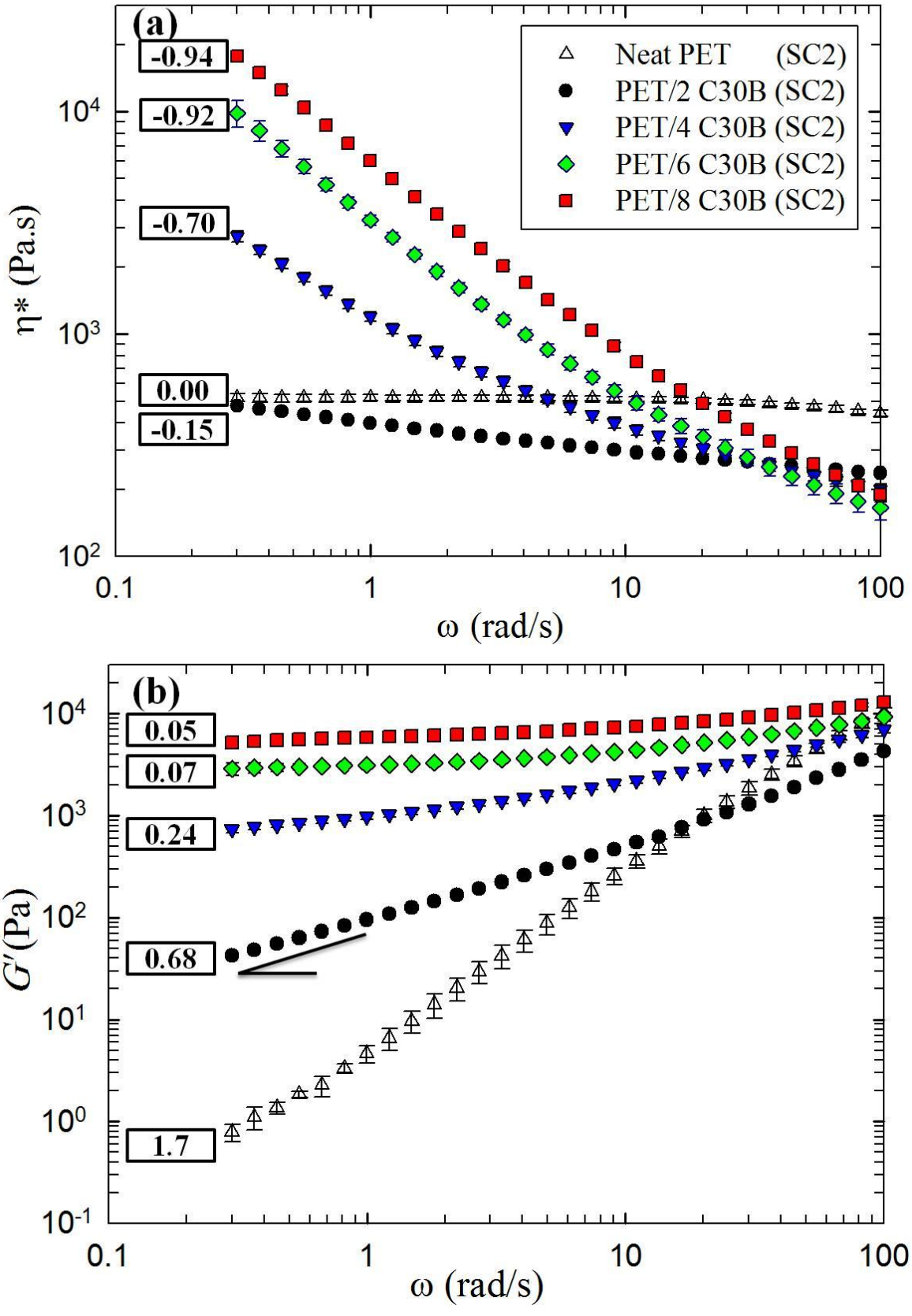
(a)
-0.94
-0.92
-0.70
0.00
-0.15
Neat PET (SC2)
PET/2 C30B (SC2)
PET/4 C30B (SC2)
PET/6 C30B (SC2)
PET/8 C30B (SC2)
η* (Pa.s)
ω (rad/s)
(b)
0.05
0.07
0.24
0.68
1.7
G′(Pa)
ω (rad/s)

Figure 6-6 Modulus of complex viscosity (a) and storage modulus (b) of PET/C30B nanocomposites (frequency sweep tests). Numbers in the text boxes represent the η* and *G'* slopes at low frequencies.

Figure 6-7 shows the reduced viscosity and reduced storage modulus of the neat PET and PET nanocomposites containing 2 to 8 wt% C30B as functions of angular frequency. The reduced viscosity (Figure 6-7a) is obtained by taking the ratio of the magnitude of the complex viscosity of the various samples to the matrix apparent viscosity estimated at 100 rad/s (Table 6-2). It is observed that the reduced viscosity increases with clay content on the whole frequency range. Hence, the normalization allows removing thermal degradation effects to highlight the clay contribution. The reduced viscosity of the PET nanocomposites exhibits a very strong solid-like behavior at high clay loadings with a slope on the log-log plots approaching -1. The reduced storage modulus (Figure 6-7b) is obtained by taking the ratio of the magnitude of the storage modulus of the various samples to the matrix apparent viscosity estimated at 100 rad/s (Table 6-2) and the frequency equal to 100 rad/s. It also increases with clay concentration and exhibits a low frequency plateau at high clay loadings. It is noteworthy to mention that the reduced storage modulus of the neat PET does not exceed the reduced storage modulus of PET nanocomposites at high frequencies, as previously seen in Figure 6-6a when thermal degradation effects are not accounted for.

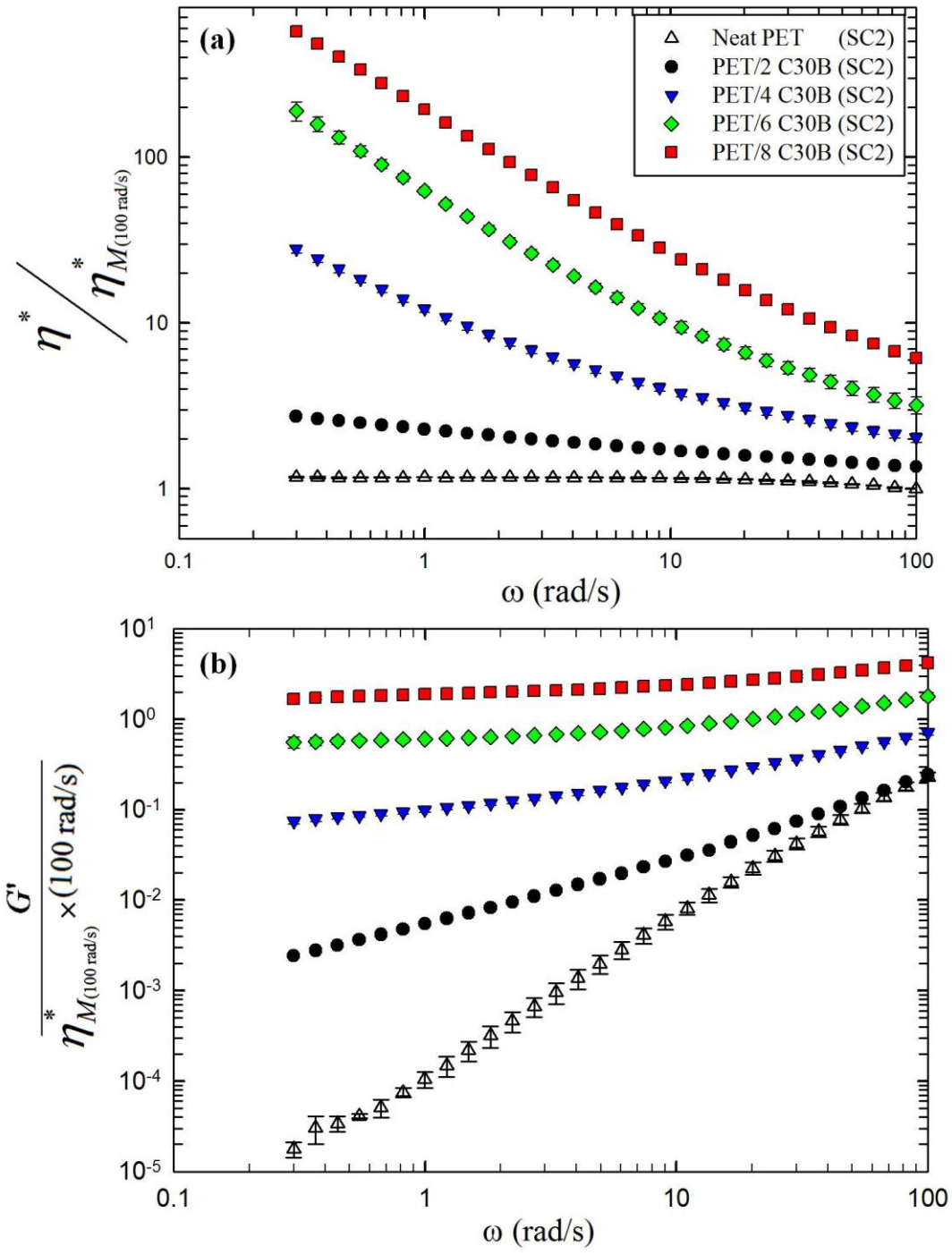

Figure 6-7: Reduced viscosity (a) and reduced storage modulus (b) of the neat PET and PET/C30B nanocomposites as functions of clay loading and frequency.

Figure 6-8 reports plots of the elastic modulus vs. the loss modulus for PET nanocomposites containing 2 to 8 wt% C30B and prepared using screw configurations #1 and #2. PET nanocomposites containing 2, 4, and 6 wt% C30B and prepared using screw configuration #2 exhibit larger values of the elastic modulus in comparison to those prepared using screw configuration #1. These observations suggest that a better dispersion of C30B particles is obtained by employing screw configuration #2, in good agreement with SEM micrographs of Figure 6-3 and Figure 6-4. The data for the PET/8 C30B nanocomposites prepared by screw configurations #1 and #2 are however very similar. It seems that when the clay concentration is very high, even the more severe screw geometry cannot help breaking down the large aggregates and disperse further the nanoparticles. Consequently, morphologies similar to that presented in Figure 6-3d are expected for PET/8C30B nanocomposites prepared using screw configuration #2. This may be attributed to the lack of sufficient space for the dispersion of clay particles, as the C30B volume fraction is equal to 0.046, which is close to the maximum packing volume fraction ($\varphi_m = 3.55 / p = 0.077$). Hence, some clay tactoids may remain undelaminated. Therefore we may expect a lower level of exfoliation and higher number of clay aggregates at increasing clay concentration, which will be proven later in this study using image analysis. At high clay loadings plots of G' vs. G'' (Figure 6-8) exhibit pseudo solid-like behavior for both screw configurations, indicating the presence of an interconnected network of individual clay platelets and/or intercalated tactoids acting like a weak solid. The differences between the elastic modulus of PET nanocomposites prepared using screw configurations #1 and #2 are more pronounced at low values of the loss modulus (low frequencies) where the effect of clay particles is more pronounced.

As observed earlier in Figure 6-7b, a significant increase (almost four orders of magnitude with respect to the neat PET) of the low frequency G' of PET nanocomposites takes place for the clay concentration of 4 wt%, and the rheological behavior changes from liquid- to solid-like. These observations suggest that percolation must happen when the C30B concentration increases from 2 to 4 wt%.

The value of the elastic modulus at low frequencies (ω = 0.3 rad/s) was used to determine the percolation threshold for PET/C30B nanocomposites. The following percolation model (Vermant et al. 2007; Khalkhal et al. 2011) was used:

$$G' \propto (\varphi - \varphi_{per})^n \tag{6-3}$$

where φ_{per} and n are the percolation threshold volume fraction and a power-law exponent, respectively. The parameter n is equal to 1.68 and 1.07 for screw configurations #1 and #2, respectively. The calculated percolation values (in wt%) are 3.4 and 3.2 for PET/C30B nanocomposites prepared using screw configuration 1 and 2, respectively, hence between 2 and 4 wt% as suggested by Figure 6-6b and Figure 6-7b. It seems that the screw configuration and residence time does not impact much the value of the percolation threshold, which is somehow surprising.

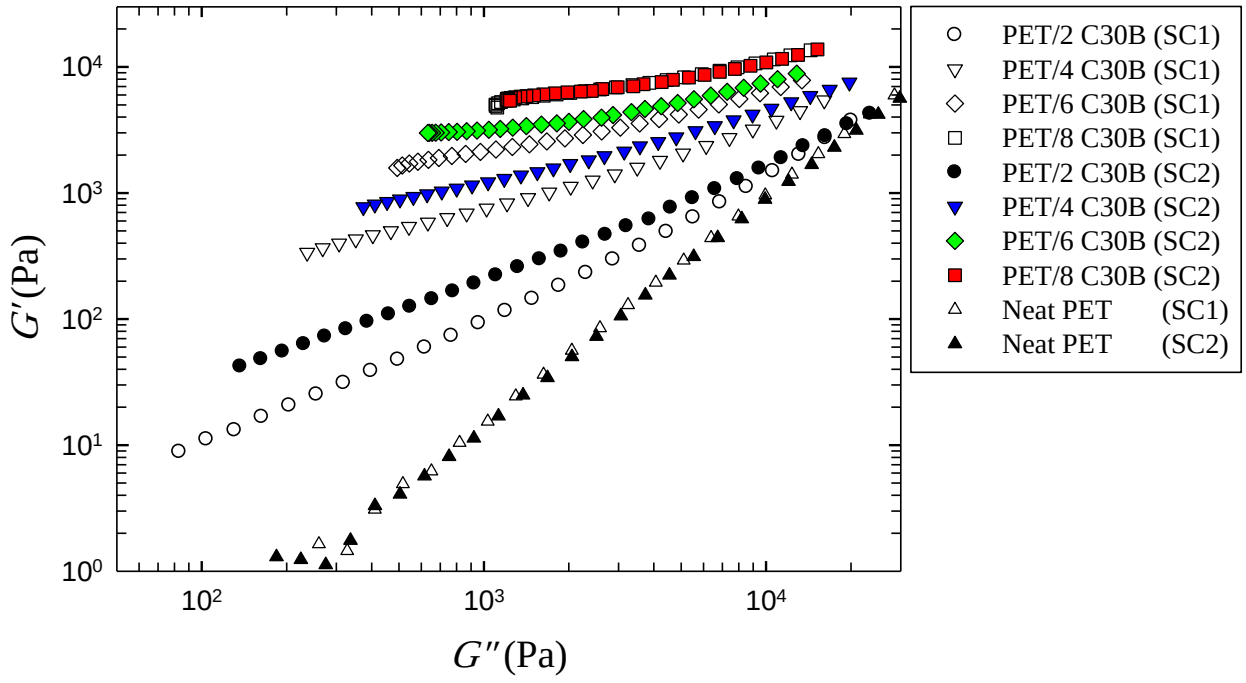

Figure 6-8: Storage modulus vs. loss modulus for the neat PET and PET/C30B nanocomposites prepared using screw configurations #1 (SC1) and #2 (SC2).

The pseudo solid-like behavior of the storage modulus at low frequencies indicates the existence of a yield stress for these systems. To observe this effect more clearly, we plot the complex viscosity vs. complex modulus in Figure 6-9 as a function of C30B concentration. A sharp increase of the complex viscosity as the complex modulus decreases indicates the existence of an apparent yield stress. This representation highlights clearly the presence of a yield stress in the PET nanocomposites with clay concentration above the percolation threshold of ~ 3 wt%. The presence of an apparent yield stress was also observed by other researchers for various nanocomposite systems (Mitchell and Krishnamoorti 2002; Abbasi et al. 2009; Mobuchon et al. 2007; Galgali et al. 2001; Aubry et al. 2005).

To estimate the apparent yield stress, a modified Herschel-Bulkley model is used as follows:

$$\eta* = \frac{G_0^*}{\omega} + k\left(\gamma^0\omega\right)^{n-1} \tag{6-4}$$

where G_0^* is the magnitude of the complex modulus at the lowest frequency, γ^0 is the strain amplitude, *k* is a constant, and *n* is the flow index which determine the behavior of the fluid.

It has been observed that yield stress, $\sigma_0 = G_0^*\gamma^0$, and *n* can be related to the microstructure of nanocomposites (Xia and Song 2006; Litchfield and Baird 2006). A lower value of *n* means a higher shear-thinning behavior, which corresponds to a stronger network. Therefore, it is reasonable to expect a lower value of *n* when clay concentration increases. Besides, stronger particle-particle and/or polymer-particle interactions results in larger apparent yield stresses (Litchfield and Baird 2006). Table 6-3 lists the calculated Herschel-Bulkley parameters for the PET-based nanocomposites, and the fits of Equation 6-4 are shown by the dashed lines in Figure 6-9 for the PET/C30B nanocomposites. The Herschel-Bulkley parameters for PET nanocomposites containing 6 wt% C15A, C25A, and N28E will be discussed later. PET nanocomposites containing C30B exhibit larger values of the yield stress at the same clay concentration. This is indicative of the stronger affinity of C30B for PET compared to the other clays. The shear-thinning exponent, *n*, decreases slightly with clay content, implying the formation of a stronger network at high clay loadings.

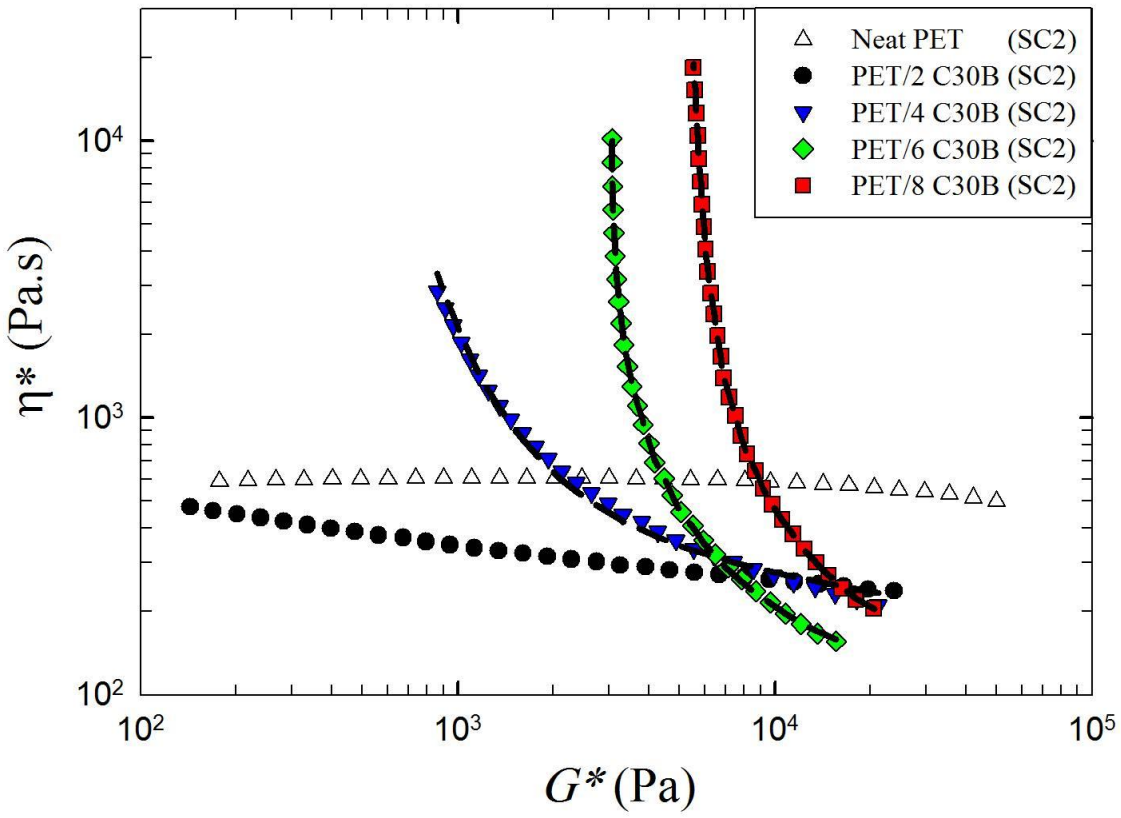

Figure 6-9: Complex viscosity vs. complex modulus for neat PET and PET/C30B nanocomposites. Dashed lines are fits of Equation 4 for clay content above 2 wt%.

Table 6-3: Herschel-Bulkley parameters for PET nanocomposites.

Sample	$\sigma_0 = G_0^* \times \gamma^0$ **(Pa)**	***k*** **(Pa.s^n)**	***n***
PET/4 C30B (SC2)	25.7	257	0.88
PET/6 C30B (SC2)	91.8	152	0.85
PET/8 C30B (SC2)	166	189	0.78
PET/6 C25A (SC2)	69.5	417	0.82
PET/6 C15A (SC2)	43.4	215	0.84

PET/6 N28E (SC2)	41.8	266	0.82

It has been reported that the limit of linearity, γ_c^0, of filled systems is very sensitive to filler content (Yziquel et al. 1999; Eslami et al. 2010; Aubry et al. 2005; Khalkhal and Carreau 2011; Vermant et al. 2007). Figure 6-10 shows the normalized storage modulus (i.e. G'/G'_0, where $G_0^{'}$ is the storage modulus at the smallest strain) as a function of strain, γ^0, for the neat PET and PET/C30B nanocomposites at 6.28 rad/s. The dashed line indicates the transition from the linear to nonlinear behavior, which is defined as the threshold where the storage modulus decreases by more than 10% from its value at the smallest strain (i.e. $G'/G_0^{'} < 0.9$) (Khalkhal and Carreau 2011). Nonlinearity appears at lower strain as the C30B concentration increases. Clay particles are solid, so the straining motion is totally concentrated in the polymer melt, which increases the effective deformation of the matrix and reduces the linearity limit (Vermant et al. 2007). The inset in Figure 6-10 illustrates the maximum strain amplitude for the linear viscoelastic behavior as a function of the clay volume fraction. It is observed that critical strain displays a power-law dependency on the volume fraction of C30B, which is approximated by the following relation:

$$\gamma_c^0 \propto \varphi^{-2} \tag{6-5}$$

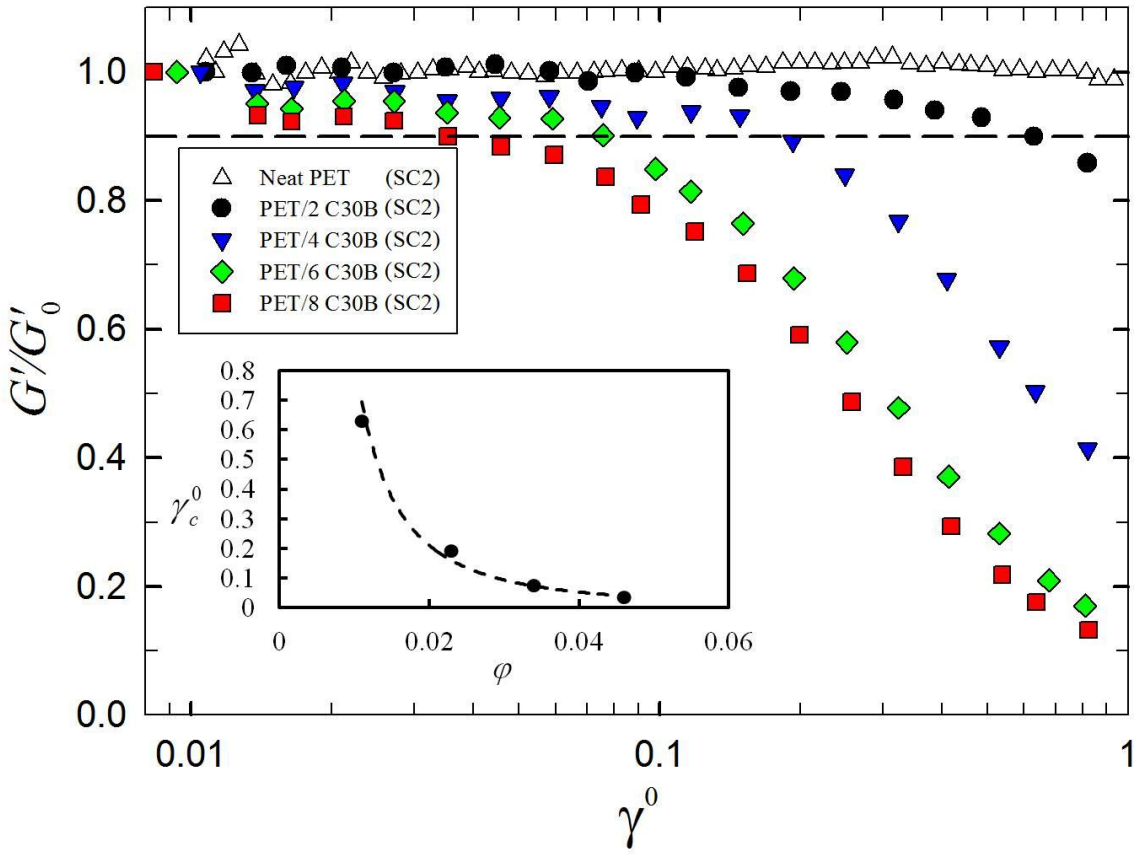

Figure 6-10: Normalized storage modulus vs. strain amplitude for the neat PET and PET/C30B nanocomposites at 6.28 rad/s. The inset shows the maximum strain amplitude for the linear viscoelastic behavior as a function of the clay volume fraction.

6.4.4 The effect of clay chemistry on the morphology and rheology of PET nanocomposites

The morphology of a polymer nanocomposite, which governs the final properties, is dependent on particle-particle interactions, but also on the degree of compatibility between the polymer matrix and the organoclay that rules polymer-particle interactions. Therefore, the existence of

strong interactions between silicate layers and a host polymer matrix is essential to achieve desirable properties. In this work, in addition to various organo-modified clays (C30B, C15A, C25A, and N28E), the effect of a pristine synthetic clay (i.e. SM100) is examined. PET nanocomposites containing 6 wt% of different clays were prepared using screw configuration #2, and their corresponding XRD patterns are shown in Figure 6-11. As expected, the PET chains are not able to diffuse within the gallery spacing of SM100 layered silicate and the gallery spacing remains the same as the clay alone (Table 6-1). The largest increase of the basal spacing, 1.55 and 1.44 nm, were obtained for C30B and C25A, respectively. The gallery spacing of N28E and C15A shows only 1.0 and 0.45 nm enhancement in their corresponding PET nanocomposites. Therefore, higher viscoelastic properties are expected for PET nanocomposites containing C30B and C25A, in comparison to those containing N28E or C15A. It has been also shown by other researchers that the higher surfactant content of C15A, which results in a high initial gallery spacing, does not guarantee a higher intercalation in a polymer matrix (Hyun et al. 2001; Ray and Bousmina 2005).

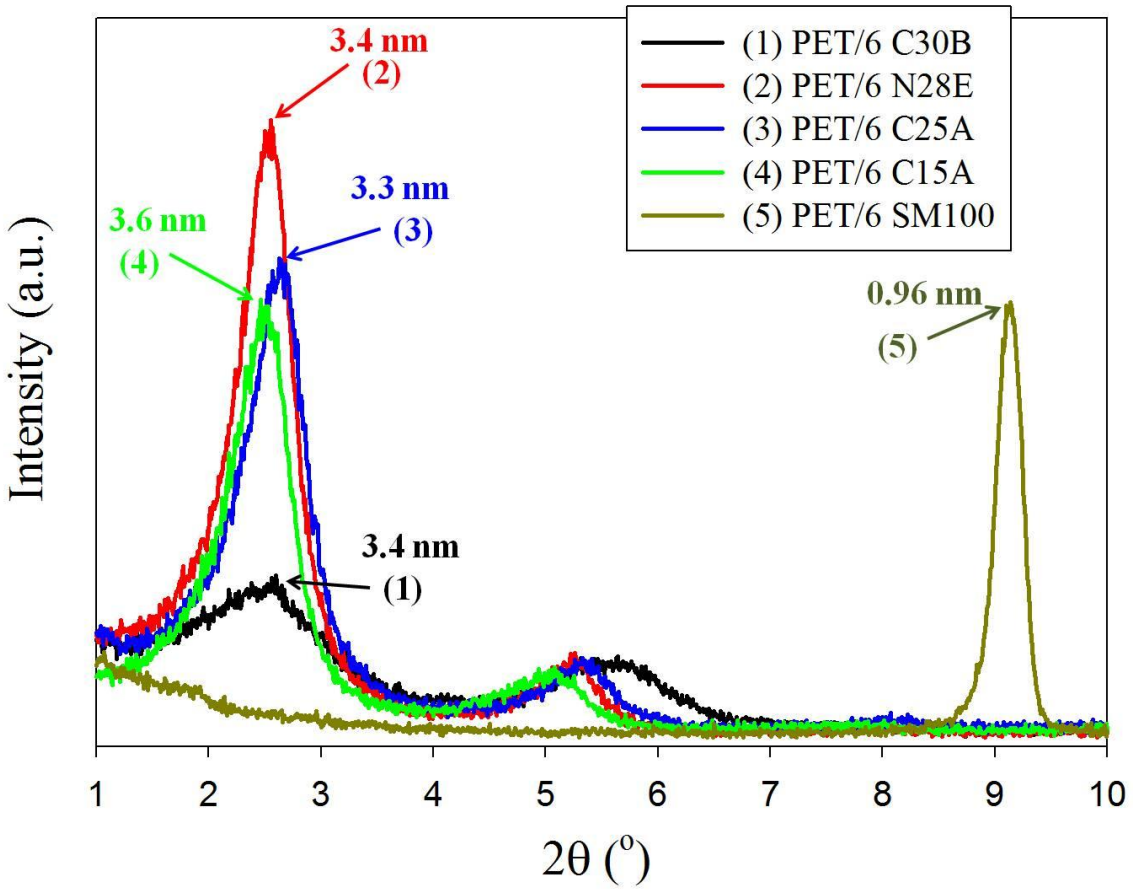

Figure 6-11: XRD patterns of PET nanocomposites containing 6 wt% clay particles prepared using screw configuration #2 (SC2).

Figure 6-12 reports the complex viscosity and storage modulus of the neat PET and PET nanocomposites containing 6 wt% of C30B, C15A, C25A and N28E prepared using screw configuration #2. All PET nanocomposites exhibit a strong solid-like behavior (Figure 6-12a), as well as a pseudo solid-like behavior at low frequencies (Figure 6-12b). These rheological observations are in good agreement with the XRD results: the lower peaks shown in Figure 6-11 at $2\theta = 2.5^{o}$ suggest a better clay dispersion for C30B and C25A in comparison to N28E and

C15A, resulting in larger values for the complex viscosity and storage modulus at low frequencies.

The solubility parameter, δ, of the different organoclay surfactants was calculated based on the Fedors group contribution method to evaluate the extent of compatibility of PET with the various organoclays (Van Krevelen and Te nijenhuis 2009). According to the solubility parameters presented in Table 6-1, the order of favorable interactions between PET and the organoclays is: $C30B > C25A > C15A > N28E$, which is in good agreement with the rheological observations.

As mentioned earlier, the yield stress can be used to quantify the solid-like character of nanocomposites. Larger yield stress means better dispersion of clay particles in nanocomposites at the same clay concentrations (Litchfield and Baird 2006; Xia and Song 2006). The Herschel-Bulkley parameters for PET nanocomposites containing 6 wt% of different organoclays are reported in Table 6-3. Experimental data of the complex viscosity vs. complex modulus are shown in Figure 6-13, along with the fits of Equation 6-4 (dashed lines). The values of the apparent yield stress exhibit the following order for PET nanocomposites containing the different organoclays: $C30B > C25A > C15A > N28E$, in good agreement with the order of favorable interactions between PET and the organoclays based on the solubility parameter. It is observed, however, that the shear-thinning exponents of PET nanocomposites containing the various organoclays are almost the same, hence the behavior of the different fluids does not change much. The better morphology and rheological properties obtained for nanocomposites containing C30B are attributed to the favorable interactions between carboxyl groups of the PET chains and hydroxyl groups of the C30B organic modifier (Ghasemi et al. 2011b).

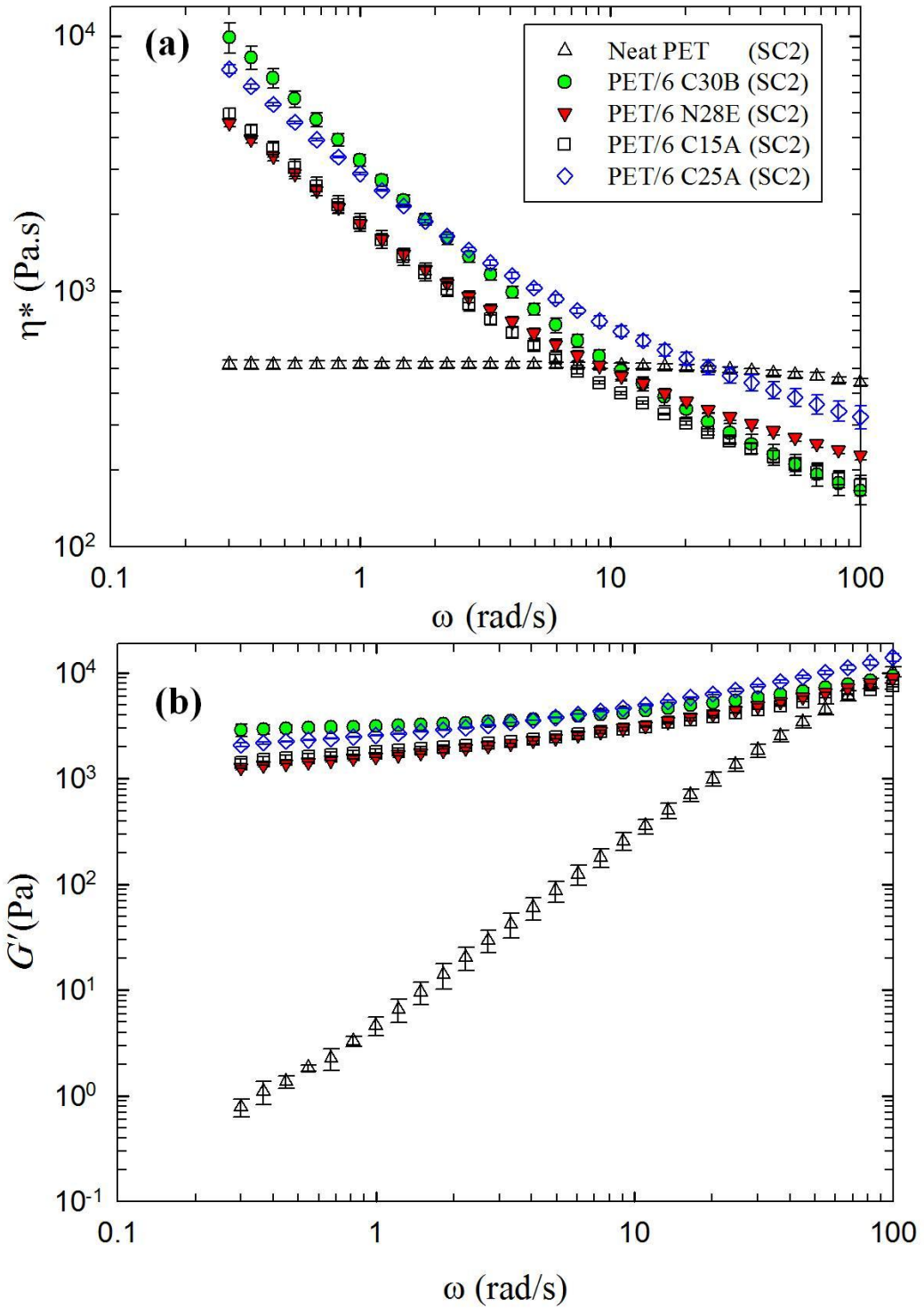

Figure 6-12: Complex viscosity (a) and storage modulus (b) for PET nanocomposites containing 6 wt% organoclays prepared using screw configuration #2 (SC2).

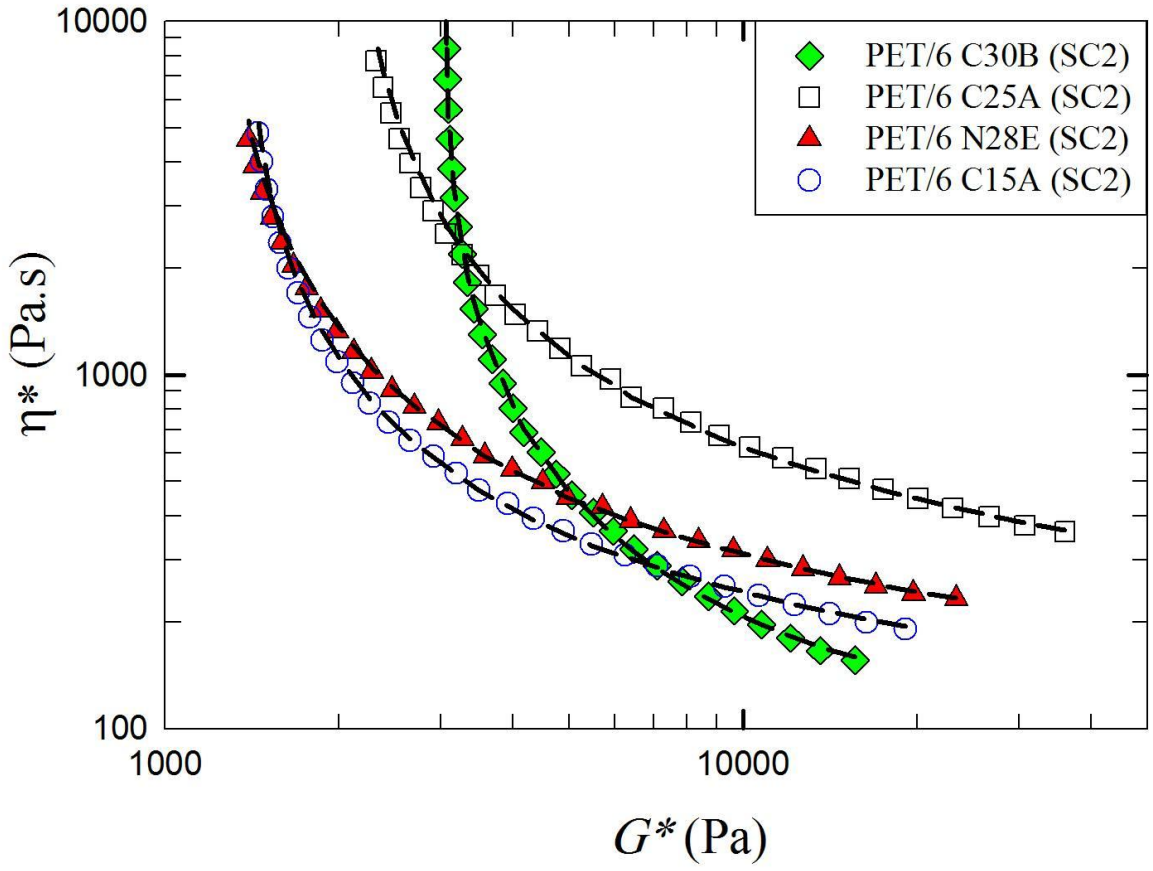

Figure 6-13: Complex viscosity vs. complex modulus for PET nanocomposites containing 6 wt% of various organoclays. Dashed lines are fits of Equation 6-4.

As done above, the apparent viscosity and apparent molecular weight of the degraded PET matrix in the nanocomposites containing 6 wt% of different organoclays are reported in Table 6-2. It is observed that the reduction of the PET matrix apparent molecular weight and apparent viscosity is dependent on the surfactant chemistry of the organoclay (Table 6-1). The highest degradation occurs for the matrix containing C30B, which can be attributed to the specific organic modifier of this organoclay. Previous studies have shown that a better dispersion of organoclays increase the exposure of silicate nanoplatelet surfaces to the polymer matrix, and results in a higher level of

thermal degradation (Fornes et al. 2003). In addition, organoclays modified with unsaturated tallow that contain double bonds in their alkyl chain result in a greater degradation, in comparison to those modified with hydrogenated tallow (Yoon et al. 2003). Surfactants with double bonds are prone to free radical formation and induce more chain scission, as the free radicals can attack polymer chains. It has also been shown that organic modifiers possessing hydroxyl-ethyl groups lead to more degradation than those having methyl groups (Fornes et al. 2003; Yoon et al. 2003). As C30B has the highest level of exfoliation in the PET matrix and its organic modifier contains unsaturated tallow as well as hydroxyl-ethyl groups (Table 6-1), a higher level of thermal degradation is expected for PET nanocomposites containing this organoclay. This is confirmed by the lowest apparent molecular weight reported in Table 6-2 (34.7 kg/mol) for a 6 wt% clay content. The amount of organic modifier used in the treatment of C15A is larger than the cation exchange capacity (CEC) of the pristine montmorillonite (125 meq/100 g clay vs. 92.6 meq/100 g clay, an excess of nearly 35%). This excess gives rise to unbounded surfactant that may cause more degradation (Mittal 2011; Cui et al. 2008). N28E has 25% excess of the organic modifier while C25A bear an excess of only 2.6%. The unbound surfactant of C15A and N28E can result in a significant degradation of the PET matrix, as confirmed by the low apparent molecular weights of 35.6 and 37 kg/mol reported in Table 6-2 for PET/6 C15A and PET/6N28E, respectively. In contrast, C25A yields the lowest thermal degradation, as confirmed by the largest apparent molecular weight reported in Table 6-2 (41 kg/mol) for the nanocomposites containing 6 wt% C25A.

Figure 6-14 presents the reduced complex viscosity and reduced storage modulus vs. frequency for the neat PET and PET nanocomposites containing 6 wt% C30B, C15A, C25A, and N28E

prepared using screw configuration #2. The reduced viscosity of all the PET nanocomposites is now larger than that of the neat PET, even at 100 rad/s, and it shows a remarkable solid-like behavior. Hence, again the normalization allows removing the effect of the PET matrix thermal degradation. As expected, PET nanocomposites containing C30B and N28E exhibit the largest and the smallest reduced complex viscosities, respectively. The reduced storage modulus of PET nanocomposites containing 6 wt% of the different organoclays is larger than that of the neat PET on the whole frequency range. The largest and the smallest reduced storage modulus are exhibited by the PET nanocomposites containing C30B and N28E, respectively. It is of interest to look more closely at their respective morphologies in order to correlate with the rheological behavior.

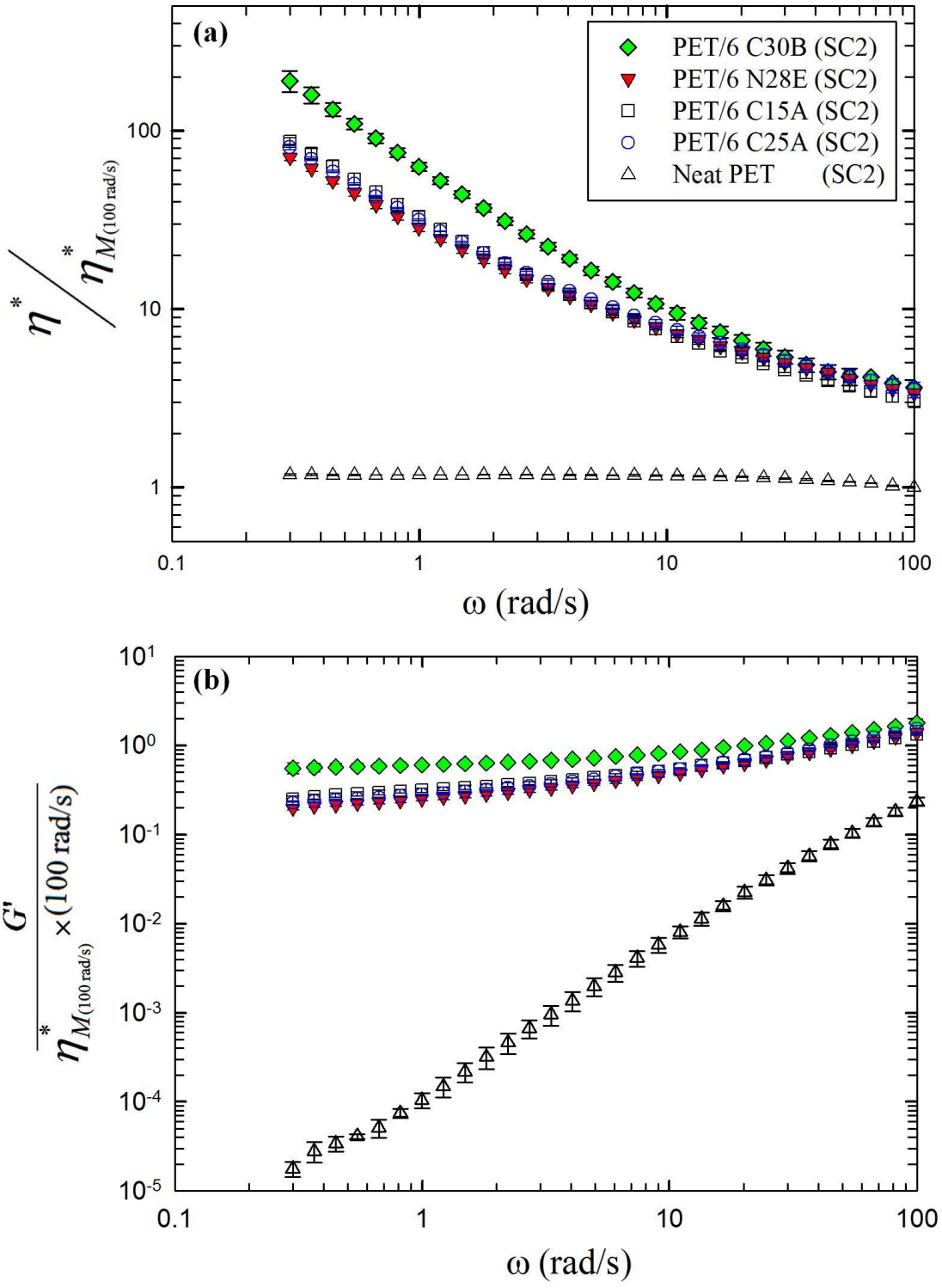

Figure 6-14: Reduced viscosity (a) and reduced storage modulus (b) for neat PET and PET nanocomposites containing 6 wt% C30B, C15A, C25A, and N28E prepared using screw configuration #2.

SEM and TEM techniques were used to examine the state of spatial distribution and dispersion of C30B and N28E particles in the PET matrix. Figure 6-15 presents SEM micrographs of PET nanocomposites containing 6 wt% C30B and N28E prepared using screw configuration #2. There are more empty spaces neighboring N28E particles than C30B particles. It seems that PET nanocomposites containing C30B exhibit higher clay density than those containing N28E. Based on the SEM observations, more particle-particle and polymer-particle interactions are expected for this nanocomposite, due to the higher clay distribution density resulting from fewer aggregates. The interpretations of the SEM micrographs are in good agreement with the XRD (Figure 6-11) and rheological results (Figure 6-14).

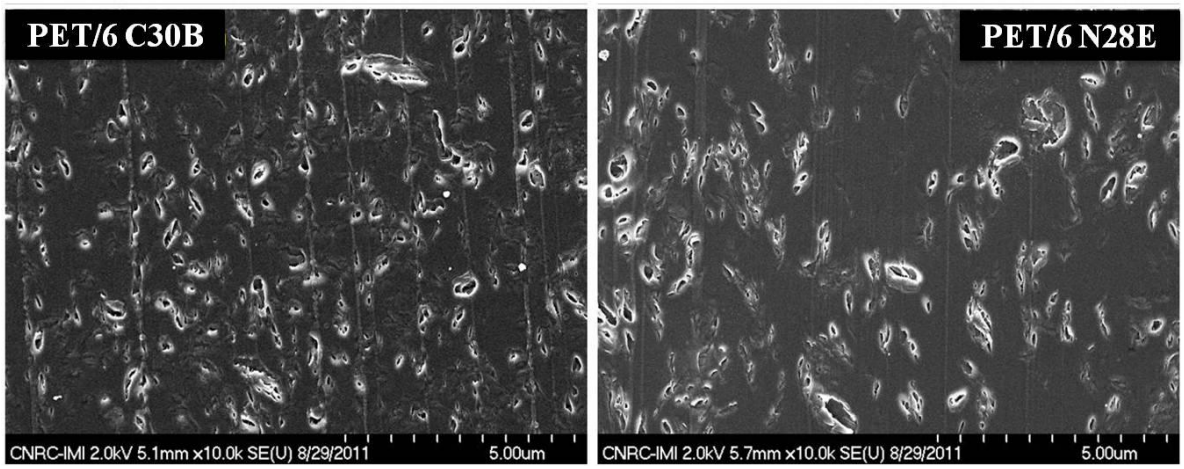

Figure 6-15: SEM micrographs of PET nanocomposites containing 6 wt% C30B and N28E prepared using screw configuration #2 (SC2).

Typical TEM bright field images of PET nanocomposites containing 2 and 6 wt% C30B and those containing 6 wt% N28E are shown in Figure 6-16. Both individual platelets and tactoid aggregates are seen in the images. It is not easy to differentiate PET nanocomposites containing 2 and 6 wt% C30B based on the high magnification of the TEM images. A better exfoliation of

C30B in comparison to N28E in the corresponding PET nanocomposites is obvious at both low and high magnification TEM images. Again, TEM results are in good agreement with XRD, SEM and rheology results presented before.

To quantitatively estimate the degree of layer dispersion in the PET nanocomposites, a technique based on free-path spacing distance introduced by Luo and Koo is used (Luo and Koo 2007, 2008). In this method, the free-path distance between the platelets is measured by drawing random lines (usually horizontal and/or vertical) to intercept silicate layers in a TEM image. After measuring the free-path distance between the platelets, the dimensionless dispersion value, $D_{0.1}$, is calculated based on the distribution of the free-path spacing distances between the clay layers according to the following equation:

$$D_{0.1} = 1.1539\times10^{-2} + 7.5933\times10^{-2}\left(\mu/\sigma\right) + 6.6838\times10^{-4}\left(\mu/\sigma\right)^2 - 1.9169\times10^{-4}\left(\mu/\sigma\right)^3 + 3.9201\times10^{-6}\left(\mu/\sigma\right)^4 \quad (6\text{-}6)$$

where μ is the mean spacing between the clay layers, and σ is the standard deviation.

A value below 4% for $D_{0.1}$ suggests an immiscible system or microcomposite, and values over 8% indicate an exfoliated structure, while values between 4 and 8% indicate intercalation. For approximately 500 measurements, performed on around 15 TEM images with 50 and 100 nm scale bars, $D_{0.1}$ values of 5.8, 5.5, and 4.3% were obtained for PET/2 C30B, PET/6 C30B, and PET/6 N28E nanocomposites, respectively. We obtained a $D_{0.1}$ value of 7.5 for a PET/2wt% C30B, but in drawn films prepared via a larger twin-screw extruder (Ghanbari et al. In press.). Higher dispersion value of PET/6 C30B in comparison to that of PET/6 N28E indicates a higher level of intercalation for this nanocomposite, in agreement with the XRD patterns and SEM

micrographs. On the other hand, a reduction of the $D_{0.1}$ value with clay concentration indicates that the level of clay exfoliation is less when the clay loading increases.

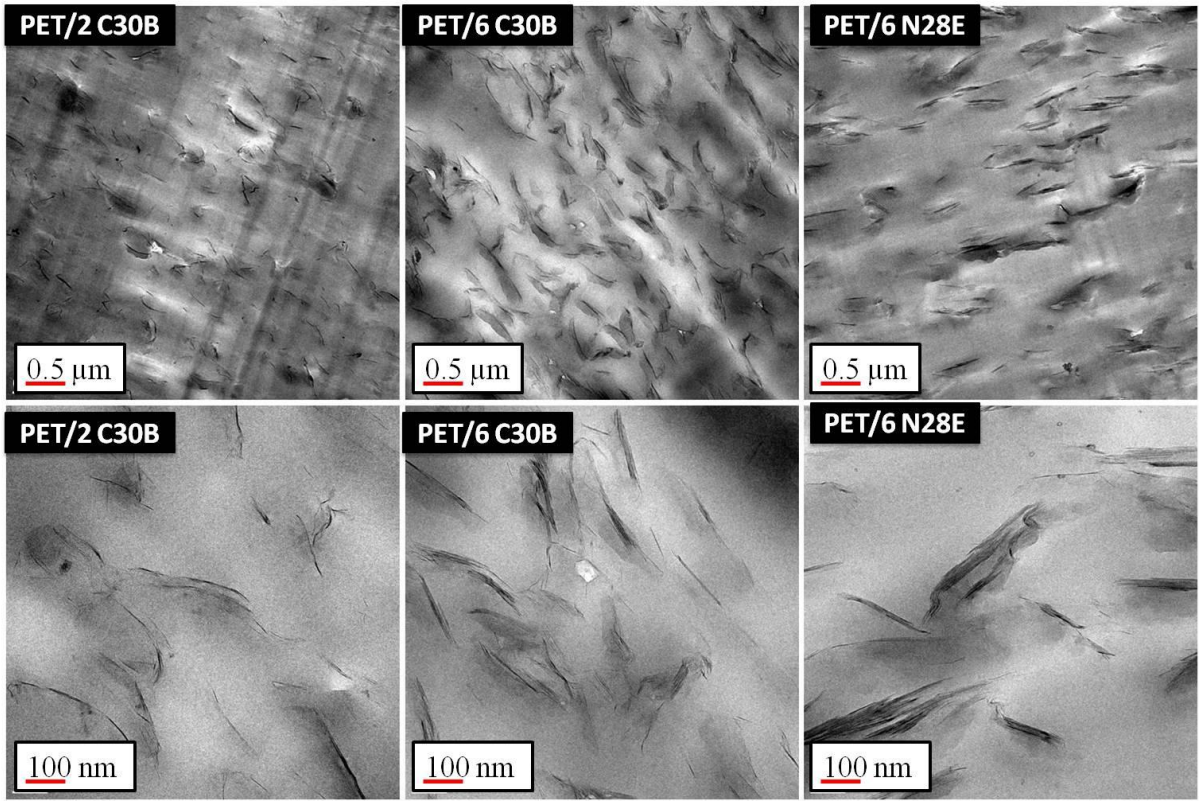

Figure 6-16: TEM images of PET/2 C30B, PET/6 C30B and PET/6 N28E nanocomposites prepared by screw configuration #2 at low and high magnifications.

To quantify the effect of clay chemistry and concentration on the morphology of PET nanocomposites, the number of layers per clay particle was manually counted using the TEM images. Figure 6-17 shows the number of platelets per clay particle histograms for PET nanocomposites containing 2 and 6 wt% C30B and that for the nanocomposite containing 6 wt% N28E. Around 400 particles were counted to ensure statistical validity of the analysis. As expected, the count for clay aggregates increases at higher clay loadings by comparing the PET/2 C30B and PET/6 C30B nanocomposites. The count for single layers and double layer particles is

also larger for PET/6 C30B in comparison to PET/6 N28E. On the other hand, the frequency of clay aggregates (5 or more layers) is higher for the nanocomposite containing N28E. Favorable interactions between layered silicates and the polymer matrix enhance diffusion of polymeric macromolecules into the gallery spacing of the clay platelets and result in morphologies with higher level of exfoliation. Among the organoclays studied in this work, C30B is the only one that has hydroxyl groups. The highest level of PET chains intercalation into the gallery spacing of C30B in comparison to other organoclays, based on XRD results is attributed to the favorable interactions between the carboxyl groups of the PET backbone and the hydroxyl groups present in the organo-modifier of C30B. Hence the higher initial gallery spacing of N28E in comparison to that of C30B (Table 6-1) does not help further intercalation of PET macromolecules. Besides, the solubility parameter of PET is closer to that of C30B in comparison to N28E, implying that C30B is more miscible with PET.

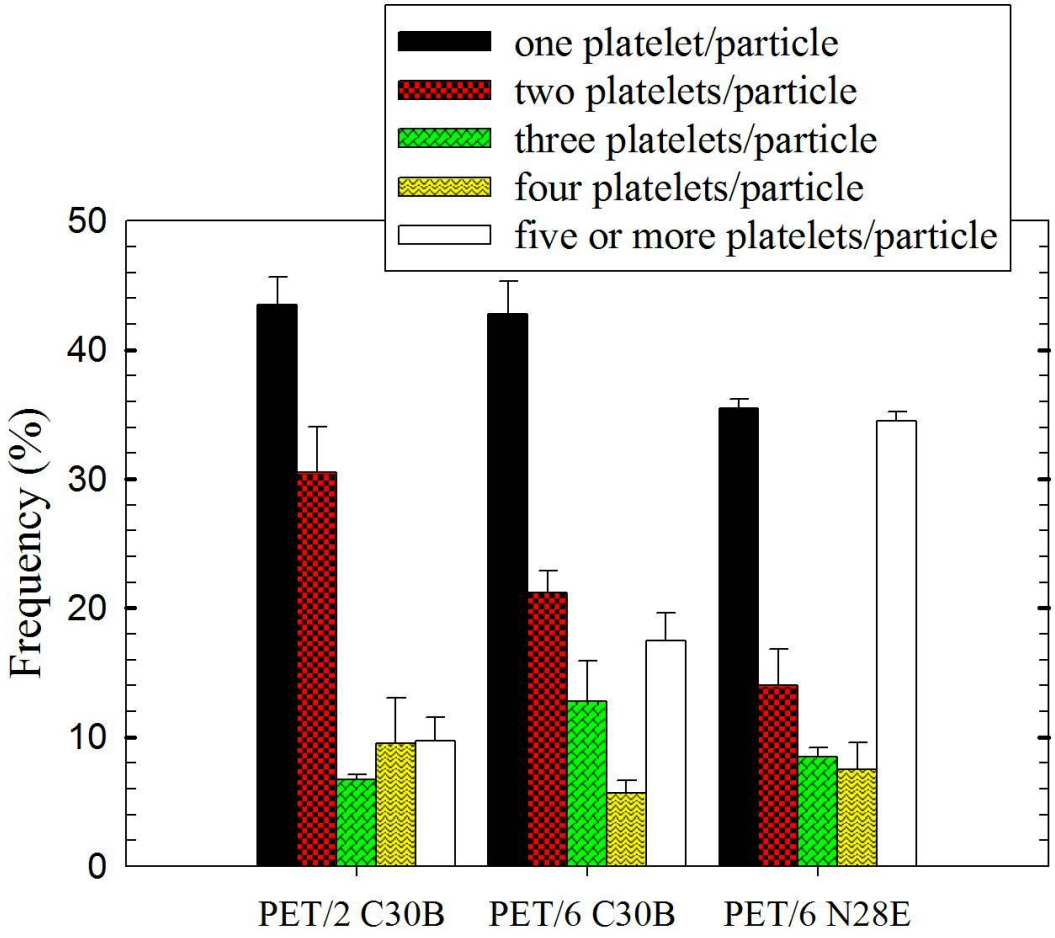

Figure 6-17: Number of platelets per particle histogram. The total number of counted particles was around 400.

6.5 Conclusion

In this work, PET nanocomposites containing C30B, C15A, C25A, N28E, and SM100 were prepared by melt compounding using a twin-screw extruder. The effect of the screw geometry, clay concentration, and surfactant chemistry of the organoclays on the morphology and rheology of the PET nanocomposites were investigated using XRD, SEM, TEM, and rheometry. The relationship between the microstructure and rheological behavior of the nanocomposites was discussed. It is observed that increasing residence time and employing more shearing elements help breaking and dispersing clay tactoids and improve the viscoelastic properties. Although

gallery spacing was found to be independent of the silicate concentration, the count for exfoliated layers was higher for nanocomposites based on C30B and decreased with clay concentration. The complex viscosity of PET nanocomposites exhibits solid-like behavior which becomes stronger with clay loading. The storage modulus shows a pseudo solid-like behavior at low frequencies and high clay concentrations, due to the formation of a percolated network. The apparent yield stress in nanocomposites has been determined using the Herschel-Bulkley model, and it was shown to increase with clay concentration and level of exfoliation. Among the various organoclays studied in this work, those being more intercalated with the PET chains exhibited larger rheological properties. The largest values of the complex viscosity and storage modulus as well as the highest degree of intercalation were obtained for C30B, which has the solubility parameter value closer to that of PET. The degradation of PET chains in the nanocomposites due to the presence of organoclays led to a lower complex viscosity for PET nanocomposites in comparison to the neat sample at high frequencies. It was possible to account for the degradation of the PET matrix by using the Maron-Pierce equation for the high frequency data. The molecular weight of the PET matrix was found to decrease from 65 kg/mol for the neat PET to 29.8 kg/mol for the PET nanocomposite containing 8 wt % C30B.

6.6 Acknowledgments

The authors are thankful to Mrs. W. Leelapornpisit for the SEM and TEM analysis. Financial support from NSERC (Natural Science and Engineering Research Council of Canada) in the context of the NRC-NSERC-BDC Nanotechnology Initiative is gratefully acknowledged.

6.7 References

Abbasi S, Carreau PJ, Derdouri A, Moan M (2009) Rheological properties and percolation in suspensions of multiwalled carbon nanotubes in polycarbonate. Rheologica Acta 48 (9):943-959. doi:10.1007/s00397-009-0375-7

Aubry T, Razafinimaro T, Mederic P (2005) Rheological investigation of the melt state elastic and yield properties of a polyamide-12 layered silicate nanocomposite. Journal of Rheology 49 (2):425-440. doi:10.1122/1.1859791

Ayyer RK, Leonov AI (2004) Comparative rheological studies of polyamide-6 and its low loaded nanocomposite based on layered silicates. Rheologica Acta 43 (3):283-292. doi:10.1007/s00397-003-0343-6

Bhattacharya S, Gupta R, Kamal M (2007) Polymeric nanocomposites: theory and practice. Hanser Gardner Publications,

Champagne MF, Huneault MA, Roux C, Peyrel W (1999) Reactive compatibilization of polypropylene polyethylene terephthalate blends. Polymer Engineering and Science 39 (6):976-984. doi:10.1002/pen.11487

Cui L, Dirnitri MKB, Christopher WBB, Hunter DL, Yoon PJ, Paul DR (2008) Effect of organoclay purity and degradation on nanocomposite performance, Part 1: Surfactant degradation. Polymer 49 (17):3751-3761. doi:10.1016/j.polymer.2008.06.029

Davis CH, Mathias LJ, Gilman JW, Schiraldi DA, Shields JR, Trulove P, Sutto TE, Delong HC (2002) Effects of melt-processing conditions on the quality of poly(ethylene terephthalate) montmorillonite clay nanocomposites. Journal of Polymer Science Part B-Polymer Physics 40 (23):2661-2666. doi:10.1002/polb.10331

Delozier DM, Orwoll RA, Cahoon JF, Ladislaw JS, Smith JG, Connell JW (2003) Polyimide nanocomposites prepared from high-temperature, reduced charge organoclays. Polymer 44 (8):2231-2241. doi:10.1016/s0032-3861(03)00082-x

Dykes L, Torkelson J, Burghardt W (2012) Shear-Induced Orientation in Well-Exfoliated Polystyrene/Clay Nanocomposites. Macromolecules in press

Eslami H, Grmela M, Bousmina M (2010) Linear and nonlinear rheology of polymer/layered silicate nanocomposites. Journal of Rheology 54 (3):539-562. doi:10.1122/1.3372720

Fornes TD, Paul DR (2003) Modeling properties of nylon 6/clay nanocomposites using composite theories. Polymer 44 (17):4993-5013. doi:10.1016/s0032-3861(03)00471-3

Fornes TD, Yoon PJ, Paul DR (2003) Polymer matrix degradation and color formation in melt processed nylon 6/clay nanocomposites. Polymer 44 (24):7545-7556. doi:10.1016/j.polymer.2003.09.034

Fox B, Moad G, vanDiepen G, Willing I, Cook WD (1997) Characterization of poly(ethylene terephthalate) and poly(ethylene terephthalate) blends. Polymer 38 (12):3035-3043. doi:10.1016/s0032-3861(96)00872-5

Frounchi M, Dourbash A (2009) Oxygen Barrier Properties of Poly(ethylene terephthalate) Nanocomposite Films. Macromolecular Materials and Engineering 294 (1):68-74. doi:10.1002/mame.200800238

Gahleitner M, Kretzschmar B, Van Vliet G, Devaux J, Pospiech D, Bernreitner K, Ingolic E (2006) Rheology/morphology interactions in polypropylene/polyamide-6 nanocomposites. Rheologica Acta 45 (4):322-330. doi:10.1007/s00397-005-0059-3

Galgali G, Ramesh C, Lele A (2001) A rheological study on the kinetics of hybrid formation in polypropylene nanocomposites. Macromolecules 34 (4):852-858. doi:10.1021/ma000565f

Galindo-Rosales FJ, Moldenaers P, Vermant J (2011) Assessment of the Dispersion Quality in Polymer Nanocomposites by Rheological Methods. Macromolecular Materials and Engineering 296 (3-4):331-340. doi:10.1002/mame.201000345

Ghanbari A, Heuzey M, Carreau P, Ton-That MT (In press.) Morphology and properties of polymer organoclay nanocomposites based on PET and sulfopolyester blends. Polymer International

Ghasemi H, Carreau PJ, Kamal MR, Chapleau N (2011a) Effect of Processing Conditions on Properties of PET/Clay Nanocomposite Films. International Polymer Processing 26 (2):219-228. doi:10.3139/217.2446

Ghasemi H, Carreau PJ, Kamal MR, Tabatabaei SH (2012) Properties of PET/clay nanocomposite films. Polymer Engineering and Science 52 (2):420-430. doi:10.1002/pen.22099

Ghasemi H, Carreau PJ, Kamal MR, Uribe-Calderon J (2011b) Preparation and Characterization of PET/Clay Nanocomposites by Melt Compounding. Polymer Engineering and Science 51 (6):1178-1187. doi:10.1002/pen.21874

Gupta R, Kennel E, Kim K (2009) Polymer Nanocomposites Handbook. 1 edn. CRC Press,

Hyun YH, Lim ST, Choi HJ, Jhon MS (2001) Rheology of poly(ethylene oxide)/organoclay nanocomposites. Macromolecules 34 (23):8084-8093. doi:10.1021/ma002191w

Khalkhal F, Carreau PJ (2011) Scaling behavior of the elastic properties of non-dilute MWCNT-epoxy suspensions. Rheologica Acta 50 (9-10):717-728. doi:10.1007/s00397-010-0527-9

Khalkhal F, Carreau PJ, Ausias G (2011) Effect of flow history on linear viscoelastic properties and the evolution of the structure of multiwalled carbon nanotube suspensions in an epoxy. Journal of Rheology 55 (1):153-175. doi:10.1122/1.3523628

Lim YT, Park OO (2001) Phase morphology and rheological behavior of polymer/layered silicate nanocomposites. Rheologica Acta 40 (3):220-229. doi:10.1007/s003970000126

Litchfield D, Baird D (2006) The rheology of high aspect ratio nanoparticle filled liquids. Rheology Reviews 1-60

Litchfield DW, Baird DG, Rim PB, Chen C (2010) Improved Mechanical Properties of Poly(Ethylene Terephthalate) Nanocomposite Fibers. Polymer Engineering and Science 50 (11):2205-2215. doi:10.1002/pen.21758

Luo ZP, Koo JH (2007) Quantifying the dispersion of mixture microstructures. Journal of Microscopy-Oxford 225 (2):118-125. doi:10.1111/j.1365-2818.2007.01722.x

Luo ZP, Koo JH (2008) Quantification of the layer dispersion degree in polymer layered silicate nanocomposites by transmission electron microscopy. Polymer 49 (7):1841-1852. doi:10.1016/j.polymer.2008.02.028

Manitiu M, Horsch S, Gulari E, Kannan RM (2009) Role of polymer-clay interactions and nano-clay dispersion on the viscoelastic response of supercritical CO(2) dispersed polyvinylmethylether (PVME)-Clay nanocomposites. Polymer 50 (15):3786-3796. doi:10.1016/j.polymer.2009.05.036

Mitchell CA, Krishnamoorti R (2002) Rheological properties of diblock copolymer/layered silicate nanocomposites. Journal of Polymer Science Part B-Polymer Physics 40 (14):1434-1443. doi:10.1002/polb.10209

Mittal V (2011) Thermally Stable and Flame Retardant Polymer Nanocomposites. 1st edn. Cambridge University Press,

Mobuchon C, Carreau PJ, Heuzey MC (2007) Effect of flow history on the structure of a non-polar polymer/clay nanocomposite model system. Rheologica Acta 46 (8):1045-1056. doi:10.1007/s00397-007-0188-5

Mobuchon C, Carreau PJ, Heuzey MC (2009a) Structural analysis of non-aqueous layered silicate suspensions subjected to shear flow. Journal of Rheology 53 (5):1025-1048. doi:10.1122/1.3193720

Mobuchon C, Carreau PJ, Heuzey MC, Reddy NK, Vermant J (2009b) Anisotropy of nonaqueous layered silicate suspensions subjected to shear flow. Journal of Rheology 53 (3):517-538. doi:10.1122/1.3094911

Nazockdast E, Nazockdast H, Goharpey F (2008) Linear and nonlinear melt-state viscoelastic properties of polypropylene/organoclay nanocomposites. Polymer Engineering and Science 48 (7):1240-1249. doi:10.1002/pen.21054

Pavlidou S, Papaspyrides C (2008) A review on polymer-layered silicate nanocomposites. Progress in Polymer Science 33 (12):1119-1198. doi:10.1016/j.progpolymsci.2008.07.008

Pogodina NV, Cercle C, Averous L, Thomann R, Bouquey M, Muller R (2008) Processing and characterization of biodegradable polymer nanocomposites: detection of dispersion state. Rheologica Acta 47 (5-6):543-553. doi:10.1007/s00397-007-0243-2

Pujari S, Dougherty L, Mobuchon C, Carreau PJ, Heuzey MC, Burghardt WR (2011) X-ray scattering measurements of particle orientation in a sheared polymer/clay dispersion. Rheologica Acta 50 (1):3-16. doi:10.1007/s00397-010-0492-3

Ray SS, Bousmina M (2005) Poly(butylene sucinate-co-adipate)/montmorillonite nanocomposites: effect of organic modifier miscibility on structure, properties, and viscoelasticity. Polymer 46 (26):12430-12439. doi:10.1016/j.polymer.2005.10.102

Ray SS, Okamoto M (2003) Polymer/layered silicate nanocomposites: a review from preparation to processing. Progress in Polymer Science 28 (11):1539-1641. doi:10.1016/j.progpolymsci.2003.08.002

Ren JX, Silva AS, Krishnamoorti R (2000) Linear viscoelasticity of disordered polystyrene-polyisoprene block copolymer based layered-silicate nanocomposites. Macromolecules 33 (10):3739-3746. doi:10.1021/ma992091u

Sanchez-Solis A, Romero-Ibarra I, Estrada MR, Calderas F, Manero O (2004) Mechanical and rheological studies on polyethylene terephthalate-montmorillonite nanocomposites. Polymer Engineering and Science 44 (6):1094-1102. doi:10.1002/pen.20102

Scaffaro R, Botta L, Ceraulo M, La Mantia FP (2011) Effect of Kind and Content of Organo-Modified Clay on Properties of PET Nanocomposites. Journal of Applied Polymer Science 122 (1):384-392. doi:10.1002/app.34087

Solomon MJ, Almusallam AS, Seefeldt KF, Somwangthanaroj A, Varadan P (2001) Rheology of polypropylene/clay hybrid materials. Macromolecules 34 (6):1864-1872. doi:10.1021/ma001122e

Soon KH, Harkin-Jones E, Rajeev RS, Menary G, McNally T, Martin PJ, Armstrong C (2009) Characterisation of melt-processed poly(ethylene terephthalate)/synthetic mica nanocomposite sheet and its biaxial deformation behaviour. Polymer International 58 (10):1134-1141. doi:10.1002/pi.2641

Stoeffler K, Lafleur PG, Denault J (2008) Thermal decomposition of various alkyl onium organoclays: Effect on polyethylene terephthalate nanocomposites' properties. Polymer Degradation and Stability 93 (7):1332-1350. doi:10.1016/j.polymdegradstab.2008.03.029

Sun L, Boo WJ, Liu J, Clearfield A, Sue HJ, Verghese NE, Pham HQ, Bicerano J (2009) Effect of Nanoplatelets on the Rheological Behavior of Epoxy Monomers. Macromolecular Materials and Engineering 294 (2):103-113. doi:10.1002/mame.200800258

Todorov LV, Viana JC (2007) Characterization of PET nanocomposites produced by different melt-based production methods. Journal of Applied Polymer Science 106 (3):1659-1669. doi:10.1002/app.26716

Utracki LA, Lyngaae-Jorgensen J (2002) Dynamic melt flow of nanocomposites based on poly-epsilon-caprolactam. Rheologica Acta 41 (5):394-407. doi:10.1007/s003970100211

Van Krevelen D, Te nijenhuis K (2009) Properties of Polymers. 4th edn. Elsevier Science,

Vermant J, Ceccia S, Dolgovskij MK, Maffettone PL, Macosko CW (2007) Quantifying dispersion of layered nanocomposites via melt rheology. Journal of Rheology 51 (3):429-450. doi:10.1122/1.2516399

Wan T, Wang B, Liao S, Clifford M (2011) Rheological Investigation on the Interaction of Polyamide 6 with Clay. Journal of Applied Polymer Science

Wang BA, Wan T, Zeng W (2011) Dynamic Rheology and Morphology of Polylactide/Organic Montmorillonite Nanocomposites. Journal of Applied Polymer Science 121 (2):1032-1039. doi:10.1002/app.33717

Wu DF, Zhou CX, Hong Z, Mao DL, Bian Z (2005) Study on rheological behaviour of poly(butylene terephthalate)/montmorillonite nanocomposites. European Polymer Journal 41 (9):2199-2207. doi:10.1016/j.eurpolymj.2005.03.005

Xia HS, Song M (2006) Intercalation and exfoliation behaviour of clay layers in branched polyol and polyurethane/clay nanocomposites. Polymer International 55 (2):229-235. doi:10.1002/pi.1948

Xu X, Ghanbari A, Leelapornpisit W, Heuzey M, Carreau P (2011) Effect of Ionomer on Barrier and Mechanical Properties of PET/Organoclay Nanocomposites Prepared by Melt Compounding. International Polymer Processing 26 (4):444-455. doi:10.3139/217.2477

Yoon PJ, Hunter DL, Paul DR (2003) Polycarbonate nanocomposites: Part 2. Degradation and color formation. Polymer 44 (18):5341-5354. doi:10.1016/s0032-3861(03)00523-8

Yziquel F, Carreau PJ, Tanguy PA (1999) Non-linear viscoelastic behavior of fumed silica suspensions. Rheologica Acta 38 (1):14-25. doi:10.1007/s003970050152

CHAPTER 7
A NOVEL APPROACH TO CONTROL THERMAL DEGRADATION OF PET/ORGANOCLAY NANOCOMPOSITES AND IMPROVE CLAY EXFOLIATION

A. Ghanbari[a], M.C. Heuzey[a], P.J. Carreau[a], M.T. Ton-That[b]

[a] *Center for Applied Research on Polymers and Composites (CREPEC), Chemical Engineering Department, Ecole Polytechnique de Montreal, PO Box 6079, Stn Centre-Ville, Montreal, QC, Canada H3C 3A7*

[b] *Automotive Portfolio, National Research Council Canada, 75 Mortagne Blvd, Boucherville, QC, Canada J4B 6Y4*

This work was submitted to *Polymer* and parts of it were presented at the 7th Modification Degradation and Stabilization of Polymer (MoDeSt) Conference, Prague, Czech Republic (2012).

7.1 Abstract

Two different types of organomodified clay, Cloisite® 30B (C30B) and Nanomer® I.28E (N28E), were melt blended with polyethylene terephthalate (PET) using a twin-screw extruder. A multifunctional epoxy-based chain extender, Joncryl® ADR-4368F (Joncryl) was added to the nanocomposites via a master-batch approach to compensate the molecular weight reduction of the matrix under processing. The morphological, rheological, mechanical, thermal, optical, and gas barrier characteristics of the nanocomposites were studied using several characterization techniques. X-ray diffraction (XRD) and transmission electron microscopy (TEM) were employed to quantify the gallery spacing and the state of the organoclays dispersion within the polymer matrix. A remarkable improvement in viscoelastic properties was observed for samples containing the chain extender due to recoupling of degraded chains. A better clay dispersion, enhanced barrier properties and increased Young modulus were also obtained for nanocomposites containing the chain extender. Compared to neat PET films, the oxygen permeability of nanocomposite films containing 4 wt % C30B and 1 wt % Joncryl decreased by 46% whereas the corresponding permeability decrease for the N28E nanocomposite was 40 %. A 66% improvement in the Young modulus was obtained for nanocomposite films containing 4 wt % N28E and 1 wt % Joncryl. The improvement of the tensile modulus for the corresponding C30B nanocomposite was slightly less.

Keywords: Polyethylene terephthalate, Organoclay, Nanocomposite, Chain extender, Rheology, Morphology, Barrier properties.

7.2 Introduction

Polyethylene terephthalate (PET) is a semi-crystalline thermoplastic polymer used in a wide variety of applications. PET is found in the manufacture of textile fibers, carbonated beverage bottles, food and non-food containers, and engineering plastics in automobile. In comparison to an equivalent glass container, PET bottles are fairly light as well as they do not shatter or break.

PET bottles are not only being used as large two- and three-liter sizes for carbonated soft drinks, but they also have taken a remarkable market share in the single serving size containers from glass and metal cans. The world market for PET resin in packaging could be doubled if PET would gain 50% of the market share in beer bottles packaging [1, 2]. Beer is a very sensitive beverage to oxygen while PET does not offer sufficient oxygen barrier properties. One promising method to enhance barrier properties of PET is the incorporation of silicate nanolayers [3-7]. When well dispersed and distributed in a polymeric matrix, the impermeable silicate nanolayers create a tortuous pathway and force the oxygen molecules to travel a longer path for diffusing through the nanocomposite [8].

The incorporation of silicate nanolayers to polymers does not necessarily lead to the formation of nanoscale structures. Microcomposites, intercalated nanocomposites, and exfoliated nanocomposites are the three main types of morphology that may be observed in practice, or a combination of the three [9]. Most polymers are hydrophobic while pristine clay is hydrophilic thus, their combination leads to the formation of microcomposites due to the lack of compatibility. Organic modification of silicate nanolayers using surfactants such as alkylammoniums is a convenient method to make pristine clay organophilic and enhance the compatibility with the polymer matrix. Besides, organic modification increases the gallery spacing of silicate nanolayers and, thus, facilitates intercalation of polymer chains [1]. However, the principal obstacle to the incorporation of commercially available organoclays in polymers with high processing temperatures is the low thermal stability of the organomodifier. Organoclays treated with various alkylammoniums undergo significant thermal degradations above 180 ºC [10]. Matrix degradation that results in a lower molecular weight and reduced viscoelastic properties as well as color formation have been reported for polymer nanocomposites that must be processed at high temperatures [3, 6, 10-13].

PET nanocomposites have been prepared via two approaches: *in-situ* polymerization [14] and melt blending [3-6, 15-17]. Ghasemi et al. [5] reported that the incorporation of 3 wt% Cloisite® 30B (C30B) in a PET matrix using twin-screw extrusion resulted in a 20% increment of the Young modulus. In another study, they demonstrated that among three different types of organoclay, including the ammonium-modified C30B and thermally stable phosphonium- and imidazolium-modified clays, C30B yielded the best intercalation with PET chains [15]. They also

reported that by employing a severe screw profile in terms of mixing and high screw rotational speed, the incorporation of 3 wt% C30B into a PET matrix led to a 27% reduction in oxygen permeability and a 30% improvement of the tensile modulus [4]. PET nanocomposites containing 3 wt% Cloisite® 15A (C15A) and Nanolin® DK2 were also prepared using a twin-screw extruder [18]. It was observed that the addition of C15A and Nanolin® DK2 to PET improved the barrier to oxygen by 16 and 30%, respectively. Soon et al. [7] reported that the addition of 5 wt% synthetic clay to PET led to a 29% reduction in oxygen permeability. Compatibilizers such as pentaerythrytol and maleic anhydride have been used by Sanchez-Solis and coworkers [17] to improve the dispersion of C15A particles in PET. The Young modulus increased with the incorporation of C15A, however the effect of the coupling agents on the Young modulus of the nanocomposites was not significant. To enhance interactions between PET chains and silicate nanolayers, an alternative approach consists of a random incorporation of sulfonated groups along the polymer backbone. Due to electrostatic interactions between clay platelets and PET sulfonated groups, nanocomposites with higher degree of intercalation were obtained [3, 6, 19].

To avoid thermal decomposition of the organic modifier of clay particles at the high processing temperature of a fiber grade PET, Chung et al. [20] dissolved PET and organoclay in a mixture of chloroform and trifluoroacetic acid. Then, the solution was added dropwise to cold methanol to eliminate the organic modifier. Next, the precipitated material was dried and melt blended with neat PET using a twin-screw extruder. This method led to a better optical transparency, thermal stability, and enhanced mechanical properties. However this procedure is tedious and not convenient because of the use of solvents. The molecular weight and viscosity of PET may decrease during melt processing as a result of thermal, hydrolytic, mechanical, and oxidative degradations [21]. During melt blending of organoclays with PET, even more severe degradation is expected due to the thermal decomposition of the clay organic modifier and reactions between the decomposition products and the polymer matrix. This may affect the thermodynamics of melt intercalation and deteriorate the exfoliation level of silicate nanolayers, which consequently affects the final properties of the nanocomposites [10, 12, 22]. The nucleophilic substitution reaction and the Hoffman elimination reaction (β-elimination) are generally believed to be the primary decomposition pathways of ammonium salts [12]. Both of these reactions lead to the formation of a tertiary amine from the decomposition of a quaternary ammonium. Nucleophilic

attack of the quaternary ammonium by a halide ion also leads to the formation of an alkyl halide [12]. On the other hand, an alkene is formed in the case of the Hoffman elimination reaction due to the presence of a basic anion (e.g. hydroxyl groups at the edges of the silicate nanolayers), which extracts a hydrogen atom from β-carbons of the quaternary ammonium salt [10, 12].

Stoeffler *et al*. [12] modified pristine sodium montmorillonite using more thermally stable phosphonium, pyridinium, and imidazolium salts to reduce the thermal decomposition of PET nanocomposites. They nevertheless found that pyridinium and phosphonium modified clays released volatiles above 250 ºC. The thermal decomposition of surfactants significantly affected the visual appearance of the nanocomposites in that study. For example, the nanocomposites containing phosphonium and imidazolium modified clays presented a yellowish/brownish color, and those containing pyridinium modified clays were reported to be dark brown.

To build back up the molecular weight of PET one approach is solid state polymerization (SSP). This post-condensation batch process must be done under high vacuum and high temperature for a time period of 12 to 20 h in special equipments for large scale operation, which makes this approach less interesting [23]. On the other hand, the use of chain extenders has been proposed as another approach to compensate molecular weight reduction induced by chain scission [11, 23-27]. Lower costs and faster reactions are the main advantages of the chain extension method over the SSP approach. Torres et al. [27] melt-blended PET with approximately 1 wt% of various chain extenders and they reported that the molecular weight of PET increased from 40.5 to 76.7 kg/mol in the presence of hexamethylenediisocyanate for a residence time of 2 min. Other bi-functional chains extenders such as dianhydrides and diepoxides have been reported to increase the molecular weight of PET [23, 28, 29]. Triphenyl phosphate was employed by Cavalcanti and coworkers [30] as another chain extender for PET and an increase in torque during mixing was associated to a chain extension reaction.

The aim of this work is to control the thermal degradation of PET and improve the properties of PET nanocomposites using a multifunctional epoxy-based oligomeric chain extender. Two different types of commercially available organoclay, C30B and Nanomer® I.28E (N28E), are employed and morphology, viscoelastic, barrier and mechanical properties of the samples are examined to assess the effects of the chain extender. To our knowledge no report has been

published on the improvement of morphology and properties of PET nanocomposites using multifunctional chain extenders.

7.3 Experimental

7.3.1 Materials

A commercial grade PET (PET 9921), with intrinsic viscosity of 0.8 dL/g and a melting point of 243 °C, was obtained from Eastman Chemical Company. The two organically modified montmorillonites, C30B and N28E, were obtained from Southern Clay Products Inc. and Nanocor Inc., respectively. C30B is modified with methyl, tallow, bis-2-hydroxyethyl, quaternary ammonium (MT2EtOH), while N28E is modified with octadecyl ammonium (ODA), according to R&D of Nanocor Inc. Joncryl® ADR-4368F (Joncryl), which is a styrene-acrylic multifunctional epoxy-based chain extender, was kindly supplied from BASF. This chain extender is designed to rebuild the molecular weight of degraded condensation polymers such as PET, polyamides, and polycarbonate. The chemical structure of Joncryl is shown in Figure 7-1. According to the supplier data sheet, the glass transition temperature (T_g) and molecular weight (M_w) of Joncryl are 54 °C and 6800 g/mol, respectively.

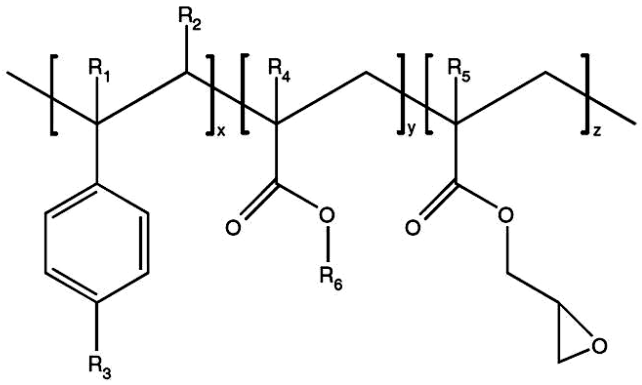

Figure 7-1: Chemical structure of the chain extender Joncryl. R1–R5 are H, CH3, a higher alkyl group, or combinations of them; R6 is an alkyl group, and x, y and z are all between 1 and 20 [26].

7.3.2 Sample preparation

The PET, organoclays, and Joncryl were vacuum dried at 90 ºC for 24 h before extrusion. To obtain a better morphology, the nanocomposites were prepared by a master-batch approach. First, PET granules were ground into a powder and dry-mixed with 6 wt% C30B or N28E to obtain uniform feeding mixtures. Next, the feeding mixtures were processed using a co-rotating twin-screw Leistritz® extruder (screw diameter = 18 mm and L/D = 40) with SC#1 geometry. Then the prepared master-batches were diluted with the appropriate amount of neat PET and Joncryl using the same twin-screw extruder, to obtain nanocomposites containing 5 wt% of organoclays (nominal value) and 1 wt% Joncryl. Hence, in this master-batch approach the initially low molecular weight PET chains could easily diffuse into the gallery spacing of the silicate layers and then delamination and exfoliation could be facilitated by the larger stresses resulting from the reaction of the chain extender with the PET. The temperature profile from the extruder feed to the die was set between 240 and 265 ºC, and the extrusion was performed at 200 rpm and feeding rate of 1.8 kg/h. A 20 cm wide slit die with a 1 mm die gap was used to prepare films. Calender rolls were employed to stretch the extrudate and an air knife was mounted on both sides of the film. The width of the films was around 19 cm, which means that the average neck-in was 5%. The thickness of the films was 50 µm corresponding to a draw ratio around 21. The same extrusion procedure was followed to prepare pellets using a circular die of 2 mm diameter. A bath containing a mixture of water and ice was used to cool the extrudate. The extruded samples were granulated and vacuum dried at 90 ºC for 24 h before compression molding. Disk-shape samples of approximately 2 mm thickness and 25 mm diameter were prepared by employing a Carver® laboratory press (model 3912) at 265 ºC for 9 min at a pressure of 20 MPa under a purge of nitrogen, followed by quenching in another Carver® laboratory press (model 30-12H) for 5 min. The compression molded samples were vacuum dried at 90 ºC for 24 h before being subjected to rheological testing.

7.3.3 Characterization

Wide angle X-ray diffraction (WAXD) was used to estimate the basal spacing (d_{001}) of silicate nanolayers. The measurements were performed on a Philips X'Pert X-ray diffractometer with CuK_{α} radiation (λ = 1.54056 Å). The generator was operated at 50 kV and 40 mA. The spectra were recorded over a 2θ range of 1-10 º using a scan rate of 0.01 °/s.

The quality of clay dispersion in PET nanocomposites, with and without chain extender, was evaluated using transmission electron microscopy (TEM) (JEOL JEM-2100F microscope, operating at 200 kV). The samples were microtomed into approximately 50-80 nm thick slices at a cryogenic temperature (i.e. -100° C) using an Ultracut FC microtome (LEICA) with a diamond knife.

Fourier transform infrared (FT-IR) spectra were recorded on a Perkin-Elmer FT-IR spectrometer from 4000 to 600 cm^{-1} in the attenuated total reflection (ATR) mode. All the spectra were obtained by accumulation of 32 scans with a spectral resolution of 4 cm^{-1} and a scanning speed of 32 kHz. This technique was employed to detect any reactions that may have occurred between the matrix and the chain extender.

To determine the exact amount of organoclays in the nanocomposite samples thermogravimetric analysis (TGA) was conducted under an air atmosphere using a TGAQ500 from TA Instruments. These tests were performed on samples of 10 mg from room temperature to 900 °C with a heating rate of 10 °C/min followed by 30 min isothermal hold at 900 °C. C30B and N28E contain around 30 wt% of organic modifier. Therefore, the ash content of the nanocomposites containing 5 (nominal) wt% C30B and N28E is expected to be 3.5%. However, the measured ash content was about 2.8%, probably due to a loss of clay during feeding in the extruder hopper, which means that the real amount of the organoclays in the nanocomposites was around 4 wt%.

Differential scanning calorimetry (DSC) of PET and the nanocomposites was performed on a DSCQ1000 (TA Instruments) on typically 10 mg of material, under a helium atmosphere to investigate thermal behavior and crystalline content of the samples. The samples were heated from room temperature to 300 ºC and held at that temperature for 3 min, then cooled to 30 ºC at a

constant rate of 10 ºC/min. This test was performed twice for each sample, always with a fresh specimen.

The rheological properties of PET and the nanocomposites were measured using a stress-controlled Bohlin Gemini rheometer. The experiments were conducted under a blanket of nitrogen to avoid oxidation of the samples. A parallel plate flow-geometry was used with a gap size of 1 mm and a plate diameter of 25 mm. Time and frequency sweeps in small-amplitude oscillatory shear were carried out on the samples at 265 ºC. The time sweep tests were performed at 0.628 rad/s over 900 s on two fresh specimens of each sample and the average value is reported. The frequency sweep tests were performed in the linear regime for four fresh specimens of each sample. Two specimens were subjected to frequency sweep from low to high frequency, and two more from high to low.

Mechanical properties of the films were measured using an Instron 3365 at room temperature according to standard ASTM D638. The tensile specimens with a rectangular geometry of 25 mm wide and 100 mm long were stretched at a cross-head speed of 12.5 mm/min. To obtain the toughness of the samples, the area under the stress-strain curve were calculated according to the Simpson 1/3 rule of integration.

A Mocon Ox-Tran Model 2/21 oxygen permeability MD module was used to determine oxygen transmission rates (OTRs) of the films at 23 °C under a pressure of 0.96 atm. 100% dry oxygen was passed over one side of the sample and a mixture of 98% N_2 (nitrogen) with 2% H_2 (hydrogen) was used as the carrier gas. The permeability coefficient [*P*, in L/(m.day.atm)] was obtained from the OTR values using the following formula:

$$P = OTR \times \frac{L}{p} \tag{7-1}$$

where *L* is the film thickness (m) and *p* is the testing pressure (atm). At least four specimens were tested for each sample.

Haze and clarity were determined using a Haze Guard Plus™ instrument (Qualitest International Inc.) according to ASTM D1003. For each nanocomposite film, at least five different specimens have been tested. Haze is defined as the percentage of the total transmitted light which deviates from the incident beam more than 2.5° when passing through the specimen. Transparency, often referred to as clarity, is defined as the percentage of light that is scattered from the incident beam by an angle lower than 0.1°. While denominator for haze is the total transmitted light (Eq. 7-2), it is the incident light for clarity (Eq. 7-3) [31]:

$$Haze = \frac{I_s > 2.5^\circ}{I_s + I_r} \tag{7-2}$$

$$Clarity = \frac{I_r < 0.1^\circ}{I_i} \tag{7-3}$$

where I_i, I_r, and I_s represents the incident light, regular transmitted, and scattered transmitted light intensity, respectively.

7.4 Results and discussion

7.4.1 Fourier transform infrared spectroscopy (FT-IR)

By comparing the FT-IR spectra of the neat materials and of PET containing Joncryl, the chemical reactions between the matrix and the chain extender may be identified. Figure 7-2a and Figure 7-2b show the FT-IR spectra of Joncryl, neat PET, and PET containing 1 wt% Joncryl in two different wavenumbers range. The peaks at 842, 908, and 1255 cm^{-1}, which are observed in the spectra of Joncryl, are assigned to the C-O stretching modes of the epoxy group [11, 32]. No peaks or weak ones occur at these wavenumbers in the spectrum of PET/1 wt% Joncryl, which means that most of the epoxy groups in Joncryl have been consumed in the PET sample treated with Joncryl. For a better comparison, these wavenumbers are identified by dotted lines in Figure 7-2b. The consumption of epoxy groups may be due to chemical reactions between these and PET end groups, as both carboxyl and hydroxyl groups can react with epoxy groups [33]. New hydroxyl groups are formed due to these reactions [33]; however, the hydroxyl end group content

is not affected if these hydroxyl groups react with epoxy groups. In contrast, due to the reaction of epoxy groups with carboxyl end groups of PET, new hydroxyl groups are formed and an increment in hydroxyl content is expected. It has been proposed by several researchers that the esterification of PET carboxyl end groups with electrophilic epoxy groups is more favorable than etherification of hydroxyl end groups [26, 33].

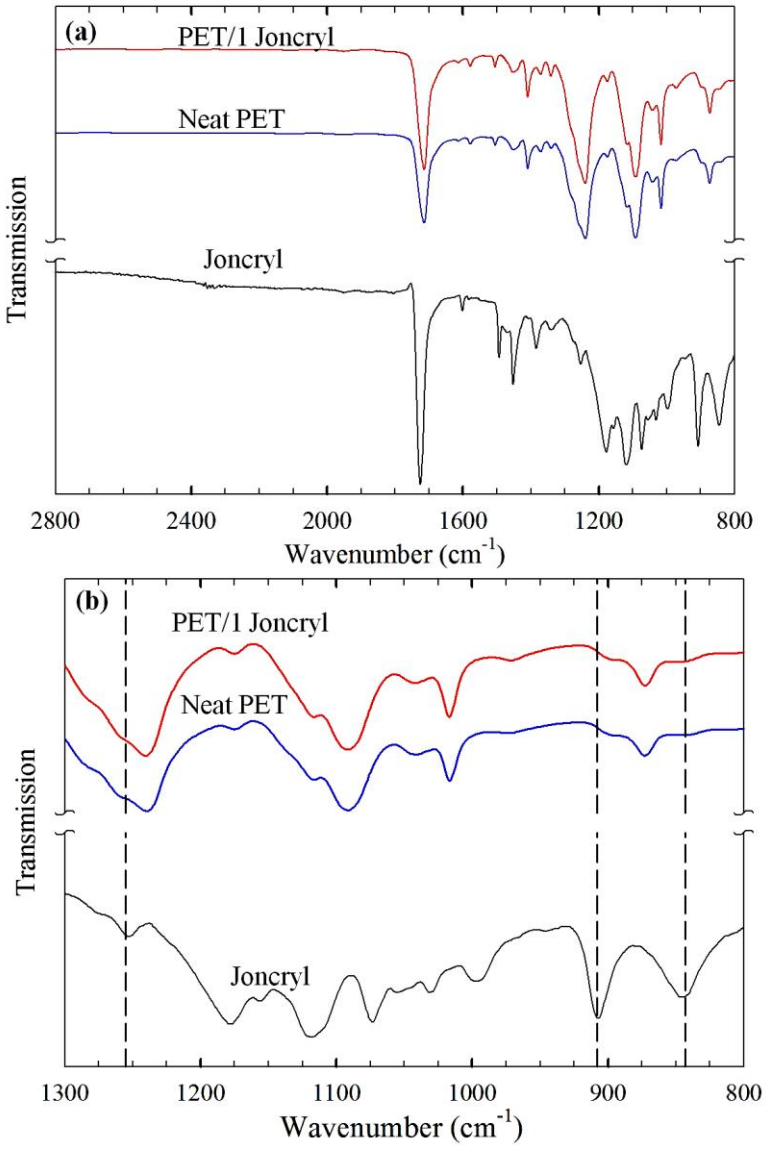

Figure 7-2: FT-IR spectra of Joncryl, PET, and PET containing 1 wt% Joncryl: (a) high wavenumber range, (b) low wavenumber range.

7.4.2 Morphology

XRD patterns of C30B and N28E and their corresponding nanocomposites with and without Joncryl are shown in Figure 7-3. By monitoring the presence, shape, intensity, and position of XRD peaks it is possible to make a preliminary assessment about the structure or morphology of the nanocomposites. The gallery spacing of both C30B and N28E increases to 3.4 nm after melt blending with PET, which illustrates the intercalation of PET chains into the basal spacing of these two organoclays. C30B exhibits a higher level of intercalation in comparison to N28E, as the increment from 1.85 to 3.4 nm of its gallery spacing is more than that of N28E (from 2.4 to 3.4 nm). XRD pattern of nanocomposite PET/4 C30B exhibits a shoulder instead of a defined peak, corresponding to a disordered intercalation, while the XRD pattern of sample PET/4 N28E shows a well-defined peak, characteristic of an ordered intercalation. The periodicities of the layers are preserved for silicate nanolayers with ordered intercalated structures, while, due to a degree of incoherence in layers, a disordered stacking is expected for nanocomposites revealing a shoulder peak [1]. The introduction of Joncryl in nanocomposites containing C30B and N28E reduces the intensity of the XRD peaks significantly. The reduction of the peak intensity in clay-containing polymers is associated with a higher level of exfoliation, as no peak is expected for exfoliated structures, and consequently smaller domains of periodicity (smaller tactoids). Note that the second peaks observed at $2\theta \approx 5.2°$ may be attributed to the d_{002} diffraction and/or to clay gallery collapse.

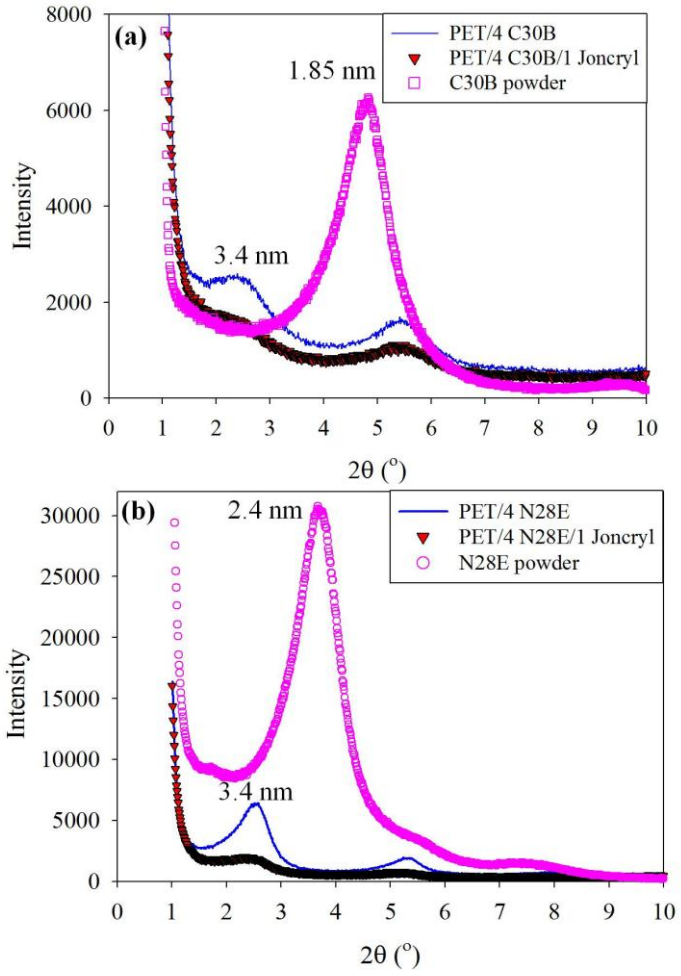

Figure 7-3: XRD patterns of the nanoclays and nanocomposites: (a) C30B and its corresponding nanocomposites, (b) N28E and its corresponding nanocomposites.

TEM was employed to obtain visual information about the internal structure of the nanocomposites at the nanometer scale. Figure 7-4 presents TEM images of nanocomposites containing N28E, with and without Joncryl, at two magnifications. Both delaminated platelets and tactoids are seen in the images. Comparing the low magnification images (Figure 7-4a and Figure 7-4c) we observe that the addition of Joncryl improves the distribution of clay particles in the PET matrix, displaying a higher clay distribution density (number of particles per unit area) and a more uniform distribution of clay particles in comparison to the nanocomposite prepared without Joncryl. The high magnification images (Figure 7-4b and Figure 7-4d) reveal that the presence of Joncryl reduces significantly the tactoid size. Clay tactoids with high number of

silicate layers per particle breakdown to more clay particles with lower numbers of platelets per particle. The reduction of the amount of large tactoids and the increase of single layer and double layer particles as shown in the next section confirm the observation of larger clay distribution density for nanocomposites containing Joncryl in the low magnification TEM images. Similar observations were made for the nanocomposites containing C30B. These results are in good agreement with XRD patterns as the peak intensity decreases for nanocomposites containing Joncryl.

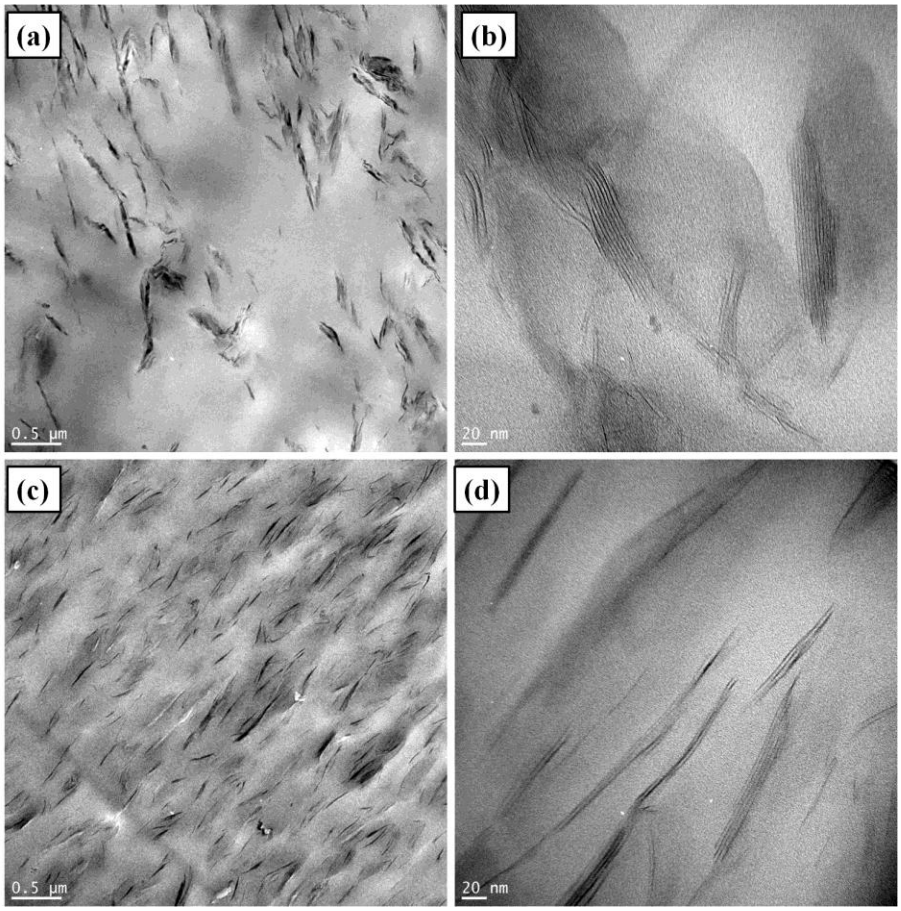

Figure 7-4: TEM images of PET/4 N28E (a, b) and PET/4 N28E/1 Joncryl (c, d) at various magnifications.

The number of platelets per tactoid was counted manually using the TEM images to evaluate quantitatively the effect of Joncryl and clay organic modifier on the level of clay dispersion within the PET matrix. Around 600 particles were counted for each sample, using around 40

TEM micrographs with 20 and 100 nm scale bars, to ensure statistical validity of the analysis. Figure 7-5 reports the histogram of the number of platelet per clay particle for PET nanocomposites containing 4 wt% C30B and N28E, with and without Joncryl. For both C30B and N28E nanocomposites, the introduction of the chain extender increases the count for single layer and double layer particles and decreases the frequency of clay aggregates (5 or more layers). It is worth noting that the PET/4 C30B nanocomposite exhibits a higher level of exfoliation than PET/4 N28E. Favorable interactions between hydroxyl groups present in the organic-modifier of C30B with PET result in a higher level of intercalation of PET chains into the gallery spacing of C30B in comparison to N28E, as suggested by the calculation of the solubility parameter of the organoclays based on the Fedors group contribution method [34]. The experimental value of the PET solubility parameter is 19.9-21.9 $J^{1/2}.cm^{-3/2}$ [34], while the calculated values for C30B and N28E are 21.5 and 16 $J^{1/2}.cm^{-3/2}$, respectively. Therefore, the solubility parameter of PET is identical to that calculated for C30B in comparison to N28E, which explains the higher level of exfoliation of C30B within the PET matrix.

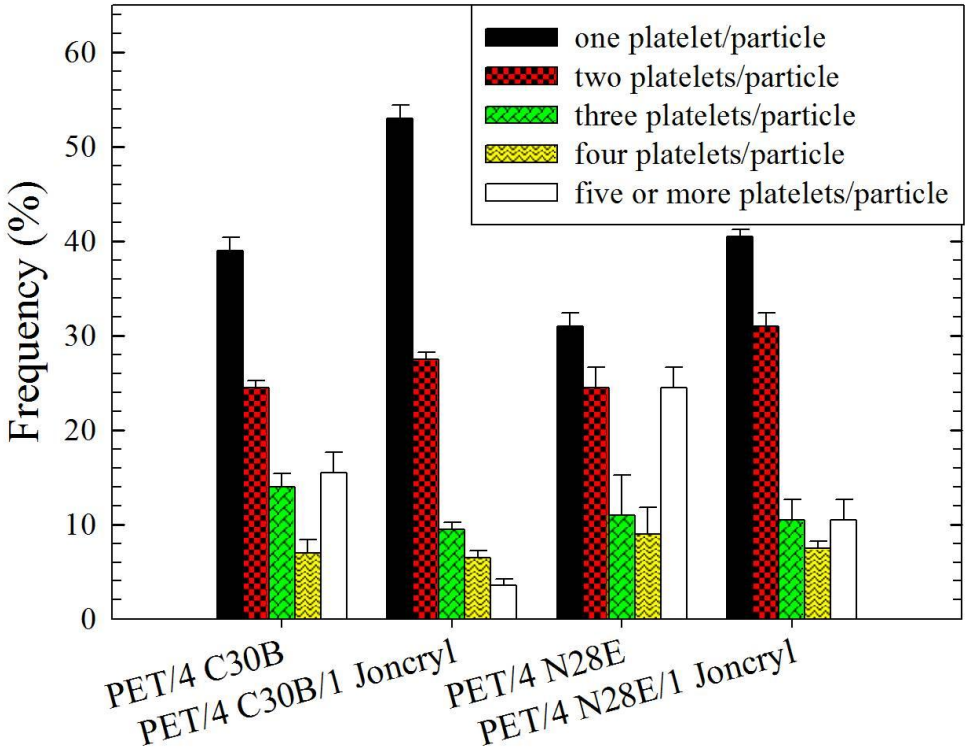

Figure 7-5: Histogram of the number of platelets per particle. The total number of counted particles was around 600.

Luo and Koo [35] introduced a TEM method to quantify the level of clay dispersion within a polymer matrix. A dimensionless parameter called the dispersion value, D_{01}, is calculated based on the distribution of the free-path spacing distances between the silicate nanolayers according to the following equation:

$$D_{0.1} = 1.1539\times10^{-2} + 7.5933\times10^{-2}\left(\mu/\sigma\right) + 6.6838\times10^{-4}\left(\mu/\sigma\right)^2 - 1.9169\times10^{-4}\left(\mu/\sigma\right)^3 + 3.9201\times10^{-6}\left(\mu/\sigma\right)^4 \quad (7\text{-}4)$$

where μ is the mean spacing between the clay layers, and σ is the standard deviation. More than 100 measurements were suggested by the authors to ensure validity of the analysis.

It has been proposed that D_{01} below 4% characterizes immiscible systems or microcomposites, and over 8% is a characteristic of exfoliated nanocomposites. The dispersion value is between 4 and 8% for intercalated nanocomposites. In this work around 600 measurements were carried out for each sample to ensure the validity of the values reported for D_{01}. The values obtained are 5.0 and 6.9 % for PET/4 C30B and PET/4 C30B/1 Joncryl, respectively; D_{01} is 4.1 and 5.6 % for PET/4 N28E and PET/4 N28E/1 Joncryl, respectively. These results suggest a higher degree of clay exfoliation for nanocomposites based on C30B and those containing Joncryl. It is worth mentioning that a value of 7.5 for D_{01} was obtained for a PET containing 2 wt % C30B in drawn films prepared via a larger twin-screw extruder [3].

7.4.3 Rheological properties

The linear viscoelastic functions, complex viscosity (η^*) and storage modulus (G'), of the neat PET and its corresponding nanocomposites with and without Joncryl are presented as functions of time in Figure 7-6a and Figure 7-6b, respectively. These tests were performed to assess if the samples exhibited a time-dependent behavior and to determine a time window for subsequent frequency sweep tests. The viscoelastic properties may be time-dependent due to possible thermal degradation of the PET matrix and/or chemical reactions between PET, clay organomodifiers, and Joncryl. Two fresh disk-shape specimens of each sample were tested and the average value, which has a maximum 5% deviation, is reported. Based on these tests, less than 10% variations took place in the viscoelastic properties of all samples up 5 min. Samples containing Joncryl displayed considerably larger viscoelastic properties than those without Joncryl. The viscoelastic properties of PET containing the chain extender increase with time. Joncryl is a multifunctional epoxy-based chain extender and it is probable the epoxy groups continue to react with the hydroxyl and carboxyl end groups of PET during the rheological tests. The residence time in the extruder, measured to be around 1 min, was probably too short for a completed reaction between Joncryl and PET. During compression molding chain scission and chain extension may also take place. However due to the low level of shearing, the probability of significant chain extension decreases due to less contact between reactive groups. The presence of organoclays accelerates

the PET degradation during melt mixing and increases the carboxyl end group content [22]. The degradation of the PET matrix in the presence of the organoclays may occur during the master-batch preparation as well as during the dilution of the master-batches. A larger carboxyl end group content increases the probability of consumption of epoxy groups of the chain extender during the master-batch dilution. That may explain why the viscoelastic properties of the nanocomposites containing Joncryl do not increase with time in the rheometer. The reaction of epoxy groups with terminal groups of PET chains increases the viscoelastic properties of the PET nanocomposites containing Joncryl. However, this reaction results in the generation of new hydroxyl groups that may attack the PET backbone and reduce the molecular weight of the PET matrix for nanocomposites containing Joncryl in the rheometer with time.

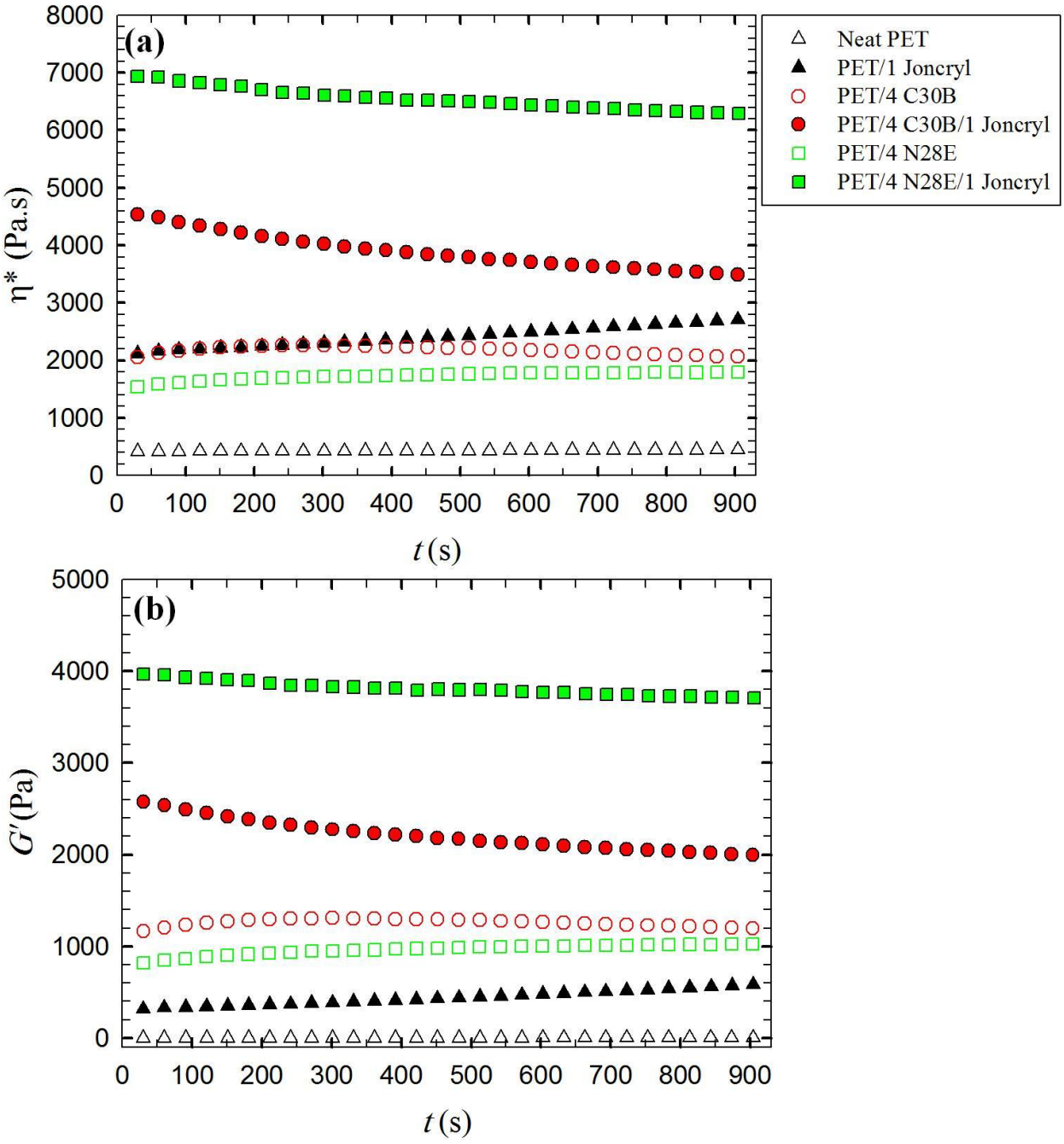

Figure 7-6: Complex viscosity (a) and storage modulus (b) as functions of time for the neat PET and its corresponding nanocomposites with and without Joncryl.

Figure 7-7a and Figure 7-7b present the complex viscosity and the storage modulus of the neat PET and PET-based nanocomposites, with and without Joncryl, as functions of frequency. The

neat PET exhibits a pseudo-Newtonian behavior, while all PET-based nanocomposites show a marked shear-thinning behavior, characteristic of nanocomposites. At low frequencies the complex viscosity and the storage modulus of PET/4 C30B are larger than those of PET/4 N28E, which is due to the higher degree of C30B exfoliation over N28E revealed by XRD and TEM results. At high frequencies, where the contribution of the matrix is more pronounced, PET/4 C30B shows a lower complex viscosity than PET/4 N28E. The better dispersion of C30B increases the exposure surface of this organoclay to the PET matrix and consequently causes a higher level of degradation. Contrary to the organic modifier of N28E, that of C30B contains unsaturated tallow with double bonds as well as hydroxyl groups which causes more degradation of the PET matrix [10]. On the other hand, the introduction of the chain extender increases the viscoelastic properties of the neat PET and its corresponding nanocomposites. As mentioned earlier, the epoxy groups of Joncryl may link the functional terminal groups of degraded PET chains and rebuild the molecular weight and viscoelastic properties [26]. The higher level of exfoliation observed for nanocomposites containing Joncryl, according to XRD and TEM results, may be explained by the larger viscosity of the matrix, which generates larger shear stresses that break down large clay tactoids into individual layers and double layer particles. The elastic modulus of the PET-based nanocomposites (Figure 7-7b) exhibit a plateau at low frequencies, corresponding to the formation of a percolated three-dimensional network of clay particles, which acts like a weak solid [36]. The introduction of Joncryl increases the viscoelastic properties of the PET nanocomposite containing N28E more than that containing C30B. Joncryl functional groups connect shorter chains in the case of PET-based nanocomposites containing C30B in comparison to those containing N28E, due to the more severe chain scission induced by C30B. Besides, the organic modifier of C30B contains hydroxyl groups that might also react with the epoxy groups of Joncryl and consequently reduce the amount of Joncryl functional groups available for chain extension.

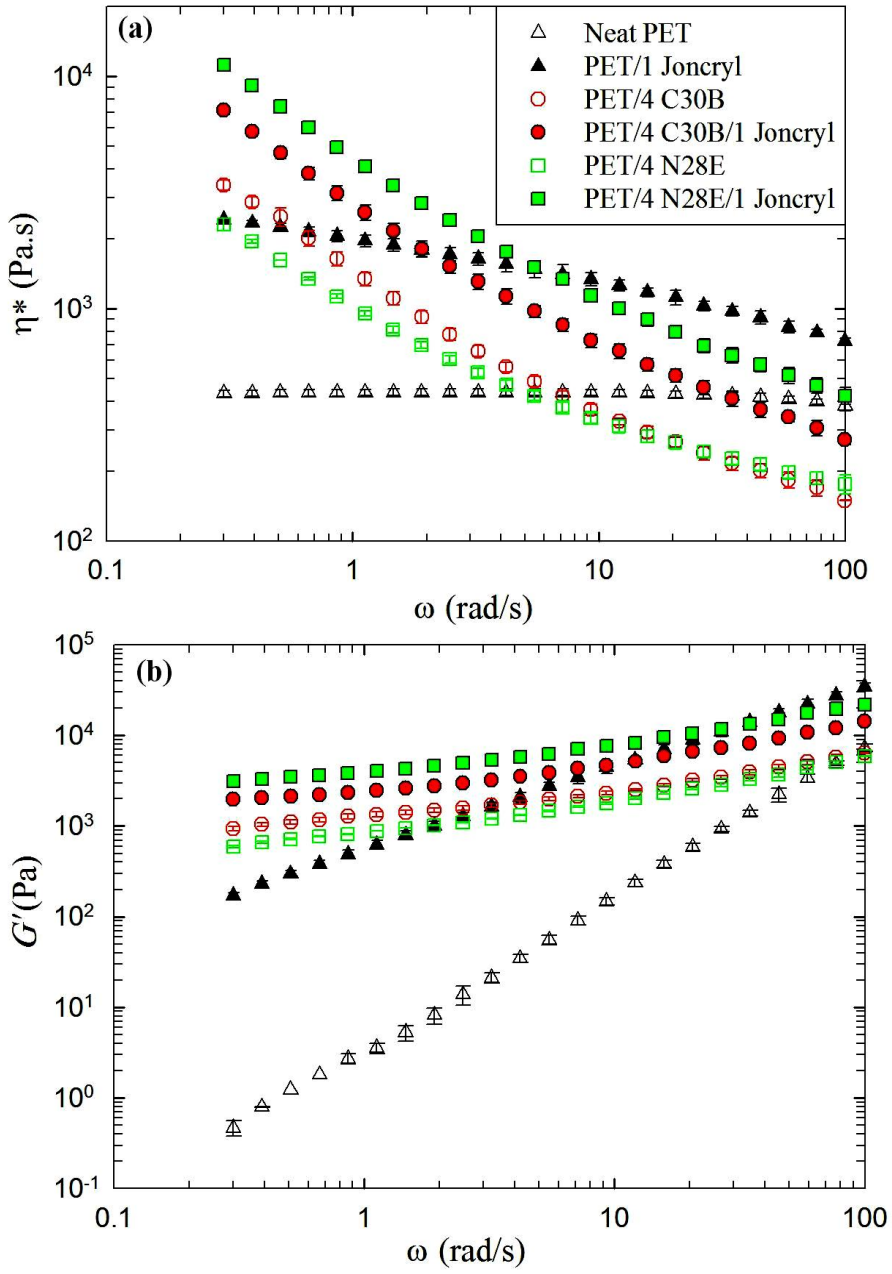

Figure 7-7: Complex viscosity (a) and storage modulus (b) of the neat PET and PET-based nanocomposites with and without Joncryl as functions of frequency.

Adding multifunctional chain extenders to linear polymers may result in chain branching and gelation. A gel content test were performed at 25 ºC by dissolving the samples containing Joncryl in a (60/40 ratio wt/wt) phenol/1,1,2,2-tetrachloroethane solution. In less than half an hour all

samples were completely dissolved in the solvent, suggesting a gel-free structure for all samples containing the chain extender. The critical mole fraction of the chain extender for gelation, α_c, may be estimated from the following equation:

$$\alpha_c = \frac{1}{f - 1} \tag{7-5}$$

where *f* is the chain extender functionality [11, 37]. For the chain extender used in this study $\alpha_c \sim$ 0.33 as the functionality of Joncryl is around 4 [26]. The weight average molecular weights of Joncryl and the PET are 6800 and 65 000 g/mol, respectively, implying that the critical weight fraction of Joncryl for gelation is 4.97%, which is remarkably larger than that used in this study.

Wood-Adams *et al.* [38] investigated the effect of molecular weight and short and long chain branching on the linear viscoelastic behavior of polyethylenes. They observed that while short chain branching does not change the viscoelastic properties of the matrix, the loss angle (δ) curves for branched polyethylenes are quite different from that of linear polyethylenes. It has been also reported by other researchers that long chain branching decreases the value of δ and changes the plot of δ vs. ω [11, 39]. Figure 7-8 presents the loss angle of the neat PET and PET containing 1 wt% Joncryl as a function of frequency. This graph clearly shows that the presence of Joncryl changes the linear molecular structure of PET, with δ = 90º at low frequencies, to a branched structure with lower δ at all frequencies.

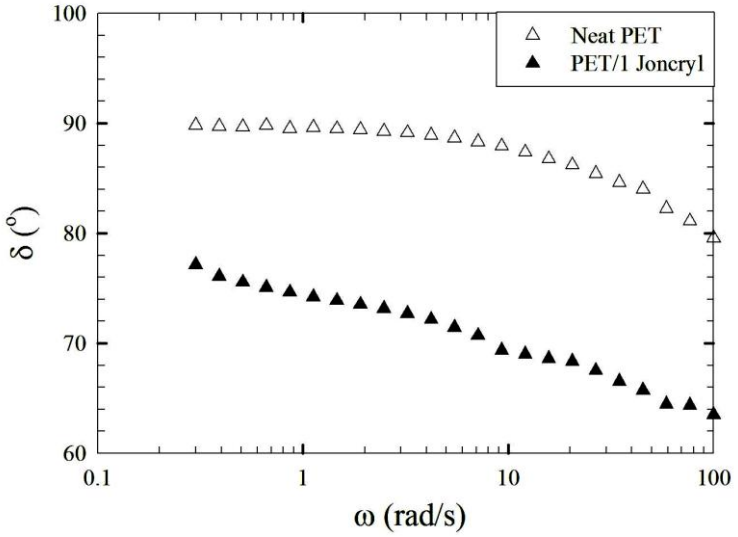

Figure 7-8: Loss angle of the neat PET and PET containing 1 wt% Joncryl as a function of frequency.

7.4.4 Thermal properties

Table 7-1 reports the effect of Joncryl and the organoclays on the glass transition temperature, T_g, the melting temperature, T_m, cold crystallization temperature, T_{cc}, hot crystallization temperature, T_{hc}, and crystal content of PET. The melting point of PET is almost unaffected by the presence of the chain extender or the organoclays, suggesting that the addition of the organoclays and/or Joncryl does not change the melting process. T_g of the nanocomposites is almost equal to that obtained for the neat PET, except for PET/4 C30B, which shows the lowest glass transition temperature that may be attributed to the severe thermal degradation of PET chains induced by C30B. The nanometric dispersion of silicate nanolayers in a polymer matrix provides a large interfacial area and promotes heterogeneous crystallization as clay platelets act as a strong nucleating agent. This explains the lower cold crystallization temperature of the nanocomposites in comparison to the neat PET. Based on the rheological results the presence of Joncryl increases the complex viscosity of the samples, which generates larger stresses during film extrusion and, consequently, we may expect more oriented chains for the films containing the chain extender. All the samples containing Joncryl display a lower T_{cc} in

comparison to those without Joncryl because the required energy for crystallization decreases as the chains become more oriented [40]. The crystal content of the films was calculated from the enthalpy of melting ΔH_m and the enthalpy of cold crystallization ΔH_{cc} according to the following equation:

$$X_c = \frac{(\Delta H_m - \Delta H_{cc})/w_{PET}}{\Delta H_m^\circ} \tag{7-6}$$

where w_{PET} is the PET weight fraction and ΔH_m° is the enthalpy of melting of 100% crystalline PET (140 J/g) [40]. The presence of silicate layers enhances the crystallinity of the PET-based nanocomposite films. Higher crystal content was also obtained for the samples containing Joncryl. The orientation of molecular segments increases the nucleation rate of crystallization. In comparison to polymer random coils in an isotropic state, oriented uncrystallized polymer chains have lower configurational entropy which reduces the entropic penalty for crystallization [41]. The heterogeneous nucleating effect of clay platelets also results in the enhancement of the hot crystallization temperature of the nanocomposites, in comparison to the neat PET. After removing the effect of processing, all samples containing the chain extender exhibit lower hot crystallization temperature in comparison to those without Joncryl. It seems that the branched structure of the samples containing Joncryl results in a steric hindrance to close packing of PET chains and affects the ability of the matrix to crystallize.

Table 7-1: Thermal properties of the neat PET and PET-based nanocomposites with and without Joncryl.

Sample	$T_g(^\circ C)$	$T_m(^\circ C)$	$T_{cc}(^\circ C)$	$T_{hc}(^\circ C)$	Crystalline degree (%)
Neat PET	78.5 ± 0.1	243.1 ± 0.1	136.4 ± 0.1	181.6 ± 0.3	4.1 ± 0.2
Neat PET/1 Joncryl	78.2 ± 0.2	242.0 ± 0.2	121.3 ± 0.1	176.0 ± 1	5.6 ± 0.3
PET/4 C30B	75.1 ± 0.3	244.8 ± 0.1	128.9 ± 0.2	198.5 ± 0.2	8.2 ± 0.1
PET/4 C30B/1 Joncryl	76.2 ± 0.1	243.4 ± 0.3	117.8 ± 0.1	194.5 ± 0.1	9.7 ± 0.2
PET/4 N28E	77.1 ± 0.4	244.5 ± 0.1	133.6 ± 0.1	199.7 ± 0.1	6.6 ± 0.4
PET/4 N28E/1 Joncryl	76.0 ± 0.1	243.5 ± 0.1	123.3 ± 0.2	196.7 ± 0.1	7.9 ± 0.6

7.4.5 Mechanical properties

The tensile modulus and the toughness of the neat PET and PET-based nanocomposites, with and without Joncryl, and in the machine direction are reported in Figure 7-9a and Figure 7-9b, respectively. The incorporation of clay particles into the PET matrix increases the tensile modulus and leads to more brittleness in comparison with the neat PET films. The Young modulus of PET/4 N28E/1 Joncryl nanocomposite films is improved by about 66% compared with the neat PET. The tensile modulus of the PET matrix is around 1.8 GPa, while clay platelets have a modulus of 178 GPa [42]. Therefore, the presence of clay particles within the PET matrix increases the mechanical properties because a significant portion of the applied load may be carried by the clay particles. The Young modulus of the samples containing Joncryl is larger than those without Joncryl, which may be attributed to the larger molecular weight and increased crystallinity of the matrix. Besides, for nanocomposites containing Joncryl, the larger Young modulus might also be attributed to a better dispersion of the silicate nanolayers in the matrix, as confirmed by the XRD and TEM results. Despite the higher exfoliation level of C30B over N28E within the PET matrix, it seems that the more severe chain scission induced by C30B results in nanocomposites with lower Young modulus values in comparison to those containing N28E. It has been reported that the introduction of clay particles to a polymer matrix leads to a reduction of the elongation at break and more brittleness [5, 15, 43, 44]. The brittle behavior of nanocomposites is probably due to the higher crystallinity, molecular weight reduction due to thermal degradation, presence of clay aggregates, and interlaminar debonding of clay particles and formation of microvoids, which can initiate the crack propagation throughout the matrix. Coalescence of the microvoids and formation of large cracks results in the embrittlement of nanocomposites [44, 45]. He *et al*. [46] reported that elongation at break of polyamide 6/Nanomer® I.30TC decreases with clay concentration, while the Young modulus increases with clay concentration. They postulated that although the adhesion between the clay particles and the matrix was adequate the clay particles promoted the formation of numerous crazes and microcracks near the interface of the clay platelets and the matrix [46]. In this work, all PET-based nanocomposite films exhibit lower toughness values in comparison to the neat PET films, due to the presence of the organoclays and higher crystallinity [47]. The presence of the chain extender and/or the organoclays increases stiffness, but deteriorates the elongation at break of the

samples at the same time (data not shown). The resulting toughness is a combination of the mentioned factors.

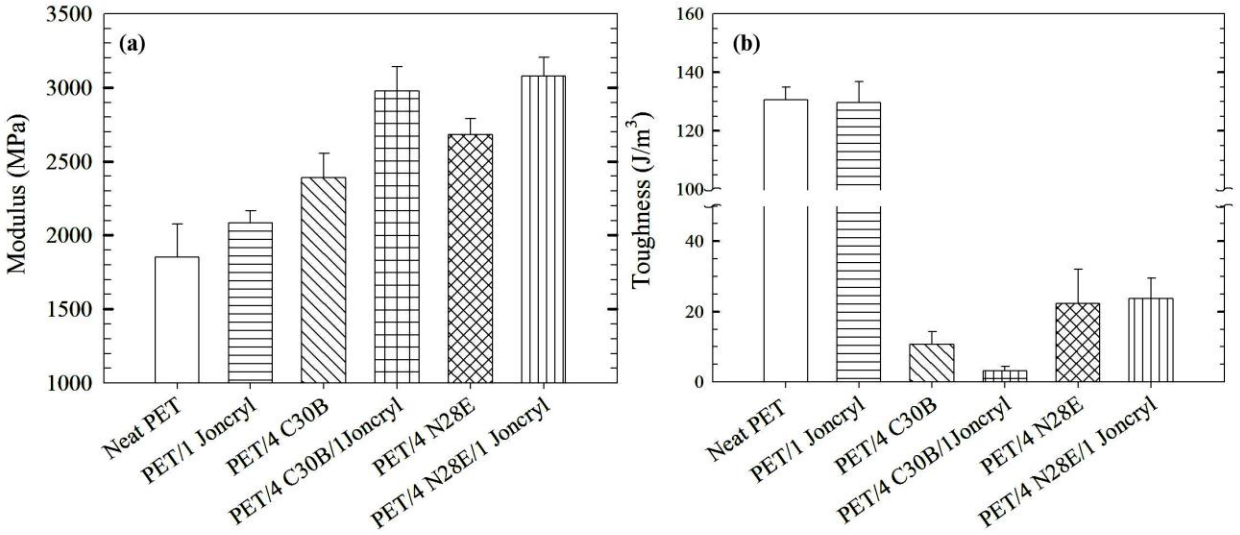

Figure 7-9: Tensile modulus (a) and toughness (b) data of the neat PET and PET-based nanocomposites with and without Joncryl.

7.4.6 Optical properties

For several applications, transparency and haze are considered as two important optical properties. Clarity correlates with the ability of the film to show the fine details of an object viewed through it. As the clarity decreases, the clear or sharp image of the object appears to be fuzzy. If a bright dot on a dark field is viewed through a film with low clarity, a halo appears around the dot and gives an out-of-focus image of the bright dot. On the other hand, high haze values are associated with seeing a smoky, milky, or cloudy image of an object viewed through the film. In this case the contrast between the bright dot and the dark field reduces and a decrease in visibility similar to what occurs in fog [31]. Crystalline regions and filler particles, which have different refractive index from the rest of the material, filler concentration, particle size, and dispersion quality of the particles influence the transparency of a film. Any chemical changes in the polymer structure such as degradation may also change the optical properties [48]. The measured haze and clarity values for the films investigated in this study are depicted in Figure

7-10a and Figure 7-10b, respectively. From these figures it can be observed that all nanocomposite films have higher haze and lower clarity with respect to neat PET. The samples containing Joncryl exhibit higher haze and lower transparency values in comparison to those without Joncryl. When the haze percentage is higher than 30%, the material is considered as translucent instead of transparent [48]. Accordingly, the PET-based nanocomposites without Joncryl are classified as transparent materials while those containing Joncryl are translucent.

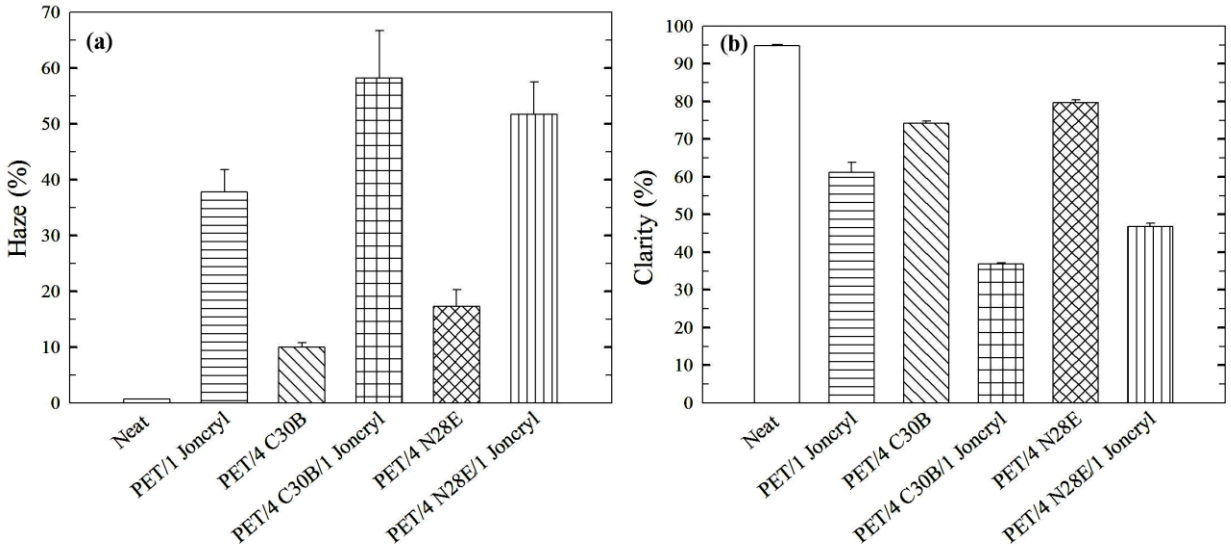

Figure 7-10: Haze (a) and clarity (b) measurements of the neat PET and PET-based nanocomposites with and without Joncryl.

7.4.7 Barrier properties

Impermeable silicate nanolayers block gases transport through a polymer matrix, and by creating a tortuous pathway force the permeant to travel longer diffusive path. Hence, higher level of exfoliation is favorable for barrier properties enhancement [1]. As mentioned earlier, the presence of clay layers increases the crystal content of the nanocomposite films. The permeability of gases through a polymer matrix depends on the available free volume of the matrix. The crystalline phase increases the barrier properties of polymers as polymer chains are efficiently packed in crystallites, which reduce the unoccupied volume of the matrix essential for gas transport. Figure 7-11 shows the measured oxygen permeability values of the neat PET and PET-based

nanocomposite films, with and without Joncryl. All nanocomposite films exhibit higher barrier properties than the neat PET due to the presence of clay layers and larger crystal content. The barrier properties of the films containing Joncryl are better than those without Joncryl, which can be attributed to the better clay dispersion and/or larger crystallinity. Overall, a 46% improvement in barrier properties was obtained for the PET nanocomposites containing C30B and Joncryl in comparison to the neat PET films. The corresponding improvement for the PET/4 N28E/1 Joncryl was 40%. According to XRD, TEM, and DSC results, the PET/4 C30B/1 Joncryl films show the highest level of exfoliation and contain the highest amount of crystals, which explains the lowest oxygen permeability. It is worth noting that barrier properties of the PET/4 C30B films are better than those of the PET/4 N28E films because of the larger crystallinity and better clay dispersion.

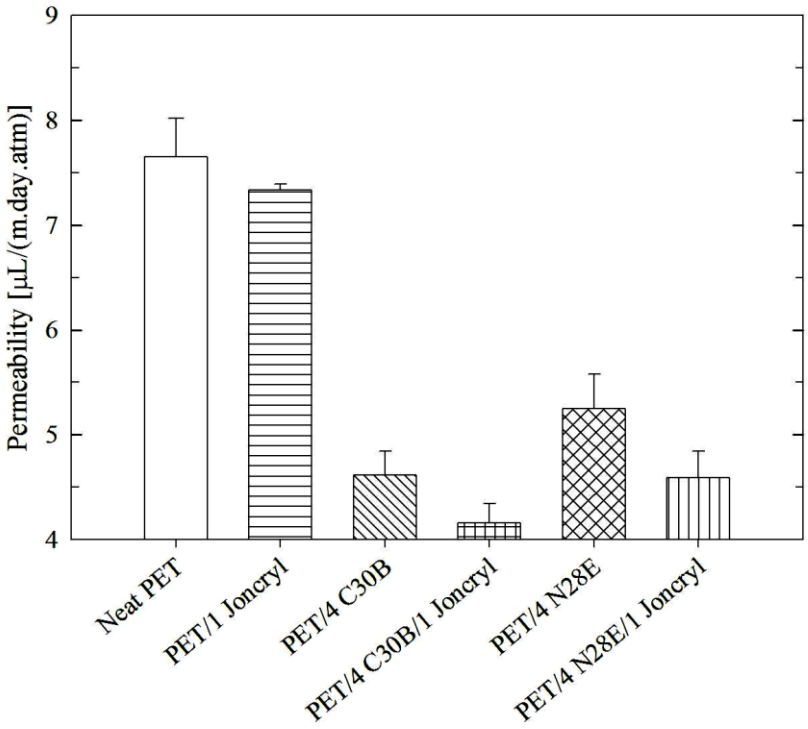

Figure 7-11: Oxygen permeability of the neat PET and PET-based nanocomposites with and without Joncryl.

7.5 Conclusion

A twin-screw extruder was used to prepare PET nanocomposites containing C30B and N28E. To rebuild the molecular weight of the degraded matrix and improve clay dispersion, a chain extender (Joncryl) was introduced in the nanocomposites via a master-batch approach. XRD and TEM were employed to evaluate the morphology and the state of delamination. The level of exfoliation improved for nanocomposites containing Joncryl. Functional groups of the chain extender reacted with PET end groups and resulted in the enhancement of the viscoelastic properties. The nanocomposite films exhibit larger crystallinity and lower cold crystallization temperature due to the nucleation effect of the clay layers. The presence of the organoclays and/or the chain extender resulted in more hazy films. Higher barrier and mechanical properties were obtained for the films containing Joncryl in comparison to those without Joncryl. The Young modulus of the nanocomposite films containing N28E and Joncryl was improved by 66%, slightly more than the corresponding C30B nanocomposites. The oxygen permeability of the nanocomposite films containing 4 wt% C30B and 1 wt% Joncryl decreased by 46% in comparison to the neat PET films. The corresponding permeability decrease for the N28E nanocomposite was 40%.

7.6 Acknowledgments

The authors are thankful to Mrs. W. Leelapornpisit for preparing the TEM images. Financial support from NSERC (Natural Science and Engineering Research Council of Canada) in the context of the NRC-NSERC-BDC Nanotechnology Initiative is gratefully acknowledged. We also thank BASF, Germany for supplying Joncryl® ADR-4368F used in this study.

7.7 References

1. Bhattacharya S, Gupta R, and Kamal M. Polymeric nanocomposites: theory and practice: Hanser Gardner Publications, 2007.
2. Brooks D and Giles GA. PET Packaging Technology, 1 ed.: Blackwell, 2002.
3. Ghanbari A, Heuzey M, Carreau P, and Ton-That MT. Polymer International In press.
4. Ghasemi H, Carreau PJ, Kamal MR, and Chapleau N. International Polymer Processing 2011;26(2):219-228.
5. Ghasemi H, Carreau PJ, Kamal MR, and Tabatabaei SH. Polymer Engineering and Science 2012;52(2):420-430.
6. Xu XF, Ghanbari A, Leelapornpisit W, Heuzey MC, and Carreau P. International Polymer Processing 2011;26(4):444-455.
7. Soon KH, Harkin-Jones E, Rajeev RS, Menary G, McNally T, Martin PJ, and Armstrong C. Polymer International 2009;58(10):1134-1141.
8. Beall G and Powell C. Fundamentals of Polymer-Clay Nanocomposites: Cambridge University Press, 2011.
9. Ray SS and Okamoto M. Progress in Polymer Science 2003;28(11):1539-1641.
10. Fornes TD, Yoon PJ, and Paul DR. Polymer 2003;44(24):7545-7556.
11. Najafi N, Heuzey MC, Carreau PJ, and Wood-Adams PM. Polymer Degradation and Stability;97(4):554-565.
12. Stoeffler K, Lafleur PG, and Denault J. Polymer Degradation and Stability 2008;93(7):1332-1350.
13. Litchfield DW, Baird DG, Rim PB, and Chen C. Polymer Engineering and Science;50(11):2205-2215.
14. Chang JH, Kim SJ, Joo YL, and Im S. Polymer 2004;45(3):919-926.
15. Ghasemi H, Carreau PJ, Kamal MR, and Uribe-Calderon J. Polymer Engineering and Science;51(6):1178-1187.
16. Sanchez-Garcia MD, Gimenez E, and Lagaron JM. Journal of Plastic Film & Sheeting 2007;23(2):133-148.
17. Sanchez-Solis A, Garcia-Rejon A, and Manero O. Macromolecular Symposia 2003;192:281-292.
18. Frounchi M and Dourbash A. Macromolecular Materials and Engineering 2009;294(1):68-74.
19. Barber GD, Calhoun BH, and Moore RB. Polymer 2005;46(17):6706-6714.
20. Chung JW, Son SB, Chun SW, Kang TJ, and Kwak SY. Polymer Degradation and Stability 2008;93(1):252-259.

21. Pielichowski K and Njuguna J. Thermal Degradation of Polymeric Materials: Smithers Rapra Press, 2008.

22. Xu XF, Ding YF, Qian ZZ, Wang F, Wen B, Zhou H, Zhang SM, and Yang MS. Polymer Degradation and Stability 2009;94(1):113-123.

23. Scheirs J and Long T, E. Modern Polyesters: Chemistry and Technology of Polyesters and Copolyesters, 1 ed.: John Wiley & Sons, Ltd, 2003.

24. Najafi N, Heuzey MC, and Carreau PJ. Composites Science and Technology;72(5):608-615.

25. Meng Q, Heuzey M, and Carreau P. Polymer Degradation and Stability 2012;in press.

26. Villalobos M, Awojulu A, Greeley T, Turco G, and Deeter G. Energy 2006;31(15):3227-3234.

27. Torres N, Robin JJ, and Boutevin B. Journal of Applied Polymer Science 2001;79(10):1816-1824.

28. Haralabakopoulos AA, Tsiourvas D, and Paleos CM. Journal of Applied Polymer Science 1999;71(13):2121-2127.

29. Awaja F, Daver F, and Kosior E. Polymer Engineering and Science 2004;44(8):1579-1587.

30. Cavalcanti FN, Teofilo ET, Rabello MS, and Silva SML. Polymer Engineering and Science 2007;47(12):2155-2163.

31. Pike L. Journal of plastic film & sheeting 1993;9:173.

32. Wang YL, Fu CH, Luo YX, Ruan CS, Zhang YY, and Fu Y. Journal of Wuhan University of Technology-Materials Science Edition;25(5):774-779.

33. Bikiaris DN and Karayannidis GP. Journal of Polymer Science Part a-Polymer Chemistry 1996;34(7):1337-1342.

34. Van Krevelen D and Te nijenhuis K. Properties of Polymers, 4th ed.: Elsevier Science, 2009.

35. Luo ZP and Koo JH. Polymer 2008;49(7):1841-1852.

36. Vermant J, Ceccia S, Dolgovskij MK, Maffettone PL, and Macosko CW. Journal of Rheology 2007;51(3):429-450.

37. Flory P. Principles of Polymer Chemistry: Cornell University Press, 1953.

38. Wood-Adams PM, Dealy JM, deGroot AW, and Redwine OD. Macromolecules 2000;33(20):7489-7499.

39. Gotsis AD, Zeevenhoven BLF, and Tsenoglou CJ. Journal of Rheology 2004;48(4):895-914.

40. Matthews RG, Ajji A, Dumoulin MM, and Prud'homme RE. Polymer 2000;41(19):7139-7145.

41. Salem D. Structure Formation in Polymeric Fibers, 1 ed.: Hanser Gardner Publications, 2001.

42. Fornes TD and Paul DR. Polymer 2003;44(17):4993-5013.

43. Fornes TD, Yoon PJ, Hunter DL, Keskkula H, and Paul DR. Polymer 2002;43(22):5915-5933.

44. Pavlidou S and Papaspyrides C. Progress in polymer science 2008;33:1119.

45. Phang IY, Liu TX, Mohamed A, Pramoda KP, Chen L, Shen L, Chow SY, He CB, Lu XH, and Hu X. Polymer International 2005;54(2):456-464.

46. He CB, Liu TX, Tjiu WC, Sue HJ, and Yee AF. Macromolecules 2008;41(1):193-202.

47. Beland S. High Performance Thermoplastic Resins and Their Composites, 1 ed.: William Andrew, 1990.

48. Ram A. Fundamentals of Polymer Engineering, 1 ed.: Springer, 1997.

CHAPTER 8
GENERAL DISCUSSION

The morphology of a polymer nanocomposite, which governs the final properties, is dependent on the degree of compatibility between components (i.e. polymer matrix and silicate layers). Silicate layers of organoclays have polar groups, therefore polymers with polar groups are capable to have strong interactions with clay particles. The exfoliated morphology of polyamide/organoclay nanocomposites and consequently, the marked improvements in barrier and mechanical properties of the matrix, show the importance of favorable interactions between silicate layers and the host polymer matrix. Accordingly, the first part of this study was devoted to investigating the effect of a PET-ionomer with sulfonated groups on the exfoliation of PET-based nanocomposites. As the final morphology of nanocomposites is also dependent on the organic part of the organoclays, two commercially available organoclays, C30B and N28E, modified with different surfactants were employed.

Contradictory results regarding the miscibility state of PET and PET-ionomer were obtained based on various characterization techniques. For all compositions of PET/PET-ionomer blends, a single glass transition temperature was observed. A continuous reduction of melting point was also observed for the blends with increasing PET-ionomer content. Although results of these two methods (i.e. the melting point depression and the T_g approach) suggest a miscible blend, a selective solvent dissolution technique followed by SEM revealed droplet-matrix and co-continuous morphologies for the blends. Therefore, any decision regarding the miscibility state of a blend based on the melting point depression and the T_g approach should be done with precautions. It is worth noting that droplets of the dispersed PET-ionomer phase were also clearly observed in TEM images, which confirm SEM results. It is worth mentioning that rheological techniques are also frequently used to assess miscibility of polymers, however since PET is very sensitive to thermal degradation, which influences the results, this approach could not be used in this work.

The advantage of C30B over N28E is that the former's surfactant contains two hydroxyl groups which could bring good compatibility between PET chains and the organoclay. Hence, a good

dispersion and distribution of C30B particles were obtained in the nanocomposites. However, migration of the C30B particles into the more polar polymer (i.e. PET-ionomer domains) restricted their uniform distribution. Due to localization of the organoclays in the PET-ionomer domains, the barrier properties were not improved as compared to the PET nanocomposite without the ionomer. It is reasonable to generalize migration of polar nanoparticles to a more polar phase to other polymer blends. Therefore, an appropriate polar polymer, which is miscible with the matrix, must be selected to take advantage of this approach. In the case of immiscible blends, adding enough of the polar polymer to obtain a co-continuous morphology may help the uniform distribution of the nanoparticles. Barrier properties of the polar polymer against transmission of oxygen in comparison to the matrix, along with optical clarity of the blend, are also challenging issues to be considered.

Another key issue to be addressed is food contact regulations of the matrix, additives, and nanoparticles. While PET 9921 produced by Eastman Chemical Company can be used for refillable carbonated soft drinks, food packaging, and health and nutrition containers, food contact regulations for ionomeric resins must be verified in the Code of Federal Regulations-Title 21: Food and Drugs (21 CFR 177.1330). According to these regulations, ethylene/methacrylic acid copolymers such as Surlyn® supplied by DuPont™ may be safely used for contacts with food. AQ 55S, supplied by Eastman Chemical Company and used as the PET-ionomer in this study, is reported safe for cosmetic and personal care applications. However, to our knowledge there is no data in the literature regarding its food contact regulations. According to the data sheet provided by Eastman Chemical Company, numerous safety studies have been performed on the determination of the toxicity of Eastman AQ™ polyesters (including AQ 55S), and results from these studies indicate that the polyester ionomers can be used in many different types of applications with wide safety margins. In terms of clay use, it has been reported that pristine natural nanoclay is approved by the U.S. Food and Drug Administration (FDA) for food contact applications [95]. The organo-modified clay C30B used in this study was also reported to be FDA approved to be used as a food contacting material [96]. Hence, while further investigation of the appropriateness of the materials used in this study is required for food and beverage applications, they *a priori* appear to be on the safe side. In addition, they may relatively easily be replaced by FDA-approved equivalents.

In the first phase of this study we observed that XRD results may be misleading in morphological characterization of nanocomposites as no peak was observed for nanocomposites containing large aggregates. It was attributed to clay dilution due to non-uniform distribution. SEM and TEM are expensive and time-consuming techniques, which examine only a very small portion of the sample, especially in the case of TEM. Besides, SEM cannot display exfoliated layers and very small tactoids. Accordingly, rheological methods must be employed as a significant volume of sample is tested which increase the reliability of the data. However care must be taken if degradation occurs during the rheological measurements since it may be misleading and hide phenomena related to nanoparticles or morphology evolution.

Various organoclays with different organic modifiers were employed to fabricate PET nanocomposites. The effect of clay loading and processing on the morphology and rheology of the nanocomposites was also investigated. XRD patterns indicated that the gallery spacing of C30B in the nanocomposites is independent of clay loadings and processing conditions. However, SEM micrographs showed that the screw configuration with more kneading blocks and longer residence time is more efficient in breaking down the large clay aggregates. SEM observations were confirmed by rheological measurements as larger viscoelastic properties were obtained for the nanocomposites processed with a more severe screw profile. Presence of the nanoparticles makes it impossible to directly measure the molecular weight of the matrix of the nanocomposites using viscometry. The presence of the nanoparticles influences the flow time of the nanocomposite solutions and lead to wrong estimation of the matrix molecular weight. That is why the Maron-Pierce equation and high frequency data were employed to determine the PET apparent viscosity and subsequently the apparent molecular weight of the matrix. Incorporating 8 wt% C30B led to more than 50% reduction in the molecular weight of the PET matrix. Therefore, incorporating high concentrations of nanoparticles may not improve the properties of nanocomposites to expected level if severe matrix degradation takes place. It should be mentioned that favorable interactions between PET and the organoclays, estimated based on the solubility parameter, follow the same order as the apparent yield stress. This finding also confirms that the rheological method can be thought as a strong tool in the characterization of nanocomposites and detecting the interactions between nanoparticles and a host polymer matrix. XRD, SEM, TEM, and rheological results indicate that the organoclay with the solubility parameter closer to that of the matrix yields a better morphology. Therefore, calculating *a priori*

the solubility parameter, based on the Fedors group contribution method, may be useful to choose an appropriate organoclay for a specific polymer matrix.

Higher amount of organic modifier in the interlayer spacing of organoclays increases the hydrophobicity of clay particles. Moreover, the initial basal spacing of the organoclays increases with surfactant loading. C15A has the highest excess of the organic modifier (35%) with the largest initial gallery spacing as compared to the other organoclays studied in this work. Nevertheless, XRD results indicated that PET nanocomposites containing this organoclay exhibited the lowest intercalation level. Besides, the unbound excess amount of the organic modifier contributed to the severe degradation of the matrix. The apparent yield stress obtained for the corresponding nanocomposite is among the lowest values obtained in this study. Saturation or high organic content of interlayer restricts the penetration of PET chains into the gallery spacing; hence nanocomposites with lower level of intercalation are obtained.

In view of our finding about the severe degradation of the PET matrix in the presence of the organoclays, the last part of this research aimed at compensating the degradation of the matrix by employing a multifunctional chain extender. Functional groups of the epoxy-based chain extender may link the terminal groups of degraded PET chains and enhance viscoelastic properties of the samples. However, high viscosity of the matrix has two opposite effects on the process of exfoliation. A PET matrix with higher viscosity imparts a higher level of shear stress onto the clay particles and facilitates the exfoliation of the silicate nanolayers within the matrix. But at the same time, it hinders the diffusion of PET chains within the interlayer spacing of the silicate layers. Considering these two antagonistic phenomena, the nanocomposites were prepared by a master-batch approach in which initially low molecular weight PET chains could easily diffuse into the gallery spacing of the silicate layers, and then by incorporating the chain extender high shear stresses were generated, which enhanced the exfoliation level. It should be mentioned that the chain extension approach proposed here is of interest only at limited concentrations of the multifunctional chain extender. In fact concentration of the chain extender must be lower than the critical mole fraction for gelation (cross-linking). Besides, according to the European Food Contact Legislation, Joncryl®ADR-4368 supplied by BASF and employed as a chain extender in this study, may be used up to 1 wt% in the manufacture of PET food packaging containers in contact with aqueous, acidic, and alcoholic (up to 10% alcohol) foods in compliance with the Framework Regulation 1935/2004/EC and the Plastic Directive 2002/72/EC.

XRD, TEM, and image analysis indicated that PET nanocomposites containing Joncryl exhibited better morphology (i.e. higher delamination level and lower clay aggregates). The chain extension reaction was confirmed with both FT-IR and rheological characterization. The Young modulus and oxygen barrier properties were also improved in the presence of the chain extender. However, more hazy films were obtained due to the presence of the organoclays and/or the chain extender as well as increased crystallinity. Generally speaking, for any polymer/particle blend experiencing degradation, employing a suitable multifunctional chain extender may rebuild molecular weight and improves dispersion of the particles within the matrix. Needless to say that although bifunctional chain extenders preserve linear structure of the matrix, multifunctional chain extenders are more efficient in increasing the molecular weight.

Secondary processing, such as bi-axial stretching, affects orientation of clay particles and the morphology and final properties of nanocomposites. During bi-axial stretching platelets may slide along the tactoids, which creates longer tortuous pathway by increasing the tactoids length, and consequently improve barrier properties [74]. On the other hand bi-axial stretching parameters (e.g. stretch ratio, temperature, etc,) must be carefully optimized as crack formation around clay particles may take place and cause barrier properties to deteriorate.

As mentioned earlier, considering that allowable oxygen concentration limit in beer is 1 ppm, it has been reported that the time limit for beer quality preservation in typical 1.5 L PET bottles is around one month [6]. Therefore, a 50% reduction in oxygen transmission rate may increase the shelf life of beer in 1.5 L PET nanocomposites bottles to about 2 months.

CHAPTER 9
CONCLUSIONS AND RECOMMENDATIONS

9.1 Conclusions

In this dissertation, PET nanocomposites containing various organoclays were prepared by melt intercalation and morphological, rheological, thermal, optical, mechanical, and barrier properties of the nanocomposites were examined by means of various characterization tools.

First, PET nanocomposite films containing 2 nominal wt% C30B and N28E were prepared by cast extrusion. A PET-ionomer was added to the nanocomposites to enhance the gallery spacing of the incorporated organoclays. A comprehensive study was performed to evaluate the state of miscibility of PET and PET-ionomer. Droplet-matrix and co-continuous morphologies of the immiscible blends were clearly displayed in SEM and TEM images. Higher affinity of the silicate layers for the PET-ionomer domains led to the migration of the organoclay into the dispersed phase. The preferential localization of the clay particles within the PET-ionomer restricted the uniform distribution of the organoclays in the nanocomposites. XRD patterns, TEM image analysis, and rheological results, however, indicated that for nanocomposites containing N28E, the PET-ionomer acted as an effective exfoliation agent and improved the level of delamination of the silicate layers. Thermal studies demonstrated the nucleating role of the silicate layers in crystallization behavior of the nanocomposite films. Compared to the neat PET film, cold crystallization and hot crystallization temperatures of the nanocomposite films decreased and increased, respectively. Crystallinity of the nanocomposite films was higher than that of the neat PET film. Incorporation of the organoclays led to gas barrier enhancements for all the nanocomposites in comparison to the neat PET film. Adding 2 nominal wt% C30B brought about 25% reduction in oxygen permeability. The highest value for the dispersion parameter, $D_{0.1}$ = 7.5%, was obtained for the nanocomposites containing C30B which is very close to the fully exfoliated value of the parameter.

The effect of clay chemistry, clay loading, and processing conditions on the morphology and the rheology of the nanocomposites were investigated in the second part of this study. According to XRD patterns, the gallery spacing of the organoclays (i.e. C30B, C15A, C25A, and N28E) was

increased due to the intercalation of PET chains, while the peak position of the pristine synthetic clay (i.e. SM100) did not shift to lower angles. XRD results showed that the interlayer distance of the clay particles is independent of the clay concentration. However, the intensity of the peaks increased with clay loading. TEM images indicated that the count for exfoliated layers decreased with clay concentration. The morphology and rheological properties of the nanocomposites improved significantly by employing a screw configuration with reverse elements and more kneading blocks.

A pseudo Newtonian-like behavior was observed for the neat PET while all PET nanocomposites exhibited a shear-thinning behavior which became more pronounced with clay concentration. A pseudo solid-like behavior was observed for the nanocomposites at low frequencies and high clay loadings, which was attributed to the formation of an interconnected network of clay particles. Due to PET degradation, induced by the presence of the organoclays, the complex viscosity of the nanocomposites was lower than that of the neat PET at high frequencies. The Maron-Pierce equation was used for estimating the matrix degradation. Incorporating 8 wt% C30B led to remarkable reduction of the matrix molecular weight, from 65 to 29.8 kg/mol. The highest degree of intercalation, the largest values of the apparent yield stress, complex viscosity, and storage modulus were obtained for the nanocomposites containing C30B. It is worth mentioning that the solubility parameter of PET is closer to that of C30B.

Finally, the last part of this thesis looked at the effect of a multifunctional epoxy-based chain extender on the control of thermal degradation of the matrix induced by the presence of the organoclays. Epoxy groups of the chain extender react with PET end groups and rebuild the molecular weight of the matrix by linking the degraded chains. Intensity of the XRD peaks reduced significantly for the nanocomposites containing Joncryl, which is a promising sign for a higher level of delamination. TEM results indicated that for nanocomposites containing Joncryl the count for single layer particles and aggregates increased and decreased, respectively. Higher clay density was obtained for the nanocomposites containing the chain extender, as clay tactoids with a high number of silicate layers per particle broke down to more clay particles with lower numbers of platelets per particle. The presence of Joncryl led to a significant improvement in the viscoelastic properties of the samples, due to connection of PET chains together. Higher degrees of crystallinity and lower cold crystallization temperatures were obtained for the nanocomposites in comparison to the neat PET. 61 and 66% improvements in the tensile modulus were obtained

for the nanocomposite films containing C30B and N28E, respectively, in the presence of Joncryl. Incorporation of Joncryl in the nanocomposite films containing C30B and N28E reduced the oxygen permeability by 46 and 40%, respectively.

9.2 Original contributions

- Comprehensive properties of PET nanocomposite films have been rarely reported. In this regard, PET nanocomposite films were prepared by extrusion and various properties of the samples such as thermal, mechanical, optical, and barrier properties were examined.
- A fundamental study was performed to investigate the state of miscibility of PET and PET-ionomer, which has not been addressed in the literature. It has been demonstrated that the melting point depression and the single T_g approaches may be misleading in predicting miscibility of a blend and microscopy techniques are required to shed more light on the state of miscibility of a blend.
- We observed that incorporation of a more polar polymer may increase the gallery spacing of silicate layers; however, clay particles migrate in the more polar PET-ionomer domains.
- In the first part of this study we observed that the complex viscosity decreases by adding 2 wt% C30B and N28E which was quite surprising at the beginning. In the second part of this work, the molecular weight reduction of the matrix in the presence of the organoclays was quantified using the Maron-Pierce equations. It was shown that the apparent yield stress of the PET nanocomposites containing various organoclays follows the same order as favorable interactions between PET and the organoclays based on the solubility parameter.
- To our knowledge, no work has been published on the control of thermal degradation of PET nanocomposites using a multifunctional chain extender. In view of our experimental results, we observed that employing of the chain extender not only increased the viscoelastic properties of the nanocomposites, but it also improved the dispersion of the organoclays and led to better barrier and mechanical properties.

9.3 Recommendations

The following subjects are proposed for future studies:

1) The presence of silicate layers in PET films reduces the elongation at break and lead to more brittleness. Toughness of the nanocomposite films may increase significantly by the addition of a small amount of an elastomer. By changing clay and/or elastomer concentration, as well as their ratio, a wide range of properties may be obtained and therefore, it may be possible to optimize properties.

2) In view of the importance of processing conditions such as screw configuration in exfoliation of silicate layers, parameters affecting mixing quality (e.g. width of kneading blocks, staggering angle, forward/backward flow) should be optimized.

3) The PET nanocomposites containing thermally stable organoclays are partially intercalated with large aggregates due to the lack of compatibility between the matrix and the organic modifier of the clays. Hence, further studies should be devoted to the chemistry of the organoclays to preserve the thermal stability of the surfactants, while improving their thermodynamic compatibility with the matrix.

4) To fabricate PET nanocomposite films containing synthetic clays. Synthetic clays with higher aspect ratios than natural clays, if modified with a suitable organic modifier, are prone to create longer tortuous pathway and consequently yield better barrier properties.

5) Considering the improvements achieved in the morphology and properties of the nanocomposites containing Joncryl, it is recommended to investigate the effect of the multifunctional chain extender on the morphology and properties of PET nanocomposites containing thermally stable organoclays. Variation of the chain extender content offers good potential to tune morphology and properties of the final product.

6) Blow molding is applied for the fabricating PET nanocomposite bottles. The effect of clay chemistry, clay concentration, and the chain extender on the barrier and mechanical properties of blow molded bottles should be studied.

REFERENCES

1. Bhattacharya S, Gupta R, and Kamal M. "Polymeric nanocomposites: theory and practice": Hanser Gardner Publications, 2007.
2. Ray SS and Okamoto M. "Polymer/layered silicate nanocomposites: a review from preparation to processing", Progress in Polymer Science; **28**, 1539-1641 (2003).
3. Pavlidou S and Papaspyrides CD. "A review on polymer-layered silicate nanocomposites", Progress in Polymer Science; **33**, 1119-1198 (2008).
4. Karayannidis GP and Psalida EA. "Chain extension of recycled poly(ethylene terephthalate) with 2,2'-(1,4-phenylene)bis(2-oxazoline)", Journal of Applied Polymer Science; **77**, 2206-2211 (2000).
5. Brooks D and G.A G. "PET Packaging Technology", 1 ed.: Blackwell, 2002.
6. Kodama H, Nakaya M, Shirakura A, Hotta A, Hasebe T, and Suzuki T. "Synthesis of practical high-gas-barrier carbon films at low and atmospheric pressure for PET bottles", New Diamond and Frontier Carbon Technology; **16**, 107-119 (2006).
7. Hussain F, Hojjati M, Okamoto M, and Gorga RE. "Review article: Polymer-matrix nanocomposites, processing, manufacturing, and application: An overview", Journal of Composite Materials; **40**, 1511-1575 (2006).
8. Mittal V. "In-situ Synthesis of Polymer Nanocomposites", 1 ed.: Wiley, 2011.
9. Giannelis EP. "Polymer layered silicate nanocomposites", Advanced Materials; **8**, 29-35 (1996).
10. Alexandre M and Dubois P. "Polymer-layered silicate nanocomposites: preparation, properties and uses of a new class of materials", Materials Science & Engineering R-Reports; **28**, 1-63 (2000).
11. Pramanik M, Srivastava SK, Samantaray BK, and Bhowmick AK. "EVA/Clay nanocomposite by solution blending: Effect of aluminosilicate layers on mechanical and thermal properties", Macromolecular Research; **11**, 260-266 (2003).
12. Lee SS, Ma YT, Rhee HW, and Kim J. "Exfoliation of layered silicate facilitated by ring-opening reaction of cyclic oligomers in PET-clay nanocomposites", Polymer; **46**, 2201-2210 (2005).
13. Kim KH, Huh J, and Jo WH. "Synthesis of thermally stable organosilicate for exfoliated poly(ethylene terephthalate) nanocomposite with superior tensile properties", Macromolecular Research; **15**, 178-184 (2007).
14. Mittal V. "Thermally Stable and Flame Retardant Polymer Nanocomposites", 1 ed.: Cambridge University Press, 2011.
15. Utracki LA. "Clay-Containing Polymeric Nanocomposites": Smithers Rapra Technology, 2004.
16. Fornes TD, Yoon PJ, and Paul DR. "Polymer matrix degradation and color formation in melt processed nylon 6/clay nanocomposites", Polymer; **44**, 7545-7556 (2003).

17. Shah RK and Paul DR. "Organoclay degradation in melt processed polyethylene nanocomposites", Polymer; **47**, 4075-4084 (2006).

18. Yoon PJ, Hunter DL, and Paul DR. "Polycarbonate nanocomposites: Part 2. Degradation and color formation", Polymer; **44**, 5341-5354 (2003).

19. Monemian SA, Goodarzi V, Zahedi P, and Angaji MT. "PET/imidazolium-based OMMT nanocomposites via in situ polymerization: Morphological, thermal, and nonisothermal crystallization studies", Advances in Polymer Technology; **26**, 247-257 (2007).

20. Scaffaro R, Botta L, Ceraulo M, and La Mantia FP. "Effect of Kind and Content of Organo-Modified Clay on Properties of PET Nanocomposites", Journal of Applied Polymer Science; **122**, 384-392 (2011).

21. Litchfield DW, Baird DG, Rim PB, and Chen C. "Improved Mechanical Properties of Poly(Ethylene Terephthalate) Nanocomposite Fibers", Polymer Engineering and Science; **50**, 2205-2215 (2010).

22. Soon KH, Harkin-Jones E, Rajeev RS, Menary G, McNally T, Martin PJ, and Armstrong C. "Characterisation of melt-processed poly(ethylene terephthalate)/synthetic mica nanocomposite sheet and its biaxial deformation behaviour", Polymer International; **58**, 1134-1141 (2009).

23. Ammala A, Bell C, and Dean K. "Poly(ethylene terephthalate) clay nanocomposites: Improved dispersion based on an aqueous ionomer", Composites Science and Technology; **68**, 1328-1337 (2008).

24. Bizarria MTM, Giraldi A, de Carvalho CM, Velasco JI, d'Avila MA, and Mei LHI. "Morphology and thermomechanical properties of recycled PET-organoclay nanocomposites", Journal of Applied Polymer Science; **104**, 1839-1844 (2007).

25. Patro TU, Khakhar DV, and Misra A. "Phosphonium-Based Layered Silicate-Poly(ethylene terephthalate) Nanocomposites: Stability, Thermal and Mechanical Properties", Journal of Applied Polymer Science; **113**, 1720-1732 (2009).

26. Jung MH, Chang JH, and Kim JC. "Poly(ethylene terephthalate) nanocomposite fibers with new organomica via in situ intercalation", Polymer Engineering and Science; **47**, 1820-1826 (2007).

27. Hwang SY, Lee WD, Lim JS, Park KH, and Im SS. "Dispersibility of clay and crystallization kinetics for in situ polymerized PET/pristine and modified montmorillonite nanocomposites", Journal of Polymer Science Part B-Polymer Physics; **46**, 1022-1035 (2008).

28. Mun MK, Kim JC, and Chang JH. "Preparation of poly(ethylene terephthalate) nanocomposite fibers incorporating a thermally stable organoclay", Polymer Bulletin; **57**, 797-804 (2006).

29. Hao JY, Lu XH, Liu SL, Lau SK, and Chua YC. "Synthesis of poly(ethylene terephthalate)/clay nanocomposites using aminododecanoic acid-modified clay and a bifunctional compatibilizer", Journal of Applied Polymer Science; **101**, 1057-1064 (2006).

30. Chang JH, Mun MK, and Lee IC. "Poly(ethylene terephthalate) nanocomposite fibers by in situ polymerization: The thermomechanical properties and morphology", Journal of Applied Polymer Science; **98**, 2009-2016 (2005).

31. Chung JW, Son SB, Chun SW, Kang TJ, and Kwak SY. "Thermally stable exfoliated poly(ethylene terephthalate) (PET) nanocomposites as prepared by selective removal of organic modifiers of layered silicate", Polymer Degradation and Stability; **93**, 252-259 (2008).

32. Lee D and Char K. "Effect of acidity on the deintercalation of organically modified layered silicates", Langmuir; **18**, 6445-6448 (2002).

33. Davis RD, Galman JW, Sutto TW, Callahan JH, Trulove PC, and De Long H. "Improved thermal stability of organically modified layered silicates", Clays and Clay Minerals; **52**, 171-179 (2004).

34. Ngo HL, LeCompte K, Hargens L, and McEwen AB. "Thermal properties of imidazolium ionic liquids", Thermochimica Acta; **357**, 97-102 (2000).

35. Cui L, Dirnitri MKB, Christopher WBB, Hunter DL, Yoon PJ, and Paul DR. "Effect of organoclay purity and degradation on nanocomposite performance, Part 1: Surfactant degradation", Polymer; **49**, 3751-3761 (2008).

36. Stoeffler K, Lafleur PG, and DenaUlt J. "Effect of intercalating agents on clay dispersion and thermal properties in polyethylene/montmorillonite nanocomposites", Polymer Engineering and Science; **48**, 1449-1466 (2008).

37. Ghasemi H, Carreau PJ, Kamal MR, and Uribe-Calderon J. "Preparation and Characterization of PET/Clay Nanocomposites by Melt Compounding", Polymer Engineering and Science; **51**, 1178-1187

38. Stoeffler K, Lafleur PG, and Denault J. "Thermal decomposition of various alkyl onium organoclays: Effect on polyethylene terephthalate nanocomposites' properties", Polymer Degradation and Stability; **93**, 1332-1350 (2008).

39. Costache MC, Heidecker MJ, Manias E, and Wilkie CA. "Preparation and characterization of poly(ethylene terephthalate)/clay nanocomposites by melt blending using thermally stable surfactants", Polymers for Advanced Technologies; **17**, 764-771 (2006).

40. Bishop C. "Roll-to-Roll Vacuum Deposition of Barrier Coatings", 1 ed.: Wiley-Scrivener, 2011.

41. Maul P. Barrier enhancement using additives. Fillers, Pigments and Additives for Plastics in Packaging Applications Pira International Conference

Brussels, Belgium, 2005.

42. Alger M. "Polymer Science Dictionary ", 2 ed.: Springer, 1996.

43. Siracusa V. "Food Packaging Permeability Behaviour: A Report", International Journal of Polymer Science; **2012**, 1 (2012).

44. Manas C and Roy SK. "Plastics Technology Handbook", 4 ed.: CRC Press, 2006.

45. Stanislav E.S and G AY. "Mass Transport & Reactive Barriers in Packaging: Theory, Applications, & Design": DEStech Publications, 2007.

46. Perkins W. "Effect of molecular weight and annealing temperature on the oxygen barrier properties of oriented PET film", Polymer Bulletin; **19**, 397 (1988).

47. Ghasemi H, Carreau PJ, Kamal MR, and Tabatabaei SH. "Properties of PET/clay nanocomposite films", Polymer Engineering and Science; **52**, 420-430 (2012).

48. Donadi S, Modesti M, Lorenzetti A, and Besco S. "PET/PA Nanocomposite Blends with Improved Gas Barrier Properties: Effect of Processing Conditions", Journal of Applied Polymer Science; **122**, 3290-3297 (2011).

49. Ozen I, Bozoklu G, Dalgicdir C, Yucel O, Unsal E, Cakmak M, and Menceloglu YZ. "Improvement in gas permeability of biaxially stretched PET films blended with high barrier polymers: The role of chemistry and processing conditions", European Polymer Journal; **46**, 226-237 (2009).

50. Yeo JH, Lee CH, Park CS, Lee KJ, Nam JD, and Kim SW. "Rheological, morphological, mechanical, and barrier properties of PP/EVOH blends", Advances in Polymer Technology; **20**, 191-201 (2001).

51. Hannay F. "Rigid Plastics Packaging - Materials, Processes and Applications": Smithers Rapra Technology, 2002.

52. Hopewell J, Dvorak R, and Kosior E. "Plastics recycling: challenges and opportunities", Philosophical Transactions of the Royal Society B-Biological Sciences; **364**, 2115-2126 (2009).

53. Duncan TV. "Applications of nanotechnology in food packaging and food safety: Barrier materials, antimicrobials and sensors", Journal of Colloid and Interface Science; **363**, 1-24 (2011).

54. Alix S, Follain N, Tenn N, Alexandre B, Bourbigot S, Soulestin J, and Marais S. "Effect of Highly Exfoliated and Oriented Organoclays on the Barrier Properties of Polyamide 6 Based Nanocomposites", Journal of Physical Chemistry C; **116**, 4937-4947 (2012).

55. Svagan AJ, Akesson A, Cardenas M, Bulut S, Knudsen JC, Risbo J, and Plackett D. "Transparent Films Based on PLA and Montmorillonite with Tunable Oxygen Barrier Properties", Biomacromolecules; **13**, 397-405 (2012).

56. Dadfar SMA, Alemzadeh I, Dadfar SMR, and Vosoughi M. "Studies on the oxygen barrier and mechanical properties of low density polyethylene/organoclay nanocomposite films in the presence of ethylene vinyl acetate copolymer as a new type of compatibilizer", Materials & Design; **32**, 1806-1813 (2011).

57. Hong SI and Rhim JW. "Preparation and properties of melt-intercalated linear low density polyethylene/clay nanocomposite films prepared by blow extrusion", Lwt-Food Science and Technology; **48**, 43-51 (2012).

58. Okamoto M. "Polymer/Layered Silicate Nanocomposites": Smithers Rapra Press, 2003.

59. Gary W. B and P CE. "Fundamentals of Polymer-Clay Nanocomposites": Cambridge University Press, 2011.

60. Picard E, Vermogen A, Gerard JF, and Espuche E. "Barrier properties of nylon 6-montmorillonite nanocomposite membranes prepared by melt blending: Influence of the clay content and dispersion state - Consequences on modelling", Journal of Membrane Science; **292**, 133-144 (2007).

61. Fredrickson GH and Bicerano J. "Barrier properties of oriented disk composites", Journal of Chemical Physics; **110**, 2181-2188 (1999).

62. Bharadwaj RK. "Modeling the barrier properties of polymer-layered silicate nanocomposites", Macromolecules; **34**, 9189-9192 (2001).

63. Nielsen LE. "Models for the Permeability of Filled Polymer Systems", Journal of Macromolecular Science (Chemistry). A1; 929-942 (1967).

64. Cussler EL, Hughes SE, Ward Iii WJ, and Aris R. "Barrier membranes", Journal of Membrane Science; **38**, 161-174 (1988).

65. Lape NK, Nuxoll EE, and Cussler EL. "Polydisperse flakes in barrier films", Journal of Membrane Science; **236**, 29-37 (2004).

66. Gusev AA and Lusti HR. "Rational design of nanocomposites for barrier applications", Advanced Materials; **13**, 1641-+ (2001).

67. Ghasemi H, Carreau PJ, Kamal MR, and Chapleau N. "Effect of Processing Conditions on Properties of PET/Clay Nanocomposite Films", International Polymer Processing; **26**, 219-228

68. Frounchi M and Dourbash A. "Oxygen Barrier Properties of Poly(ethylene terephthalate) Nanocomposite Films", Macromolecular Materials and Engineering; **294**, 68-74 (2009).

69. Goitisolo I, Eguiazabal JI, and Nazabal J. "Stiffening of poly(ethylene terephthalate) by means of polyamide 6 nanocomposite fibers produced during processing", Composites Science and Technology; **70**, 873-878 (2010).

70. Calcagno CIW, Mariani CM, Teixeira SR, and Mauler RS. "The effect of organic modifier of the clay on morphology and crystallization properties of PET nanocomposites", Polymer; **48**, 966-974 (2007).

71. Ghasemi H, Carreau PJ, and Kamal MR. "Isothermal and non-isothermal crystallization behavior of PET nanocomposites", Polymer Engineering and Science; **52**, 372-384 (2012).

72. Bandyopadhyay J, Ray SS, and Bousmina M. "Thermal and thermo-mechanical properties of poly(ethylene terephthalate) nanocomposites", Journal of Industrial and Engineering Chemistry; **13**, 614-623 (2007).

73. Soon K, Harkin-Jones E, Rajeev RS, Menary G, Martin PJ, and Armstrong CG. "Morphology, barrier, and mechanical properties of biaxially deformed poly(ethylene terephthalate)-mica nanocomposites", Polymer Engineering and Science; **52**, 532-548 (2012).

74. Rajeev RS, Harkin-Jones E, Soon K, McNally T, Menary G, Armstrong CG, and Martin PJ. "Studies on the effect of equi-biaxial stretching on the exfoliation of nanoclays in polyethylene terephthalate", European Polymer Journal; **45**, 332-340 (2009).

75. Sanchez-Solis A, Garcia-Rejon A, and Manero O. "Production of nanocomposites of PET-montmorillonite clay by an extrusion process", Macromolecular Symposia; **192**, 281-292 (2003).

76. Chisholm BJ, Moore RB, Barber G, Khouri F, Hempstead A, Larsen M, Olson E, Kelley J, Balch G, and Caraher J. "Nanocomposites derived from sulfonated poly(butylene terephthalate)", Macromolecules; **35**, 5508-5516 (2002).

77. Xu XF, Ghanbari A, Leelapornpisit W, Heuzey MC, and Carreau P. "Effect of Ionomer on Barrier and Mechanical Properties of PET/Organoclay Nanocomposites Prepared by Melt Compounding", International Polymer Processing; **26**, 444-455 (2011).

78. Hayrapetyan S, Kelarakis A, Estevez L, Lin Q, Dana K, Chung YL, and Giannelis EP. "Non-toxic poly(ethylene terephthalate)/clay nanocomposites with enhanced barrier properties", Polymer; **53**, 422-426 (2012).

79. Vidotti SE, Chinellato AC, Hu GH, and Pessan LA. "Preparation of poly(ethylene terephthalate)/Organoclay nanocomposites using a polyester lonorner as a compatibilizer", Journal of Polymer Science Part B-Polymer Physics; **45**, 3084-3091 (2007).

80. Hwang SY and Im SS. "PET-Ionomers and PETi/MMT Nanocomposites: A Comparison of the Effect of Ionic Groups on Their Crystallinities and Physical Properties", Polymer Composites; **32**, 259-267 (2011).

81. Barber GD, Calhoun BH, and Moore RB. "Poly(ethylene terephthalate) ionomer based clay nanocomposites produced via melt extrusion", Polymer; **46**, 6706-6714 (2005).

82. Nazockdast E, Nazockdast H, and Goharpey F. "Linear and nonlinear melt-state viscoelastic properties of polypropylene/organoclay nanocomposites", Polymer Engineering and Science; **48**, 1240-1249 (2008).

83. Eslami H, Grmela M, and Bousmina M. "Linear and nonlinear rheology of polymer/layered silicate nanocomposites", Journal of Rheology; **54**, 539-562 (2010).

84. Ray SS and Bousmina M. "Poly(butylene sucinate-co-adipate)/montmorillonite nanocomposites: effect of organic modifier miscibility on structure, properties, and viscoelasticity", Polymer; **46**, 12430-12439 (2005).

85. Vermant J, Ceccia S, Dolgovskij MK, Maffettone PL, and Macosko CW. "Quantifying dispersion of layered nanocomposites via melt rheology", Journal of Rheology; **51**, 429-450 (2007).

86. Aubry T, Razafinimaro T, and Mederic P. "Rheological investigation of the melt state elastic and yield properties of a polyamide-12 layered silicate nanocomposite", Journal of Rheology; **49**, 425-440 (2005).

87. Solomon MJ, Almusallam AS, Seefeldt KF, Somwangthanaroj A, and Varadan P. "Rheology of polypropylene/clay hybrid materials", Macromolecules; **34**, 1864-1872 (2001).

88. Dykes LMC, Torkelson JM, and Burghardt WR. "Shear-Induced Orientation in Well-Exfoliated Polystyrene/Clay Nanocomposites", Macromolecules; **45**, 1622-1630 (2012).

89. Cassagnau P. "Melt rheology of organoclay and fumed silica nanocomposites", Polymer; **49**, 2183-2196 (2008).

90. Krishnamoorti R and Yurekli K. "Rheology of polymer layered silicate nanocomposites", Current Opinion in Colloid & Interface Science; **6**, 464-470 (2001).

91. Loiseau A and Tassin JF. "Model nanocomposites based on laponite and poly(ethylene oxide): Preparation and rheology", Macromolecules; **39**, 9185-9191 (2006).

92. Wu DF, Zhou CX, Hong Z, Mao DL, and Bian Z. "Study on rheological behaviour of poly(butylene terephthalate)/montmorillonite nanocomposites", European Polymer Journal; **41**, 2199-2207 (2005).

93. Li J, Zhou CX, Wang G, and Zhao DL. "Study on rheological behavior of polypropylene/clay nanocomposites", Journal of Applied Polymer Science; **89**, 3609-3617 (2003).

94. Khalkhal F, Carreau PJ, and Ausias G. "Effect of flow history on linear viscoelastic properties and the evolution of the structure of multiwalled carbon nanotube suspensions in an epoxy", Journal of Rheology; **55**, 153-175

95. Hegde RR, Bhat GS, and Deshpande B. "Morphology and Properties of Nylon 6 Blown Films Reinforced with Different Weight Percentage of Nanoclay Additives", International Journal of Polymer Science;

96. Sothornvit R, Hong SI, An DJ, and Rhim JW. "Effect of clay content on the physical and antimicrobial properties of whey protein isolate/organo-clay composite films", Lwt-Food Science and Technology; **43**, 279-284

97. Khalkhal F, Carreau PJ, and Ausias G. "Effect of flow history on linear viscoelastic properties and the evolution of the structure of multiwalled carbon nanotube suspensions in an epoxy", Journal of Rheology; **55**, 153-175 (2011).

APPENDIX A:
PERCOLATION THRESHOLD

The following percolation model [85, 97] was used to determine the percolation threshold in the nanocomposites:

$$G' \propto (\varphi - \varphi_{per})^n \qquad \text{(A-1)}$$

where φ_{per} and n are the percolation threshold volume fraction and a power-law exponent, respectively. The parameter n is equal to 1.68 and 1.07 for screw configurations #1 and #2, respectively.

The calculated percolation values (in wt%) are 3.4 and 3.2 for PET/C30B nanocomposites prepared using screw configuration #1 and #2, respectively. The following Figure shows the fit for the percolation threshold.

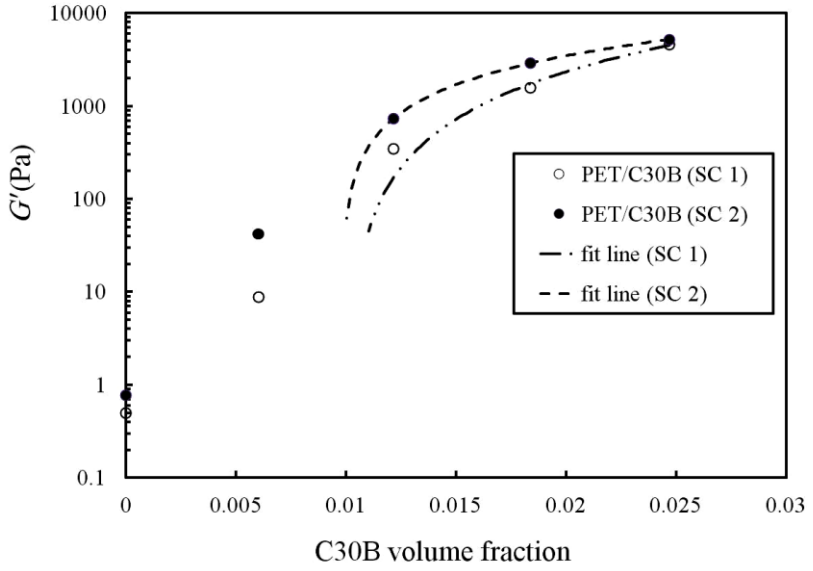

Figure A-1: Storage modulus of the PET/C30B nanocomposites as a function of clay loading for screw configurations #1 and #2 (data at 0.3 rad/s).

APPENDIX B:
INTRINSIC VISCOSITY

An Ubbelohde viscometer was used with the goal of measuring the intrinsic viscosity of the neat PET and the PET nanocomposites containing 2, 4, 6, and 8 wt% C30B at 30 °C according to ASTM D-4603. The main objective of this part was to determine the matrix degradation induced by the presence of the organoclay. PET and all the nanocomposites were dissolved in a mixture of (60/40 ratio wt/wt) phenol/1,1,2,2-tetrachloroethane to prepare solutions at 0.50 wt% concentration. Elimination of the clay particles from the solutions is required to rule out the effect of the particles on the intrinsic viscosity of the samples. To this end syringe filters with 220, 100, and 20 nm pore sizes were employed. The syringe filters were kindly supplied by Whatman™ Company.

The intrinsic viscosity, η, of the samples determined using the Billmeyer relationship, cited in the ASTM D-4603:

$$\eta = 0.25(\eta_r - 1 + 3\ln\eta_r)/C$$

where C is the polymer concentration (g/dL), η_r is the relative viscosity obtained by taking the ratio of the average solution flow time (s) to the average solvent flow time (s).

While all the samples passed easily through the syringe filters with 220 nm pore size, those with 100 and 20 nm pore sizes were clogged by the clay particles after filtering a few droplets. Therefore, the PET-based nanocomposites were filtered by employing only the syringe filters with 220 nm pore size, which meant that the filtered solutions most probably still contained clay particles.

Table B-1: Intrinsic viscosity and molecular weight of the neat PET and the nanocomposites containing C30B filtered by syringe filters with 220 nm pore size.

Sample	Average flow time (s)	Relative viscosity	Intrinsic viscosity (dL/g)	Apparent viscosity-averaged molecular weight (kg/mol)
Solvent	76.5	-	-	-

Neat PET	107.8	1.41	0.719	61.7
PET/2 C30B	108.9	1.42	0.741	64.3
PET/4 C30B	104	1.36	0.640	52.6
PET/6 C30B	96.2	1.26	0.472	34.7
PET/8 C30B	96.1	1.25	0.470	34.5

Obviously the presence of the remaining clay particles in the samples has influenced the flow time of the solutions. For example, while the thermal degradation of the matrix of the nanocomposite containing 2 wt% C30B was already verified by the rheological results and color formation, a larger intrinsic viscosity and molecular weight were obtained for this sample in comparison to the neat PET. Besides, intrinsic viscosity and molecular weight of the nanocomposites containing 6 and 8 wt% C30B are very close to each other, which is not expected.